Development of a Fast Gas-Solid Flow Simulation for Control of the Pneumatic Conveying System on Air Seeders

A Thesis Submitted to the
College of Graduate and Postdoctoral Studies
in Partial Fulfillment of the Requirements
for the degree of Master of Science
in the Department of Mechanical Engineering
University of Saskatchewan
Saskatoon

By
Jason D.M. Cousins

Permission to Use

In presenting this thesis in partial fulfilment of the requirements for a Postgraduate degree from the University of Saskatchewan, I agree that the Libraries of this University may make it freely available for inspection. I further agree that permission for copying of this thesis in any manner, in whole or in part, for scholarly purposes may be granted by the professor or professors who supervised my thesis work or, in their absence, by the Head of the Department or the Dean of the College in which my thesis work was done. It is understood that any copying or publication or use of this thesis or parts thereof for financial gain shall not be allowed without my written permission. It is also understood that due recognition shall be given to me and to the University of Saskatchewan in any scholarly use which may be made of any material in my thesis.

Requests for permission to copy or to make other use of material in this thesis in whole or part should be addressed to:

Head of the Department of Mechanical Engineering
57 Campus Drive
University of Saskatchewan
Saskatoon, Saskatchewan S7N 5A9 Canada

OR

Dean
College of Graduate and Postdoctoral Studies
University of Saskatchewan
116 Thorvaldson Building, 110 Science Place
Saskatoon, Saskatchewan S7N 5C9 Canada

Abstract

Limitations of the pneumatic conveying system are an obstacle to the improvement of air seeding technology. Operators often run conveying velocities far above the minimum requirement. This is common because lower conveying velocities - which could reduce waste, energy consumption and hydraulic requirements - put the system at risk of blockages and non-uniform distribution. Furthermore, new precision technologies such as variable rate application and sectional control introduce imbalances to the highly coupled and distributed conveying system. Incorporating adaptive control mechanisms has been theorized as a potential means of improving conveying system performance.

Real-time prediction of conveying system flow conditions is a prerequisite for the proposed control strategies. There is limited existing research regarding control and modeling for air seeders or similar pneumatic conveying systems. While there is extensive research for multiphase flow modeling, few examples prioritize computational efficiency to the extent that real-time simulation is feasible. Application to control dictates that computational speed, in addition to accuracy, is essential. The purpose of this research was to identify, develop and validate a method for predicting flow conditions within a pneumatic conveying system that is suitable for control applications.

A low-computational cost, one-dimensional model and simulation have been developed for fast prediction of bulk multiphase flow conditions within the pneumatic conveying system. The model is a simplified form of the Eulerian-Eulerian (two-fluid) equations for fluid-particle flows. The differential model equations were discretized via the finite volume method and solved using computational fluid dynamics techniques. Specifically, the SIMPLER algorithm for the solution of coupled equations was used. The simulation program, which employs the numerical methods to obtain solutions to the discrete equations, was implemented in MATLAB ®.

Experimental data were collected using a laboratory apparatus which approximated a straight horizontal pneumatic conveying line. The inner diameter of the experimental conveying line was 57.4 mm. Spherical plastic particles with a mean diameter of 3.56 mm were conveyed. Testing consisted of dilute flows only that were relevant for air seeding condi-

tions. Experiments covered air velocities of 20 to 30 m/s and mass loadings of 0.84 to 4.68. Recorded data included steady-state and transient measurements for fluid pressure and bulk particle velocity. The experimental data were used to validate simulation results.

The accuracy of the model for steady-state conditions was acceptable for sufficiently dilute and well-developed flow. The simulation predicted experimental fluid pressure within 6% in all tests. For moderate mass loadings, simulation error for particle velocity was below 10%. At higher mass loadings, accuracy for particle velocity began to deteriorate and an error of $>$ 25% was observed. Analysis of the model's accuracy for transient conditions was inconclusive. Evidence suggested that transient simulation results may be quite good. However, limitations of the continuous equations and experimental factors complicated the analysis, preventing a definitive verdict regarding transient accuracy.

Simulation performance with respect to computing time was excellent. Simulation results were found to be relatively insensitive to the size of time and spatial step used, allowing for the program to execute in less time than was being simulated. The fastest execution recorded required 5.0 sec to simulate 60 sec of transient flow, and results deviated minimally from higher resolution simulations. Results indicated the potential for optimization between speed and accuracy. While the simplified model only calculates a limited number of bulk flow properties, it delivered timely results with reasonable accuracy and with relatively low computational effort.

Assessment of the developed model and simulation has concluded a suitable potential for control application. Acceptable accuracy and computing speed were obtained to justify further development efforts. The prescribed methodology provides a foundation for future expansion and improvement. There is potential to incorporate fast multiphase flow simulation into control infrastructure to improve the performance of the air seeder conveying system.

Acknowledgements

I would like to offer my sincere thanks to my research supervisor, Professor Scott Noble, for his mentorship and project guidance. Our often not-so-brief conversations were a source of constant encouragement and inspiration. Perhaps most of all, his patience and support while I pursued my degree, along with a host of other distractions, did not go unnoticed and was greatly appreciated.

Secondly, my colleagues: Tyrone Keep for his frequent assistance with equipment in the Air Handling Lab; Arsh Brar for his assistance with the experiments, stimulating intellectual discussions, and encouragement; and my two office mates for their companionship, conversation and occasional distractions.

Thirdly, Mr. Joel Gervais and CNH Saskatoon for providing the project, continued interest in its completion, and support in supplying working space and resources.

Finally, the financial support of both CNH Industrial and the Natural Sciences and Engineering Research Council (NSERC) in the form of the Industrial Post-graduate Scholarship is gratefully acknowledged; without which this research would not have been possible.

To my parents, Keith and Karen, whose confidence and support over these past years, and long before, have been immeasurable.

Contents

List of Tables

List of Figures

Nomenclature

C_D	Drag coefficient	[-]
Cr	Courant number	[-]
d	Pipe inner diameter	[m]
d_p	Diameter of a particle	[m]
e_{ss}	Coefficient of restitution for particle-particle collisions	[-]
e_{wall}	Coefficient of resitution for particle-wall collisions	[-]
f	Darcy friction factor	[-]
g	Acceleration due to gravity	[m/s^2]
g_0	Radial distribution function	[-]
M_i	Interphase momentum transfer vector	[N/m^3]
Ma	Mach number	[-]
$\dot{m}_f$	Mass flow rate of the fluid phase	[kg/s]
$\dot{m}_s$	Mass flow rate of the solids phase	[kg/s]
p	Static fluid pressure	[Pa]
p^s	Solids pressure	[Pa]
$\tilde{p}$	Normalized fluid pressure	[-]
Re	Pipe Reynolds number	[-]
Re_s	Solids Reynolds number	[-]
Stk	Particle Stokes number	[-]
S^f	Total fluid momentum source term	[N/m^3]
$S^f_{friction}$	Fluid momentum source due to wall friction	[N/m^3]
$S^f_{gravity}$	Fluid momentum source due to gravity	[N/m^3]
S^s	Total solids momentum source term	[N/m^3]
$S^s_{friction}$	Solids momentum source due to wall friction	[N/m^3]
$S^s_{gravity}$	Solids momentum source due to gravity	[N/m^3]

t	Time	[s]
u	Average fluid velocity in the streamwise direction	[m/s]
u_k	Fluid velocity vector in k dimensions	[m/s]
υ	Average solids velocity in the streamwise direction	[m/s]
V	Volume	[m^3]
υ_k	Solids velocity vector in k dimensions	[m/s]
x	Spatial coordinate in streamwise direction	[m]
x_k	Cartesian spatial coordinate in k dimensions	[m]
z	Mass loading ratio	-
β	Drag friction coefficient	[kg/$m^3 s$]
Δt	Temporal step-size for numerical computation	[s]
Δx	Spatial step-size for numerical computation	[m]
$\tilde{\delta p}$	Normalized difference in pressures	[-]
$\tilde{\delta u}$	Normalized difference in fluid velocites	[-]
ϵ	Relative pipe roughness	[-]
ε_f	Volume fraction of the fluid phase	-
$\varepsilon_{s,max}$	Maximum packing density of particles	[-]
ε_s	Volume fraction of the solids phase	-
λ	Fluid bulk viscosity	[Pa s]
λ^s	Solids bulk viscosity	[Pa s]
μ	Fluid dynamic viscosity	[Pa s]
μ^s	Solids dynamic viscosity	[Pa s]
ρ_f	Fluid density	[kg/m^3]
ρ_s	Solids phase density	[kg/m^3]
σ	Fluid stress tensor	[Pa]
σ^s	Solids stress tensor	[Pa]
τ_p	Particle response time	[s]

τ^s_{wall}	Solids-wall shear stress	[Pa]
Θ	Granular temperature	[J/kg]
θ	Angle between pipe axis and direction of gravity	[rad]
$()_{\text{exp}}$	Experimental data	
$()_{\text{set}}$	Experiment setpoint	
$()_{\text{sim}}$	Simulation data	

Chapter 1

Introduction

1.1 Introduction

The agriculture and food industries have seen tremendous change over the past few decades. Continued development in mechanization and agronomy, introduction of new plant breeds and precision agriculture technologies have helped to revolutionize food production; driving population and economic growth in many regions. Today, the face of agriculture is still changing, and must continue to do so in the future if it is to meet the challenges that face the industry, and our species. The human population is continually growing and must be fed, clothed and sheltered from the same finite resources. According to the United Nations (2017), the world will need to produce at least 50% more food than it currently does by mid-century in order to sustain a predicted population of 9 billion people. To add to the difficulty, the continued trend toward urbanization means this increase in production must be achieved with a diminishing workforce. Simultaneously, agriculture's impact on the environment, which is substantial, must be minimized. Currently, more than one third of the earths surface is consumed by agricultural activity (Roser and Ritchie, 2017) and approximately 25% of GHG emissions come from agriculture and related land use changes (World Bank Group, 2015). To overcome these challenges, the agricultural food production industry must grow and improve; becoming more productive, more efficient, and more sustainable as it strives to feed an ever-growing world.

Agriculture and related industries are an important part of the economies of both Canada and more locally, Saskatchewan. The Canadian economy relies heavily on the exportation of raw goods, extracted from a large land mass and abundant natural resources. In 2016, Canadian crop exports totaled approximately $20.5 Billion or 4% of the total exports for

the year (Industry Canada, 2017), with the majority of Canadian crops being produced in the Western "prairie" provinces. For instance, in the province of Saskatchewan agricultural production and export is a primary component of the provincial economy. In 2016, 16 of the provinces' top 25 exports were agricultural products (Saskatchewan Trade & Export Partnership, 2016). Further, the five largest crop exports (canola, lentils, wheat, durum and peas) amounted to nearly half of the province's total exports; worth more than $11.5 Billion. In addition to direct export of agricultural commodities, a number of support industries related to agricultural production are also prominent in Saskatchewan, including agricultural equipment manufacturing, equipment dealers and distributors, agronomy and crop inputs, seed growing and transport for agricultural materials. Design and improvement of agricultural equipment are of particular interest and are the focus of the present work; specifically, air seeding equipment and technology.

Air seeders are an important agricultural implement used in crop planting and tillage processes. Air seeding technology was developed in the 1950's and 1960's primarily as a seed planting method for conservation tillage operations, and has since become a common sight across the Canadian prairies and elsewhere in the world. Modern air seeders typically consist of two main components. First, is the air cart which stores, meters (i.e. controls application rates), and distributes seed and granular products such as fertilizers. The second component is the air hoe drill, which interacts with the soil to prepare the seed bed, deposit the product into the soil and cover the furrow. Seed and granular products are moved between the air cart and the air hoe drill by means of a pneumatic conveying system – transport of particles through a network of multiple pipes or lines using an air stream – which lends the "air" to the names of the equipment. A tractor unit tows the air seeder through the field, while also providing hydraulic and electrical power. The use of air seeders allows for seeding, fertilization and tillage to be completed simultaneously in a single operation, providing several benefits over traditional practices in many locations and situations.

The benefits they provide have positioned air seeders as an important part of agricultural crop production in Western Canada and other regions. Air seeders play a prominent role in conservation tillage practices (including no-till), which is a major development in agriculture technology and has had a tremendous benefit towards the sustainability of the agricultural

food supply. Conservation tillage, which limits pre-seeding soil disturbance, has numerous benefits including reduced soil erosion by up to 90%, less fossil fuel consumption, increased soil organic matter (Minnesota Department of Agriculture, 2017) and decreased green house gas emissions (Conservation Technology Information Center, 2017; Janzen, 2004). The significant benefits associated with conservation tillage have led to wide spread adoption of the practice and currently more than 80% of all tilled land in Canada is considered either no-till or conservation till practice (Statistics Canada, 2017). Additional benefits outside of conservation tillage also contribute to the popularity of air seeding equipment. Modern air seeders allow for a large variety of crop types to be seeded quickly and efficiently, in a single pass and with few operators, reducing time and labour requirements. The largest units available have drill widths of 30 meters and cart capacities of 45,000 litres, allowing large areas of land to be seeded quickly with less equipment. The success of the technology and equipment, particularly in Western Canada, has lead to the growth of a number of leading manufacturers; many of which are headquartered or have production centres in Saskatchewan.

1.2 Problem

Air seeding technology is developing and changing, being driven by the demands of the industry. Reliability and ease of maintenance are no longer the solitary concerns of customers. Farmers have come to expect innovative features and superior performance as justification for what has become an enormous investment (new top model air seeders now run around $1M for a complete unit). The motivation for development and innovation among air seeder manufacturers can be broadly summarized as perusing increases in three primary areas: productivity, efficiency, and agronomic performance. Manufacturers seek to deliver increased productivity by designing larger equipment that can operate at higher speed, allowing more acres to be seeded in less time. Larger, faster equipment introduces challenges such as designing structures that can handle increased stress, achieving predictable behaviour in inherently rough terrain, and increasing conveying capacity to supply seed and fertilizer at higher rates. A second major trend, the pursuit of greater efficiency, focuses primarily on reducing power consumption and wasting less of the expensive crop inputs, providing cost

savings to farmers. Examples include reducing seeding overlap with sectional control, better management of crop inputs through variable rate application, and reducing seed attrition and power consumption by conveying at lower air speeds. The final trend, better agronomic performance, involves having more precise control over seed placement (depth and spacing), fertilizer placement, and less seed damage (i.e. higher germination); ultimately resulting in higher crop yields. Agronomic performance is closely related to the previous aspects because the behaviour of the cart and drill significantly affect seed placement, germination rates, etc. Achieving higher performance is not a trivial matter, and necessitates overcoming a number of challenges in addition to creating some new ones.

It is clear that there is significant interest in finding ways to improve the performance of air seeding equipment. One component of the technology that simultaneously presents both an obstacle and an opportunity for improved performance is the pneumatic conveying system. Performance of the conveying system can be generalized as having two interrelated aspects: uniformity and efficiency. Uniformity refers to uniform stable flow ensuring consistent seed placement, no line blockages, and even distribution across the width of the drill. Efficiency implies conveying at lower speeds; reducing hydraulic demand and fuel consumption, reducing seed damage, and improving seed placement. Unfortunately, these two aspects oppose each other - inadequate airflow being a major threat to uniformity - and it can be difficult to achieve acceptable levels of both simultaneously. Consequently, it is common practice to run excessive conveying speeds to reduce the chance of blockages at the expense of efficiency. Optimization of the conveying speeds would provide some significant benefits to performance. However, this is not easily achieved with the existing technology. The complexity inherent in the conveying system is a major barrier to improving performance. The fan which supplies airflow is highly nonlinear, as is the two-phase air-particle flow in the conveying lines. Reliance on a single fan for supplying the air to multiple conveying lines also means that the lines are tightly coupled and changes in one can have an impact on the flow in other lines (aggravated further by variable rate and sectional control). Add to this a complex, distributed geometry with multiple lines, bends, elbows, splits and dozens of outlets and the difficulty yet increases. Thus, the pneumatic conveying system presents a significant opportunity for better performance and a significant challenge in realizing it.

Active control mechanisms are one potential way of improving the operating characteristics of the conveying system. Better control capabilities over the conveying system could take several forms. Active control of the fan (i.e. air supply) could allow for optimal conveying velocities to be maintained as operating conditions change during regular use. Further to this, manipulation of individual conveying lines would provide a finer level of control not possible using the fan alone. Control over individual lines would allow for the system to be balanced, preventing lines with less resistance from shorting the air supply and starving adjacent lines. These capabilities would allow the system to operate under optimum conveying speeds, reducing seed damage, wear and hydraulic power consumption while still avoiding blockages and non-uniform flow problems. Even small reductions in conveying velocity could produce a noticeable performance increase, since both particle attrition and fan power have nonlinear relationships with conveying velocity. In the case of seed and particle damage, the relationship to air velocity is exponential (Baker et al., 1986). However, as has been discussed previously, the complexity of the conveying system – nonlinearity, geometry, size and coupling – makes this a challenging prospect. A reactive, feedback control system, for example, would be difficult and expensive to implement in such a system, and likely would deliver less than ideal results. Alternatively, a proactive, feed-forward system is likely better suited to handle the complexity of the system, particularly the coupling between lines, and deliver superior results. However, implementation of feed-forward control requires information, about the behaviour of the system and how it will respond to internal and external conditions. Modeling and simulation offer a potential means of providing this required information, giving the ability to predict operating conditions and responses of the conveying system. Providing a method for accurately predicting conditions within the conveying system through modeling will be the focus and goal of the present research.

1.3 State of Air Seeder Modeling and Control

A survey of the available literature was conducted to determine the current state of the art regarding modeling and control of the air seeder pneumatic conveying system. The initial review of existing literature encompassed three primary focus areas: application specific

research studying air seeder conveying systems, control of pneumatic conveying systems or related technologies, and prediction of pneumatic conveying and/or more general multiphase flows.

The body of published literature examining air seeder conveying systems was found to be limited. A thorough search revealed a relatively small number of applicable examples; the majority of which have been conducted at the University of Saskatchewan. Proprietary interest of manufacturers, the primary facilitators of such application-specific research, is a plausible reason for the lack of publicly available research. Existing research focused on air seeder conveying systems conducted at this institution included the work of Keep (2016) which examined the flow and entrainment characteristics of agricultural materials and their implications for conveying power and efficiency, the work of Binsirawanich (2011) and Hossain (2015) which both developed methods for estimation of solids mass loading through correlation with pressure drop and air velocity, and that of Mittal (2017) who examined pressure drop for different radius bends in the conveying line. The previous work of this research group provides experimental data, parameter correlations and insight into the underlying physics that may be useful for further modeling and simulation of the conveying system. Development of a system level model, particularly for application to real-time control, however, has not been considered previously. Thus, guidance and direction for applying these concepts to the air seeder conveying system will need to be sourced from a broader collection of literature.

Information on the design and operation of pneumatic conveying systems, being a mature technology, is quite prevalent. Surprisingly, the subject of control (particularly model-based control) of pneumatic conveying systems under dynamically varying loads/conditions does not appear to have been thoroughly examined and a literature search returned comparatively few examples. Barbosa and Seleghim (2003) and Salahshoor et al. (2013) have both employed artificial neural networks (ANN) in the control and optimization of multiphase flows. The former made use of ANNs to identify flow regime and implement a relatively simple non-linear controller with the objective of optimizing conveying velocity and reducing power consumption in pneumatic conveying. The latter implemented model predictive control (MPC) to regulate and stabilize multiphase flow in a production oil well using a

dynamic ANN as the plant model (i.e. ANN model of the multiphase flow). MPC was again applied to pneumatic conveying in the work of Satpati et al. (2014) but in this case system identification techniques and a generic non-linear model structure were used to represent the conveying system. Although good results were obtained, calculation of the model can become problematic as the size and complexity of the system increases. Wu et al. (2017) made use of computational fluid dynamics (CFD) in the development of MPC for single-phase flow. However, control calculations were based on a simplified linear plant model while CFD was used to simulate the closed loop system as a means of controller validation. Thus, the CFD model was not involved in the implementation of predictive control. The above examples all represent viable means of implementing model-based control for pneumatic conveying. None of these, however, makes use of a theoretical model derived from first principles to implement MPC. In the case of the air seeder conveying system, which has many inputs/outputs and a high degree of coupling, using a process model with a theoretical basis is likely to be more robust and potentially easier to scale. Given the lack of examples in the literature, predictive control of pneumatic conveying using a theoretical model seems to be a relatively unexplored topic.

In contrast to the previous two topics, there is a very large amount of literature discussing modeling, simulation and prediction of multiphase flows; including pneumatic conveying. Examples consist of experimental studies, investigations into behaviour and physical principals, theoretical discussion, modeling and simulation. In the case of pneumatic conveying, practical guides on design and operation are also abundant. Due to the enormous volume and breadth, a concise summary of literature on pneumatic conveying and multiphase flow modeling and prediction is not attempted. Instead, relevant information regarding description, physical behaviour and modeling methodologies are presented, in context with the present work, in chapters 2 and 3. It is nevertheless of interest to note that despite the large volume of literature there are apparent gaps associated with some specifics of this project. First, examples featuring flow conditions relevant to air seeders, namely dilute, dispersed flow of large non-spherical particles in distributed systems, are underrepresented. Second, simulation studies examining dynamic flow conditions are infrequent. Finally, studies focused on modeling and simulation rarely place significant emphasis on computing speed.

1.4 Objectives

The motivation for this research is the proposition that predictive (feed-forward) control measures can be applied to existing air seeding technology to improve performance and efficiency, particularly when using sectional control and variable rate strategies. An important requirement for realization of predictive control is the ability to accurately predict system operating conditions and response to internal and external stimuli. In the case of the product distribution system of air seeders, this translates to accurate prediction of multiphase flow conditions inside multiple parallel pneumatic conveying conduits. Modeling and simulation are a means of providing information for control purposes and are the primary goal of this research. However, using modeling and simulation to provide information in the context of control raises several important research questions which must be answered. What techniques exist for modeling the given flow conditions that would be suitable for the intended application? Can a model and simulation be developed using the available techniques to allow prediction of flow conditions within the conveying system? Once developed, can the simulation provide results that are both accurate and delivered fast enough to be useful for control application?

To deliver the desired results and to answer the above research questions, the present research had the following objectives:

1. To research existing modeling methodologies and select a suitable candidate for the given conditions and application,

2. To develop a model and simulation for prediction of multiphase flow conditions within an air seeder conveying system,

3. To validate the model and simulation using experimentally collected data,

4. To assess the suitability of the developed model and simulation for future expansion and for control system application.

1.5 Scope

Although the development of a complete model for the entire conveying system may ultimately be required for successful implementation of advanced control strategies, achieving this is not feasible within the timeline of this work. Therefore, the present work investigated modeling and simulation only for a single, straight section of the primary conveying system. Considerations for the chosen scope include:

- Boundary conditions for the primary conveying lines are more easily obtained than for other portions of the conveying system, because inputs to the primary lines are directly controlled, either individually or collectively.
- Fan dynamics may be important for overall system behaviour, but will be coupled with line conditions, and thus should be addressed only once a line model has been validated. Excluding fan dynamics simplifies the boundary conditions.
- A model and simulation for the primary lines will validate the methodology and provide a starting point from which to expand. Additional system elements can be incorporated in future development.

1.6 Contribution

This research has identified a model and developed a simulation for predicting multiphase flow in a single line of the primary conveying system. The developed simulation and methodology employed thereto provide a foundation for future work; including expansion to the entire conveying network. The ability to predict flow conditions in the conveying system will facilitate the implementation of active control strategies within the existing technology and improve the performance of air seeding equipment.

Active control strategies, implemented with the aid of this work, would provide several improvements over existing technology. It would allow for prediction and avoidance of blockages, lowering system downtime and improving the uniformity of seed application. Optimization of conveying conditions through active control and better system design would allow seed

and granular product to be conveyed at lower speeds than are typical of current practice. Lower conveying speeds translates to better seed placement, lower fan speed, lower power requirements and less seed damage. Less seed damage and improved placement increase germination rates, maximizing food production and reducing input costs for farmers. Reducing fan power saves energy and reduces fossil fuel consumption, making food production more energy efficient and more sustainable.

1.7 Organization

Including the introductory matter, this thesis document contains five chapters, followed by references and appendices. Chapters are organized as follows:

Chapter 1 provides context and direction for the present work. It describes the current industry climate, the motivation for this project, defines the problem to be addressed, identifies the objectives, and sets the scope for this research.

Chapter 2 offers background information and introduces important technical topics critical to the understanding of the later material. It contains a survey of relevant literature and provides the basis and justification for the methodology employed herein.

Chapter 3 describes the mathematical model and simulation which are the subject of this report. The modeling equations are presented and simplified using assumptions and the numerical methods used for solving the equations are outlined.

Chapter 4 is comprised of an evaluation of the model's accuracy and simulation performance. Results of model validation using experimental data are reported and discussed. Performance of the simulation computer program with respect to computing time is investigated and its implications for control application discussed.

Chapter 5 summarizes the completed work and concludes the key research findings. Limitations of the model and recommendations for future work are stated.

References and appendices follow the main report body.

Chapter 2

Background

A technical problem cannot be properly understood without context and adequate foundational knowledge. It is the purpose of this chapter to provide these. Relevant background information concerning the air seeder system, control applications, and multiphase flow are offered. Subsequently, a review of existing modeling methodologies applicable to pneumatic conveying flow is conducted. The potential methods are evaluated, and a suitable candidate selected for continued development; as per the first project objective.

2.1 The Air Seeder System

The motivation for the present work is the improvement of the air seeding technology used in agricultural crop production. It is therefore helpful to have a basic understanding of the modern air seeder and it's conveying system to provide proper context. The air seeder system (figure 2.1) is comprised of two primary components, the *air cart* (A) and the *air drill* (B), both of which are towed and powered by a *tractor* unit (C). The air cart is the centre storage and distribution hub of the air seeder, storing one or more granular products – typically seed, fertilizer, or nutrients – in multiple internal compartments. Air carts provide significantly greater storage capacity than more conventional seeding equipment; capacities of ~1000 bu. (27 tons, wheat) and larger are available from most major manufacturers. Air carts also provide the fan (air supply) and the metering components of the pneumatic conveying system. The fan speed (air flow rate) and metering rates (particle flow rate) are the two means by which the conveying system is controlled on existing equipment and are an integral part of the operation of air seeders.

The second portion of the air seeder is the air drill which is the ground engaging imple-

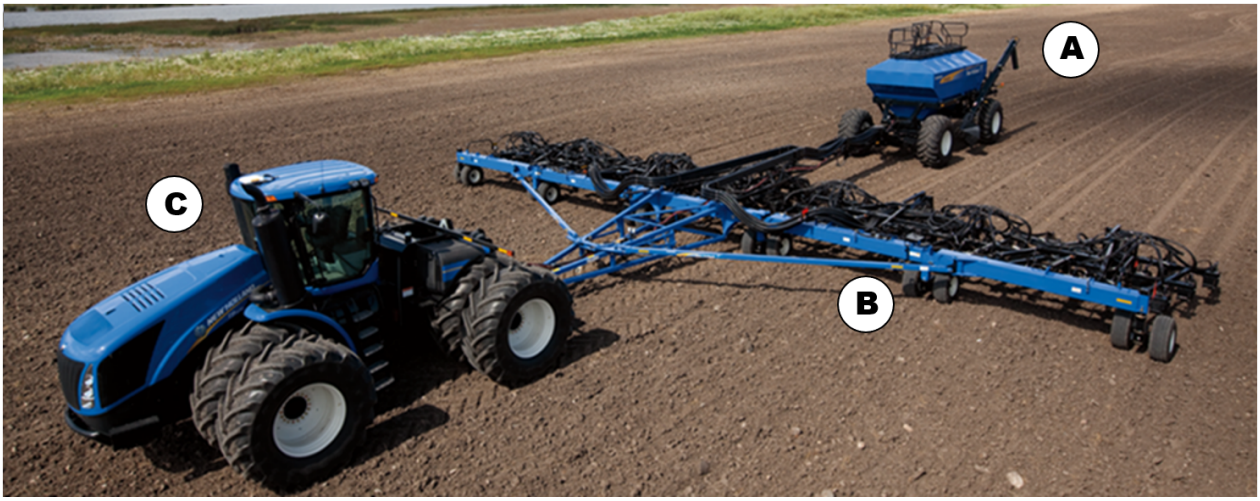

Figure 2.1: Typical air seeding equipment, comprised of the air cart (A), air drill (B) and tractor unit (C). Image credit: www.newholland.com (Accessed April 2016)

ment. The air drill has several functions, including soil tillage, preparation of the seedbed and placement of seed, fertilizers and other nutrients into the soil. The air drill is comprised of three main elements: the *primary frame* (the large horizontal beam seen in blue in figure 2.1), multiple *row units* (figure 2.2), and a network of pipes and tubing which form part of the conveying system and supply each row unit. Row units are the functional element responsible for tillage and seed placement. Each contains a form of tillage tool (a hoe drill is shown here although other types are available) that scours the soil opening the furrow in which seed is deposited. Air drills are commonly available from most major manufacturers at working widths (on larger models) in the 20-30 m range. Air drills are highly configurable

Figure 2.2: A typical air seeder row unit. Image credit: www.caseih.com. (Accessed February 2018)

for differing row spacing, seeding depths, shoot configurations, etc., and can accommodate many crop types. The versatility and large working widths of air drills make them highly productive, particularly in areas with large scale farming operations.

Together, elements of both the air cart and the air drill make up the *pneumatic conveying system*; a critical component of the air seeder and the focus of the present research. The air seeder conveying system is responsible for moving granular products – seed, fertilizers and nutrients – from the air cart's central storage and distributing it to the numerous openers (i.e. row units) across the width of the air drill. The pneumatic conveying system is formed from several functional elements[1]. Referring to figure 2.3, these are: (1) pressurized product tank, (2) hydraulic fan and plenum which generates the air flow supply for each primary conveying line, (3) metering system and induction manifold where product is introduced into each primary conveying line, (4) the routed primary conveying lines which convey product out to a section of the drill, (5) a secondary distribution header where the primary line terminates, splitting into multiple secondary lines, and (6) the secondary conveying lines which branch out from the secondary distribution header and convey product down to each individual opener within a section of the drill. These elements function together to create the product distribution system employed on modern air seeders.

During operation, granular products are metered from the air cart's tanks into each *primary conveying line*. Flow rates in individual lines can be controlled independently on many of the latest designs (e.g. variable rate and sectional control). The primary conveying lines – of which there are typically between 8 and 12 supplied by a single fan – span the width of the drill and will have different lengths and geometries. The primary lines are a combination of metal piping and heavy plastic hose, with a diameter in the range of 50-75 mm. Each primary line terminates at a *distribution header* where the air and product flow is split between as many as a dozen *secondary conveying lines*.

The configuration of the air seeder conveying system gives rise to two important characteristics which distinguish it from other examples of pneumatic conveying. The air seeder conveying system can be described as both "parallel" and "distributed". The designation of

[1]Note, there are several types of air seeder distribution systems. The most common Type-B configuration is described herein.

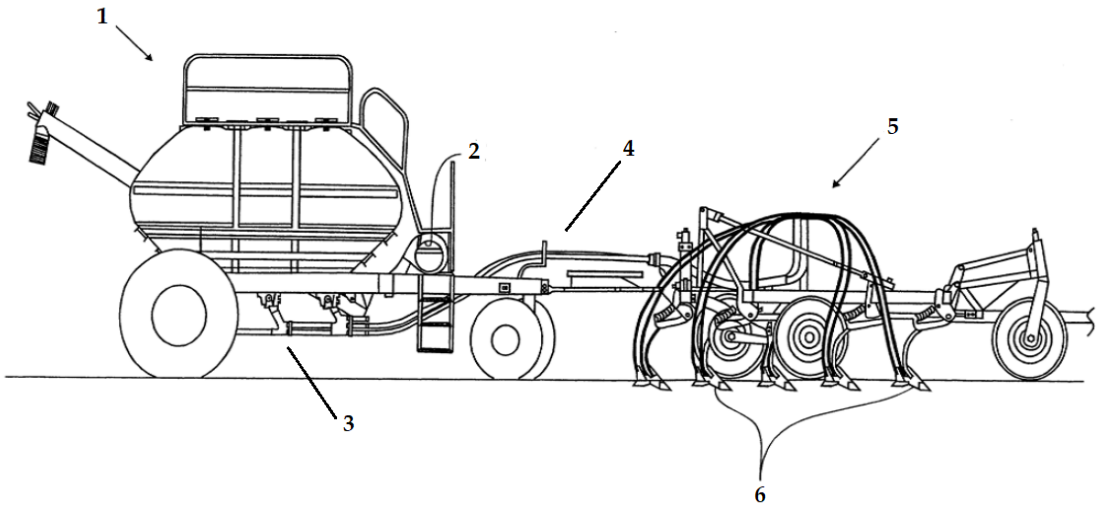

Figure 2.3: The basic components of an air seeder. Adapted from: Patent US6296425B1. (Accessed February 2018)

"parallel" makes note of the fact that there are multiple similar conveying lines running side by side. The conveying lines are all fed by the same single air supply (i.e. fan) and all eventually terminate open to atmosphere. Pointedly, reliance on a single air supply means that the primary conveying lines are tightly coupled; each one able to significantly affect the conditions in others. The designation "distributed" refers to the geometric aspects of the conveying network. The conveying lines have many termination points located across the drill, with significant variation in geometry between individual primary and secondary lines. For example, lines routed to the outside of the drill are longer and possess more bends than inner lines (figure 2.1). Furthermore, air and product flow rates in each line are dynamic and can vary between lines. This means that while conveying lines are similar and run in parallel, they do have significant differences which must be accounted for. These attributes (parallel and distributed) are not common among example applications of pneumatic conveying and introduce additional complexity that must be considered and addressed when working with air seeder conveying systems.

2.2 Improved Performance Through Control of the Conveying System

The addition of active control measures is a potential way to improve the performance of large distributed pneumatic conveying systems. The current control regime for air seeder conveying systems is an example of an *open-loop* control system, meaning that control of the system is based only on the input or command signal. Excluding blockage sensors – which are only capable of detecting a problem that has already occurred – air and granular product flow in the conveying lines are not typically monitored. Without measurement of the output, open-loop control is not able to compensate for *disturbances* in the system (Ellis, 2004). In the present case, changes to product rate in one or more conveying lines would be an example of a disturbance. This lack of capability to deal with the unexpected has led to the current practice of operating with excessive conveying velocities as a means of ensuring that unstable flows and blockages are avoided. Introducing improved control capability to the conveying system could produce significantly better performance. Blockages and unsteady flow could be avoided even while lowering conveying speeds, reducing product attrition, and improving the efficiency of the system.

Design of an improved control structure to realize improved performance is beyond the scope of the current work. Yet, it is easy to identify areas of the current system where control could be integrated to advantage. The most obvious starting place is the air supply, i.e. the fan. The air cart fan is driven by a hydraulic motor to produce air flow. Typical fans exhibit nonlinear relationships between fan speed, airflow, back-pressure, and power requirements. System efficiency could be improved simply by lowering the fan speed to achieve lower conveying velocities. The danger of doing so is that it leaves conveying lines vulnerable to airflow disturbances caused by changes in back-pressure, which the existing open-loop system is not able to compensate for. To safely run lower conveying speeds, the system would need to be capable of responding quickly to changes in back-pressure so that air flow is relatively constant. This is especially important when there are frequent and drastic changes in back-pressure, such as might be generated by the changing product rates

in sectional control and/or variable rate application. A second avenue would be to manipulate individual conveying lines directly. Resistance to air flow in the primary conveying lines can vary significantly due to variations in length, geometry and product rates. The significance of this is that a conveying line with lower resistance will draw more air flow from the common supply, potentially starving other lines and changing the overall system back-pressure. A means of manipulating line resistance, perhaps with a special valve or variable orifice, would allow for the conveying lines to be balanced to compensate for differences. This would give a higher degree of control than using the fan alone and could be used to mitigate fluctuations in air flow and back-pressure for each conveying line and the system as a whole.

While it is relatively easy to identify areas that control could be implemented to advantage, implementation is a far less trivial matter. Without going into extensive detail, there are several control strategies that could potentially be employed. The most obvious of these is the prototypical *feedback control* (figure 2.4a), covered in any introductory control systems course or textbook. Feedback control requires measurement of the output variable, which is then fed back through the controller. This *closed-loop* system produces far better dynamic and steady-state performance along with the ability to compensate for disturbances ($D(s)$). The only real disadvantage versus open-loop control is additional complexity and the cost associated with measuring the output variable. A second strategy is to supplement the traditional feedback control loop with knowledge of the system to improve performance. This is done by the addition of a *feed-forward* control loop, as can be seen in figure 2.4 b). In feed-forward control, the command signal (setpoint) is processed outside and ahead of the main control loop, allowing a best-guess of the ideal controller signal to be routed ahead of the feedback controller. The feed-forward controller produces much of the initial excitation to the system, thereby unburdening the main control loop of this responsibility. With an accurate estimation of the plant's behaviour (F_{est}), the feed-forward loop can significantly improve overall control performance and has the added benefits of low sensitivity to controller gains and low impact on system stability (Ellis, 2004). Also shown in figure 2.4b is the concept of *disturbance decoupling*, which is a similar concept to the feed-forward control but applied specifically to compensate for the disturbance, $D(s)$. Analogous to feed-forward, the success of the disturbance control loop relies on the ability to accurately predict the response

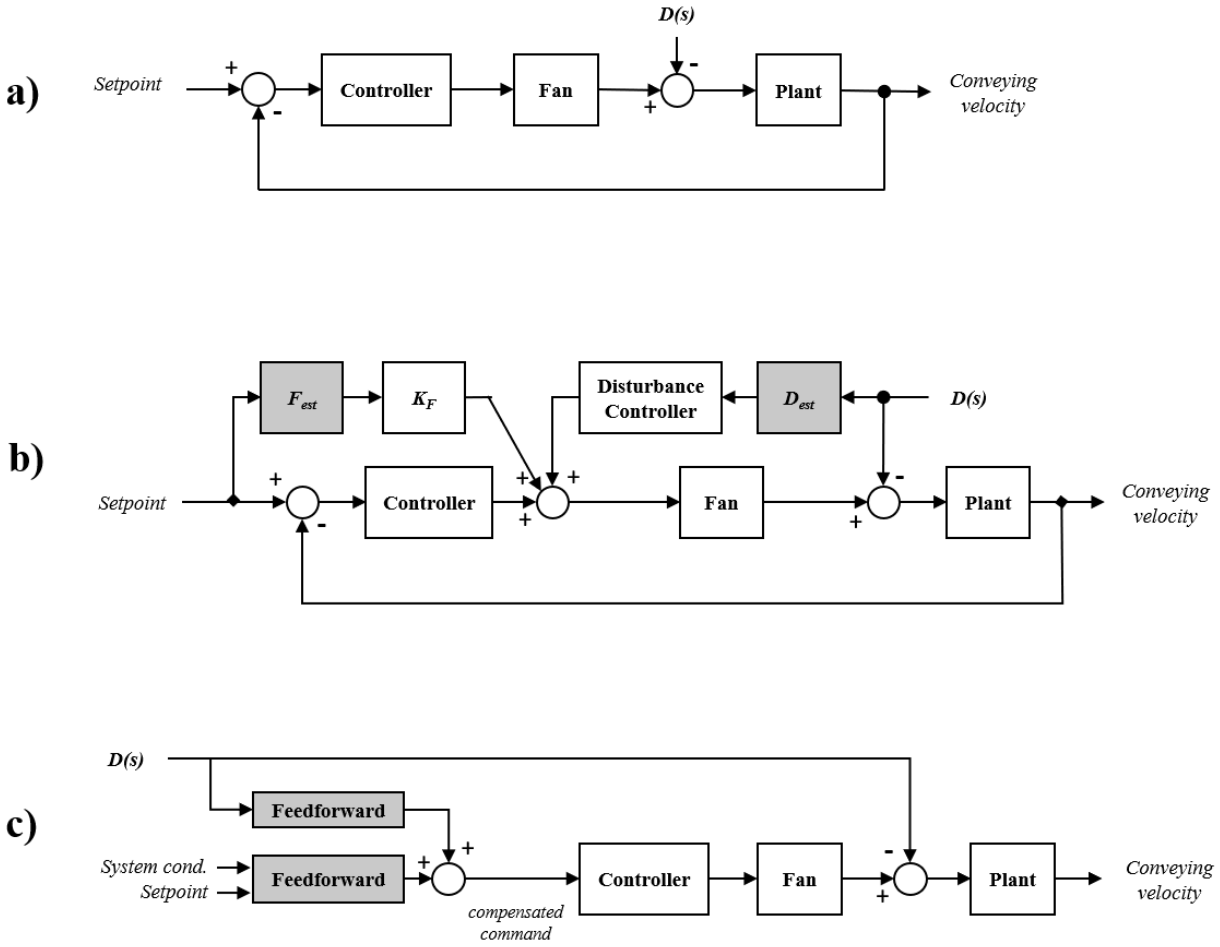

Figure 2.4: Potential control system configurations for improving conveying system performance and their relation to flow prediction. The configurations include: a) feedback control, b) feedback with feed-forward compensation and c) stand-alone feed-forward control which estimates a command based on the setpoint and system conditions. Elements which rely on flow prediction are shaded grey.

of the plant to disturbances (D_{est}) and thus requires prior knowledge of the system to be implemented. A third strategy is to remove measurement of the output variable (i.e. feedback) and instead rely entirely on feed-forward control. Essentially, this is a more informed version of the existing open-loop control. The effectiveness of feed-forward only control alone relies on the ability to accurately estimate or predict how the system will respond to different conditions, commands and disturbances. If these factors are known - and their effect can be accurately predicted using prior knowledge of the system – then the command signal can be appropriately corrected to compensate for the expected effects. Although less robust, it eliminates the additional cost of measuring the output variable.

The generalized strategies presented are by no means exhaustive but give a brief overview of the potential approaches for control of the parallel and distributed conveying system. Of those mentioned, it is hypothesized that some utilization of feed-forward control (alternatively *model predictive control* or MPC) is the most likely to be successful for the given application. Although feedback control is the most common option, it has several disadvantages. First, it requires measurement of the controlled variables - i.e. flow in the conveying lines – which can be expensive due to the large number of conveying lines. Second, the conveying system is a complex, nonlinear, *multiple-input-multiple-output* (MIMO) system for which a standard feedback control design with high performance and robust stability may be difficult to achieve. In contrast, feed-forward offers some advantages, such as flexibility as stand-alone or augmenting feedback, lower sensitivity to instability, lower instrumentation and measurement cost, and more capable of handling nonlinearity and MIMO. The primary disadvantage is that feed-forward control requires a priori knowledge of the system and how it will respond to commands and/or disturbances. In practice, the system knowledge for feed-forward control – shown greyed out in figure 2.4 b and c – is acquired either by measurement or estimation using a mathematical model of the system. Again, due to the size of the system, estimation is a more attractive alternative to measurement as a means of providing the requisite information for feed-forward control.

Developing an appropriate means of predicting operating conditions and the response of the system to commands and disturbances is the motivation for the present research. As mentioned, this is usually achieved by employing a mathematical model representing the

system. To be practical for control, the method of estimation must operate in near real-time, making speed and computational efficiency of particular importance. Furthermore, it must be capable of predicting unsteady or transient conditions in addition to steady-state operation. Transient response – how a system transitions from one stable condition to another – is almost always of importance in control application for practical reasons of performance and stability. Thus, investigation and eventually selection of a method to predict flow conditions in the conveying system will be influenced strongly by the requirements of its application to control.

2.3 Multiphase Flow

The term *multiphase flow* describes any flow process where two or more constituents are present simultaneously (i.e. a mixture), and these constituents are either of a different phase (i.e. gas, liquid, solid) or of the same phase but with significantly different physical properties. Multiphase flow is a topic of enormous size and breadth, seen in many different technologies, industries, engineering disciplines, and with research spanning decades. The term multiphase flow can be used to describe: liquid-liquid flow such as oil and water emulsions, liquid-gas flow where boiling or cavitation is present, liquid-solid flows like chemical mixtures or suspended solids in waste water, and gas-solid flows like conveying of particles. When the term pneumatic conveying is used, it refers to a gas-solid multiphase flow where the conveying gas is usually air and the flow is bounded by a conduit, often a pipe. Examples of pneumatic conveying include the transport of pulverized coal for gasification, clean transport of pharmaceutical powders, and distribution of grain and fertilizer on air seeders. All multiphase flows have elements in common, such as terminology, engineering approaches and, to some extent, behaviour. Yet, there are also substantial differences. Most of the discussion herein will be focused on gas-particle (also fluid-particle) flows as it relates to pneumatic conveying, and particularly on conditions relevant to air seeding. The purpose of this section is to introduce some of the important concepts and terminology associated with multiphase flow, with special attention to pneumatic conveying.

Categorization is an important initial step in the study of multiphase flow, because of

the great potential for variation and diverse behaviour. Multiphase flows are commonly classified by their *mode* (alternatively *flow regime*) as being an example of either a *separated* or a *dispersed* flow. In separated flow, the constituent phases are all continuous mediums, separated by an unbroken surface and in constant contact. Conversely, in a dispersed flow at least one of the phases is comprised of discrete, unconnected elements. Fluid-particle flow is an example of the latter. Further classification of fluid-particle flow is possible based on the behaviour of the dispersed phase (i.e. particles). *Dilute* flow occurs when particle motion is influenced predominantly by interaction with the carrier fluid, for example through viscous drag. *Dense* flow occurs when particle collisions with the wall and other particles is the dominant factor influencing particle motion (Crowe, 2006). Pneumatic conveying systems are typically designed to operate in either dilute or dense modes but rarely both[2]. The distinction is an important one, as differences in behaviour between dense and dilute flow are significant and greatly influence design and modeling decisions.

Although classification as dilute or dense phase flow is meant to differentiate between the prominence of different internal flow mechanisms, concentration of the dispersed phase is often used as a qualifier for reasons of practical convenience. Klinzing et al. (2010) give the division between dilute and dense phase flow at a mass flow ratio of 15, where *mass flow ratio* is the ratio between the mass of the conveyed solids and the carrier fluid. This definition puts the conveying conditions found on air seeders well within the dilute flow classification. The foundational definition based on mechanisms of particle motion is more difficult to evaluate.

Still closer observation reveals the presence of distinctive and recognizable patterns in multiphase flows, particularly when bounded by a pipe or channel. Several common *flow patterns* for fluid-particle case are shown in figure 2.5. Certain flow patterns are associated with either dense or dilute phase flow, while others may be observed during transitions between the two. Furthermore, multiple flow patterns can manifest within the same conveying mode, change with conveying velocity and solids loading ratio, and are heavily influenced by properties of the particulate phase (Klinzing et al., 2010). Flow patterns may be stable or unstable; the latter type often an indication that eventual plugging will occur. In the case of dilute pneumatic conveying employed in air seeding, uniform homogeneous flow (figure 2.5)

[2]In pneumatic conveying applications, dilute and dense are alternatively termed the conveying mode.

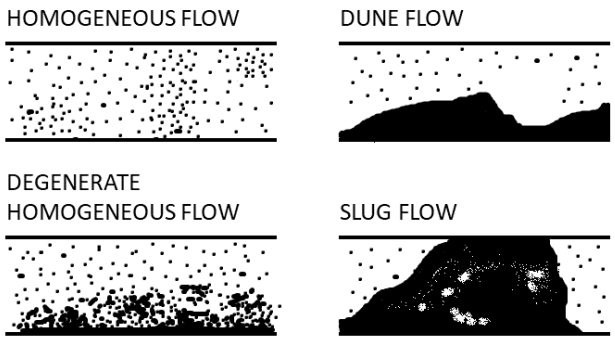

Figure 2.5: Flow patterns in horizontal gas-solid multiphase pipe flow, showing degeneration as the flow becomes more dense. Adapted from Wen (1959).

is ideal and deviation there from is considered undesirable.

Mass loading ratio is an important quantity in the description of multiphase flows involving particle transport. It is defined as the ratio between mass flow rate of the solid phase to that of the carrier fluid, such that

$$z = \frac{\dot{m}_s}{\dot{m}_f}. \tag{2.1}$$

Similarly, *volume fraction* is common terminology and used extensively in mathematical descriptions of multiphase flow. Analogous to concentration, volume faction is the proportion of total volume occupied by the respective phase:

$$\varepsilon_i = \frac{V_i}{V}, \tag{2.2}$$

where the subscript i is substituted with f and s for the fluid volume fraction and solids volume fraction, respectively. The fluid volume fraction can also be referred to as the *void ratio* or simply as *voidage*.

Particle characteristics such as density, size, and shape significantly affect flow behaviour. Particle response time (τ_p) and Stokes number (Stk), both functions of particle size and

density, are commonly used to describe the interaction between the continuous and dispersed phases. In general, small and light particles (low τ_p and Stk) are very responsive to the fluid phase. Their motion will consequently have a similar trajectory to that of the fluid. In contrast, large and heavy particle (high τ_p and Stk) are comparatively unresponsive to the fluid phase. Their motion will be more independent of the fluid, instead dominated by collisions with the wall and other particles. Furthermore, the relation between particles and fluid turbulence, including attenuation and amplification effects, is highly dependent upon particle size (Gore and Crowe, 1989; Mando et al., 2009). Particle shape modifies the drag relationship between fluid and particles, making the mathematically convenient spherical approximation erroneous. Particles encountered in pneumatic conveying of agricultural products are comparatively large, have high response times and Stokes number, and are often non-spherical.

In any multiphase flow there is interaction between the constituent phases, the details of which determine the nature of the flow. Mass, momentum and energy are transferred between the phases whilst being conserved in the overall system. Mass is transferred through such processes as absorption, evaporation, and chemical reactions. Momentum exchange (in the case of fluid-particle flow) occurs predominantly through drag forces acting on the particles, but can also include more complex mechanisms such as "virtual" or "added" mass, Magnus, Saffman, and Basset forces. Energy exchange most commonly takes the form of heat transfer and affects phase changes and reactions.

Interactions also occur within the dispersed phase. Particle-particle collisions occur more frequently as the concentration of the dispersed phase increases. In the case of large particles and/or dense flows, these collisions can dictate motion of the dispersed phase. Electrostatic forces, particle rotation, deformation, turbulent dispersion, and particle-turbulence modulation can also be of importance in certain situations.

The relative significance and direction of phase interactions is expressed as the degree of coupling. *One-way coupling* describes the case where the continuous phase influences the dispersed phase but the reverse is not significant. When the effect of the dispersed phase on the continuous phase is also of importance, the term *two-way coupling* is used. Finally, *four-way coupling* indicates that interactions within the dispersed phase (e.g. particle-particle colli-

sions) also play a significant role in determining the overall flow behaviour. This terminology is especially prevalent in literature regarding the modeling of multiphase flows.

For further reading on multiphase flows refer to the sources for the present section, namely: Crowe (2006); Klinzing et al. (2010); Gidaspow (1994) and Brennen (2005).

2.4 Modeling of Multiphase Flows

There are numerous examples of modeling pneumatic conveying flow in the literature, and even more for general multiphase flow. Models provide a mathematical description of the flow or property of interest and can be developed using a variety of theoretical and empirical principles. Modeling types or families based on a common methodology are identified and summarized, providing the basis of an informed decision as to which method is most suitable for the application herein.

Modeling methods can be broadly classified as either experimental or theoretical. Experimental models rely predominantly on experimental data to develop equations for predicting similar conditions. These include empirical and semi-empirical models. Theoretical models, in contrast, use fundamental principles to derive equations which describe the phenomenon of interest. Theoretical models can be further divided into correlations, computational models and analytical models. Correlations and computational models will be discussed in the subsequent subsections. Analytical models, which represent exact solutions to differential equations are quite prevalent in fluid mechanics. However, due to the high degree of nonlinearity in multiphase flows, analytical models are not common in this context and have been omitted from the following discussion.

2.4.1 Empirical Models

Empirical equations represent one methodology that has been applied to modeling multiphase flows, including specific examples of pneumatic conveying systems. These types of models are always derived in some part through experimentation, using collected data to estimate equations and parameters which predict the observed results. Examples of empirical models found in the literature can be further categorized based on differences in the exact

methodology used. Fully empirical models, which rely on little or no theoretical basis and therefore entirely on experimental data, include the work of Gasterstadt (1924), Cabrejos and Klinzing (1992) and Binsirawanich (2011). Semi-empirical models have a greater reliance on theory in addition to experimental study. The form of semi-empirical modeling equations is hypothesized from theoretical knowledge and then "fit" to measured data by empirical estimation of model parameters and coefficients. Semi-empirical methods were employed in developing models for the acceleration region on air seeder conveying lines (Hossain, 2015), and to bends in pneumatic conveying lines (Mason et al., 1998). A third method, analogous to system identification methods used in control system design, empirically estimates a time domain transfer function model for the conveying system using measured system input and output data (Sæther et al., 2009; Satpati et al., 2014; Wu et al., 2017). A special case are those works involving the use of artificial neural networks (ANN) (Barbosa and Seleghim, 2003; Salahshoor et al., 2013) to model flow conditions, as discussed in section §1.3. Dynamic neural networks (a special type of ANN where network output are functions of not only the current input but also previous inputs, outputs and network states) can be trained using experimental data to develop computationally efficient predictive models for dynamic systems. While these later methods have some advantages and potential, primarily due to efficient computation and development, they are less common in literature pertaining to multiphase flow and pneumatic conveying.

Empirical models are ideal for certain applications but poorly suited for highly variable systems and control application. Strengths of empirical models include ease of understanding and application, computational efficiency and high accuracy in predicting particular flow conditions. However, the range of conditions in which they can be accurately applied is usually limited, making empirical models inflexible, and often new equations must be developed for each new condition encountered. Furthermore, empirical equations often provide limited insight regarding the physics and structure of the flow, a restriction not shared by models employing more theoretical direction to their development.

2.4.2 Correlations

Correlations are another technique frequently applied to pneumatic conveying systems when pressure drop along the conveying line is the primary interest. Using correlations, the pressure drop is presented as a sum of contributing factors from both the fluid and particulate phases. Henthorn et al. (2005) give six contributions to pressure drop: fluid acceleration, fluid weight, fluid-wall friction, particle acceleration, particle weight, and particle-wall friction. This analysis seems to be common and is simply an application of the conservation principle to bulk axial momentum. Source terms are derived from basic fluid mechanics principles where possible, while more complex components - such as solids-wall friction loss - are determined empirically. Konno and Saito (1967) developed an empirical relation for particle-wall friction analogous to that of single-phase flow and were able to predict pressure loss for a straight vertical pipe with reasonable accuracy. Indeed, their correlation was found to give more accurate pressure drop prediction than modern numerical methods, if only for simple cases (Henthorn et al., 2005).

Like empirical models, correlations are mathematically modest, easily understood and computationally inexpensive. Correlations are easier to scale and provide greater physical insight than empirical relations. The drawback of correlations comes from simplification of the flow as it limits the information which they can provide. Correlations generally only provide a prediction of pressure loss. Additionally, they are normally developed under the assumption of steady-state conditions, preventing analysis of dynamic systems and transients.

2.4.3 Computational Models

The most advanced types of modeling involve the formulation and solution of differential equations. These equations, based on principles of conservation of mass, momentum, and energy, have long been applied to the study of fluid mechanics and the study of multiphase flows. Pneumatic conveying being an application of multiphase flow can, therefore, be modeled in this way and has been quite extensively. Such models form the basis of all modern computational fluid dynamics (CFD) programs, both commercial and academic, and offer some significant advantages over the model types already discussed. However, significantly

different methodologies have been developed for formulating the differential equations which govern multiphase flows. In all methodologies, the fluid phase is modeled using the well established Navier-Stokes equations. Where they differ is the mathematical framework used to describe the particulate phase. Multiphase flow models can, therefore, be classified into types or families based on the methods used to describe the particle phase, each with their own advantages and disadvantages.

2.4.3.1 Eulerian-Eulerian Framework

The Eulerian-Eulerian class of multiphase flow models, as the name would suggest, used a Eulerian mathematical framework to describe the dispersed phase (Anderson and Jackson, 1967; van Wachem and Almstedt, 2003; Brennen, 2005; Crowe, 2006). The defining feature of Eulerian models, therefore, is that both phases – the continuous fluid phase and dispersed (i.e. particle) phase – are approximated as interpenetrating continua. This approximation ignores the discrete nature of the particles, electing instead to treat the collective assembly of particles as a second fluid (the solids phase). Indeed, the Eulerian-Eulerian model is commonly referred to as the two-fluid model. The result is two sets of very similar partial differential modeling equations, one set for the fluid phase and the other for the particulate phase. These partial differential equations represent effective conservation of mass, momentum and energy for each phase. The equations must also contain terms accounting for the interaction between the phases resulting from the exchange of mass, momentum and energy and thereby coupling the two equations sets; requiring that they be solved simultaneously in many cases. For model closure, the Eulerian-Eulerian framework requires auxiliary equations and constitutive relations to account for phase interactions as well as the fluid-like terms that appear in the momentum balance equation, such as solids stresses and pressure. These auxiliary equations often have an empirical basis (Henthorn et al., 2005) as direct calculation can be difficult when the discrete nature of the particles is overlooked. The kinetic theory for granular flows is often employed in the derivation of closure equations for use in the Eulerian-Eulerian model.

The Eulerian-Eulerian framework has both advantages and disadvantage compared to other modeling techniques. Like the other computational models, it makes use of partial differential equations derived from theoretical principles to describe multiphase flow. This

gives it three distinct advantages versus the methods already described earlier in section §2.4, namely: generally applicable to a wide range of flows and conditions, a greater number of flow properties predicted and the ability to predict unsteady, transient conditions. Similarity between governing equations for the fluid and particle phases allows for a more convenient numerical solution procedure. Lower computational cost relative to other modeling methodologies is an additional benefit of the Eulerian-Eulerian framework, making it the recipient of much early attention in the field when limits on computational power made other methods impractical for many applications (van Wachem and Almstedt, 2003; Crowe, 2006). Disadvantages of the Eulerian framework include: limits on its applicability to certain flows due to assumptions inherent to the averaging used to approximate the discrete dispersed flow using continuous equations (Brennen, 2005; Anderson and Jackson, 1967), inability to capture some complex phenomena associated with the dispersed phase (Pirker et al., 2010), heavy reliance on constitutive relations and susceptibility to their accuracy limitations (van Wachem and Almstedt, 2003), and difficulty in accurately specifying some boundary conditions (Brennen, 2005).

2.4.3.2 Eulerian-Lagrangian Framework

In the Eulerian-Lagrangian family of computational models, the fluid phase is again modeled in the continuous Eulerian domain. The dispersed phase, however, is modeled as discrete entities in a Lagrangian reference frame (van Wachem and Almstedt, 2003; Brennen, 2005; Crowe, 2006; Laín and Sommerfeld, 2012). In the Lagrangian framework, the motion of individual particles – or in some cases clusters of particles – through the domain are calculated and tracked. Consequently, the Eulerian-Lagrangian method is also commonly referred to in the literature as the discrete or trajectory model. The Lagrangian formulation involves the application of Newton's second law of motion to a particle to produce a set of equations, in the form of ordinary differential equations, describing the motion of the particle. Both translational and rotational motion can be included as appropriate. The particle motion equations account for external forces such as gravity, the influence of the fluid on the particle, and particle collisions with the wall and other particles. Fluid-particle interaction can be determined by two methods, either through empirical/theoretical equations yielding a resultant point

force (e.g. drag on a sphere) or by fully resolving the pressure and viscous forces across the particle's surface. The modeling equations for the continuous fluid are again partial differential equations representing conservation of mass, momentum, and energy. When relevant, the effect of particles on the fluid motion must be accounted for in the fluid governing equations. Typically, this is accomplished by tracking the number of discrete particles located within a particular computational cell in the Eulerian domain and employing similar closure equations as used in the Eulerian-Eulerian method. Particle-particle and particle-wall collisions can be tracked and calculated directly in the Lagrangian framework using various collision models.

The Eulerian-Lagrangian framework is based on differential governing equations and enjoys the same advantages as the Eulerian-Eulerian approach (section §2.4.3.1) with respect to empirical models and correlations, including application to unsteady flows. Preservation of the discrete nature of the dispersed phase allows collisions and interactions to be calculated directly, without the strict reliance on empirical closure and the averaging procedures needed for the continua approximation. Furthermore, the discrete treatment of particles allows for certain complex phenomenon to be captured (such as rope formation) more accurately than in two-fluid models (Brennen, 2005; Pirker et al., 2010; Laín and Sommerfeld, 2012). The Lagrangian formulation is capable of producing very detailed and accurate results, particularly when few simplifications are made, and fluid-particle interactions are fully resolved; such simulations are often termed direct numerical simulation (DNS). The cost of detail and accuracy, however, is complexity and computational cost. The need to incorporate two different calculation domains (Eulerian and Lagrangian) increases the complexity of the numerical implementation (Crowe, 2006). The computational effort of tracking large numbers of particles is large and can limit the practicality of the Lagrangian models for certain applications, such as large system (van Wachem and Almstedt, 2003; Henthorn et al., 2005). It should be noted, however, that computational intensity can vary significantly and is highly dependent upon the characteristics of the flow being modeled, such as particle size and concentrations (Crowe, 2006).

2.4.3.3 Kinetic Theory for Granular Flows

The kinetic theory for granular flows is formulated along similar means to its predecessor which was originally developed to describe the behaviour of gases. In this methodology, an analogy is made between the motion and behaviour of suspended particles and the chaotic motion of gas molecules. Using analysis and correlations adapted from the kinetic theory of gases, the particulate phase is described using parameters such as granular temperature, granular pressure and viscosity. The importance of these constitutive relations for closure of the Eulerian-Eulerian model has already been stated; and indeed, the kinetic theory approach is formulated within a fixed Eulerian reference frame and so might be considered to belong to section §2.4.3.1. In point of fact, kinetic theory can be used to alternatively derive the same governing equations used in the Eulerian-Eulerian models (i.e. Navier-Stokes equations) as is shown by Gidaspow (1994). However, there are examples in the literature which are best described as a separate type of kinetic theory model rather than a subset of the Eulerian-Eulerian methodology. These models rely on the kinetic theory approach for more than just model closure and can be distinguished by their use of additional transport equations for the kinetic properties (e.g. granular temperature). Notable examples in the literature include Gidaspow (1994) who provides a comprehensive presentation of the kinetic theory approach and Eskin et al. (2007) who apply it to the simulation of pneumatic conveying.

The kinetic theory for granular flow benefits from a well established and rigorous mathematical derivation. It is of immense importance in the closure of other modeling methods, and in that regard has been well studied. Kinetic theory also boasts the ability to describe important phenomenon present in granular mixtures – when more than one type or size of particle is present – such as granular diffusion and particle-particle drag (Gidaspow, 1994). However, except for Eulerian model closure, full modeling based on the kinetic theory for granular flow is not nearly as prevalent in the literature as the previously introduced Eulerian and Lagrangian methodologies. This makes it difficult to assess its advantages and disadvantages with respect to other model types. It is also perhaps somewhat less intuitive than other methodologies partially due to the rigorous mathematical and statistical treatment required in its derivation.

2.4.3.4 Hybrid Models

The fourth type of computational model addressed herein is hybrid methods (Andrews and O'Rourke, 1996; Pirker et al., 2010; Schellander et al., 2013). Hybrid models combine the standard Eulerian-Eulerian and Eulerian-Lagrangian approaches to circumvent some of their inherent limitations when used individually. Most hybrid methods seek to provide the computational efficiency of using the Eulerian-Eulerian framework while enhancing its capabilities with information gained from the discrete treatment of particles available in the Lagrangian framework. This is achieved by calculating particle behaviour simultaneously in both the Eulerian and Lagrangian domains and employing translation or "mapping" techniques to couple (i.e. move information between) the two calculation domains. For example, the location and velocity of particles – or commonly clusters of particles – can be calculated in the Lagrangian domain and then imported to the Eulerian domain for coupling with the fluid equations. This allows for greater particulate phase detail and accuracy than achievable with the Eulerian-Eulerian model with particle torque, rotation, lift forces, rough wall collisions and improved particle drag estimates becoming accessible. These can be especially important in predicting microscopic flow details and behaviour associated with the particles (Pirker et al., 2010). Additionally, the availability of both the Eulerian and Lagrangian domains allows for simulations to selectively use the more efficient method as volume fraction changes; calculation effort of the former being independent of volume fraction and the later being highly dependent (Schellander et al., 2013).

Hybrid models have many of the advantages of both the Eulerian-Eulerian and Eulerian-Lagrangian models while mitigating their respective disadvantages. Hybrid methods are practically applicable to both dense and dilute flow regimes (Andrews and O'Rourke, 1996; Schellander et al., 2013). They can model flows with multiple particle types and sizes and are better able to capture particle movement and complex phenomenon – particularly separated flow - than standard two-fluid models. Hybrid models generally have lower computation and memory requirements compared to full Lagrangian methods and enhanced detail and accuracy versus two-fluid models (Schellander et al., 2013). The disadvantage of hybrid models is in the increased complexity of the model and numerical solvers required to implement the

required coupling between the Eulerian and Lagrangian domains.

2.5 Model Selection

The conveying system found on modern air seeders is large, distributed and contains parallel conveying lines with relatively complex geometry. Multiphase flow within the conveying system is dilute and contains large particles, however, flow conditions can vary significantly during operation and for different use cases. For application to control, information must be delivered in near real-time with reasonable accuracy for both steady-state and transient conditions. The information that will actually be useful is probably limited to a relatively small number of bulk flow quantities, since microscopic details of the flow are unlikely to influence control decisions. Consideration of these factors forms the basis for the selection of a suitable model.

From these considerations, several criteria were identified and used to evaluate the different modeling methodologies. In order of importance, these were:

1. Computational efficiency (i.e. computing speed)

2. Simulation of transient conditions

3. Accuracy

4. Generality (i.e. wide applicability)

Computational speed and the ability to simulate transient conditions are of paramount importance. Simulation data even with extraordinary accuracy is not useful if it cannot be delivered quickly enough to be used for control decisions. Accuracy, therefore, is of secondary importance to speed. The simulated data does not need to predict the real conditions perfectly and certainly, every microscopic detail of the flow is not required. Rather, predictions of "suitable accuracy" to allow control decisions to be made with reasonable certainty is satisfactory. Finally, the generality of the model is an obvious advantage: reducing the need for further development in expanding it to the rest of the conveying system and increasing

Table 2.1: Qualitative comparison of different modeling approaches

Criteria	Empirical	Correlation	EE	EL	Kinetic	Hybrid
Real-time operation						
Computational efficiency	++	++	+	−−	+	~
Simplification potential	~	~	+	−	+	−
Transient conditions	N	N	Y	Y	Y	Y
Accuracy	++	++	~	++	~	+
Applicability for dilute flow	+	+	−	+	~	+
Generality	−−	−	++	~	++	+

Symbols: Yes (Y), No (N), Very Good (++), Good (+), Marginal/not applicable (~), Poor (-), Very Poor (--)
Abbreviations: EE – Eulerian-Eulerian, EL – Eulerian-Lagrangian, Kinetic – Kinetic Theory Granular Flows

applicability as conveying and operating conditions vary. A brief qualitative assessment of the different modeling techniques according to the above criteria is given in table 2.1.

The most appropriate modeling methodology was selected based on the comparison shown in table 2.1, information available in the literature, and inference from the form of the different modeling equations. Firstly, the majority of empirical and correlation methodologies (section §2.4.1 and section §2.4.2) can be excluded for the reason that they cannot predict transient conditions. The exception to this is the system identification and ANN techniques which are capable of modeling transient conditions. However, due to a smaller volume of literature and the advantages of theoretical models (physical insight, robustness, generality and scalability), these methods were rejected for the current study; although future investigation may be warranted. Thus, aspiring towards a theoretical basis capable of modeling transient conditions eliminates all but the differential equation based models presented in section §2.4.3, namely the Eulerian-Eulerian, Eulerian-Lagrangian, kinetic theory and hybrid methods. Secondly, the Eulerian and kinetic theory models are expected to be both more computationally efficient and appropriate for simplification (e.g. to a 1-D representation) than either of the Lagrangian or hybrid methods. The latter two both rely on discrete tracking of particles and collisions, suggesting that simplification to lower dimensions would significantly impact their accuracy. Furthermore, the computational intensity is less constant and increases with particle loading, which is non-deterministic, and therefore undesirable for control system integration. Although they provide advantages in accuracy, the critical importance of computational speed means that the methods involving Lagrangian treatment

of the discrete phase are less likely to meet the specific application requirements and can be eliminated. The remaining candidates thereafter are the Eulerian-Eulerian and kinetic theory methods. The final two methods are quite comparable with respect to the evaluation criteria, which might be anticipated based on their similar forms. However, the Eulerian-Eulerian model is slightly simpler, arguably more intuitive and also much more prevalent in the literature. Therefore, the Eulerian-Eulerian or two-fluid modeling methodology was selected as the most appropriate method and the most likely to successfully meet the requirements of the current research.

The goal of this project was to develop a Eulerian-Eulerian mathematical model and to simplify the model where possible to improve computational efficiency while keeping it as general as possible. Thus, it was hypothesized that a simplified model of the conveying flow, based on the Eulerian-Eulerian framework, could be developed that is computationally efficient enough to be useful for control application, while still providing suitable prediction accuracy. Testing this hypothesis - through development and validation of the model and simulation - is the focus of the subsequent chapters.

2.6 Summary

In this chapter, relevant background information and an investigation of modeling methods were presented. A description of air seeding equipment and its basic function was offered. The proposition that active control infrastructure could be used to improve the performance of the air seeder conveying system was put forward. Several generalized control schemes were introduced and the relation between system control and prediction of multiphase flow conditions was established. A brief overview of important multiphase flow topics and terminology was communicated. Additionally, a review of the literature regarding potential modeling methodologies was conducted. To conclude, the available modeling methodologies were evaluated with respect to the intended application and the most appropriate candidate was selected.

Chapter 3

Model and Simulation Development

The process of modeling and simulation for any physical system generally involves the same basic progression. This includes defining the problem and relevant concepts, development of a mathematical description of the system, selection of appropriate numerical methods, implementation of the numerical procedure and solving the equations, and finally, processing and interpretation of the results. In fulfillment of objective #2, the purpose of this chapter is to define a mathematical model and numerical procedure which are the basis for simulation.

3.1 Mathematical Model

The previous chapter concluded with the statement that the Eulerian-Eulerian framework was the most suitable basis for developing the mathematical model. It uses a stationary reference frame for deriving the governing equations of both the fluid and particles. Both phases are treated as interpenetrating continua, and so the analysis and derived equations of both phases are similar. The general derivation of the governing equations (G.E.'s) for a continuous medium (i.e. a fluid) is conducted by applying conservation laws for mass, momentum, and energy over a fixed control volume. For a complete description, this results in a set of three partial differential governing equations, of which one is a vector with three components. The process of deriving the conservation equations, particularly for fluid-only flows, can be found in most textbooks on fluid mechanics and/or computational fluid dynamics (example, see Wendt, 2009). For multiphase flows when following the Eulerian-Eulerian framework, the conservation laws are applied separately for each phase. Although the presence of the dispersed phase complicates the derivation, the result is similar in form to fluid-only flow

but with twice the number of governing equations. In addition to the partial differential G.E.'s, auxiliary equations are usually required to replace approximate values for unknown terms and provide closure for the mathematical model. Once properly closed, the modeling equations can be solved numerically.

3.1.1 Assumptions and Simplifications

A complete, three-dimensional mathematical description of fluid-particle flow requires a large set of equations. A minimum of six coupled partial differential governing equations are required, some of which are also nonlinear. If additional phenomena are included - for example, fluid turbulence - then additional transport equations are required to fully close the model. With the aid of modern computers and numerical methods, it is possible to solve this large system of complex equations. This is the function of commercial CFD programs. However, these simulations require significant computational resources, and even on high-performance hardware can take hours or days to compute. To reduce computational effort and simulation time, the modeling equations must be simplified. To this effect, the assumptions and simplifications employed herein were:

A1. Temperature variation within the system is negligible and therefore the system is considered isothermal

A2. The fluid phase (air) is assumed to be incompressible and of constant density

A3. A simplistic one-dimensional representation of the flow is suitable to capture the properties and behaviour of interest for the given application, with the implications that

   a. Flow properties are constant in directions y and z except at the pipe wall

   b. Velocity components in the y and z directions are zero everywhere

   c. Viscous shear stresses will be approximated as pipe wall friction

Justification for the first assumption (A1) was drawn from the observation that for normal operating conditions, the air seeder conveying system does not experience significant

internal temperature variation. First, the entire system is subject to the same environmental conditions. Second, pressure changes expected within the system are not capable of causing a significant change in temperature. Third, there is no need to account for changes in state with gas-solid flows. Temperature variation within the conveying system was therefore assumed to be negligible, eliminating the need to solve the energy equation.

Similarly, the fluid phase was assumed to be incompressible (A2) due to relatively low pressure and temperature variations within the conveying system. The anticipated pressure difference produces variations in air density of less than 5% when calculated using the ideal gas law. Furthermore, the low *Mach number* condition ($Ma < 0.3$) for incompressible flow is observed in the present case, with expected air velocities yielding Mach numbers of $Ma \approx 0.1$ and below (White, 2011). Both assumptions A1 and A2 were equally valid for the laboratory apparatus used for experimental data collection.

The third and most important assumption made was that a *one-dimensional* representation of the flow is acceptable (A3). Simplification to a one-dimensional model implies that flow properties are constant in all but the axial direction, and non-axial velocities are everywhere zero. Flow properties such as axial velocity and particle concentration were therefore averaged across the pipe cross-section. This simplified the governing equations substantially, requiring only the continuity and a single component of the momentum equation for the axial direction. The assumption of one-dimensional flow does prevent modeling of much of the internal structure of the flow. However, the smaller set of modeling equations reduced the computational effort required for the simulation. Because simulation speed was of primary importance, simplification to one-dimension was a necessary compromise. Recalling that for the control application, only bulk flow quantities were of interest gave further argument in favour of the simplified model. Determining if the one-dimensional assumption is justified and can provide suitable prediction accuracy was one of the objectives of this work. Assumptions A1-A3, having been discussed, were used to simplify the general two-fluid governing equations for fluid-particle flow.

3.1.2 Governing Equations

The seminal work of Anderson and Jackson (1967) is frequently cited in the literature as one of the first and most formal derivations of the Eulerian-Eulerian modeling equations for fluid-particle flows. In their work, they conduct rigorous mathematical averaging to develop locally-averaged properties and equations for fluid and particles. This is done for continuity, the fluid Navier-Stokes equations and the equation of motion for a single particle. The result of this analysis is a set of equations representing conservation of mass (i.e. continuity) and locally averaged momentum for gas-particle flow in an Eulerian reference frame. Assumptions A1 (isothermal) and A2 (incompressible) were likewise included in the original analysis and so are already reflected in their model. For reference, the three-dimensional governing equations of Anderson and Jackson (1967) follow, represented in tensor notation with the summation convention implied.

The three-dimensional continuity (conservation of mass) equations for the fluid phase and the solids phase are, respectively

$$\rho_f \frac{\partial \varepsilon_f}{\partial t} + \rho_f \frac{\partial}{\partial x_k} (\varepsilon_f u_k) = 0 \tag{3.1}$$

and

$$\rho_s \frac{\partial \varepsilon_s}{\partial t} + \rho_s \frac{\partial}{\partial x_k} (\varepsilon_s v_k) = 0 \tag{3.2}$$

where ρ_f and ρ_s are densities of the fluid and solids phase in kg/m^3, ε_f and ε_s represent the volume fractions of fluid and solids and are unitless, u_k and v_k are velocity vectors for the fluid and solids phases respectively in m/s, t is time in seconds and x_k represents three-dimensional Cartesian space. Note that inclusion of the density terms is not strictly necessary.

The conservation of momentum equations (i.e. the Navier-Stokes equations[1]) for the fluid phase and the solids phase are, respectively

[1]For further discussion on the momentum equations and their alternative form see Appendix B.

$$\rho_f \varepsilon_f \left[\frac{\partial u_i}{\partial t} + u_k \frac{\partial u_i}{\partial x_k} \right] = \varepsilon_f \frac{\partial \sigma_{ik}}{\partial x_k} + \varepsilon_f \rho_f \mathrm{g}_i - M_i \tag{3.3}$$

and

$$\rho_s \varepsilon_s \left[\frac{\partial \upsilon_i}{\partial t} + \upsilon_k \frac{\partial \upsilon_i}{\partial x_k} \right] = \varepsilon_s \frac{\partial \sigma_{ik}}{\partial x_k} + \varepsilon_s \rho_s \mathrm{g}_i + \frac{\partial \sigma^s_{ik}}{\partial x_k} + M_i \tag{3.4}$$

where σ and σ^s represent the fluid and solids stress tensors respectively, g is acceleration due to gravity in $\mathrm{m/s^2}$, and M represents momentum transfer between the phases due to particle-fluid interaction in $\mathrm{N/m^3}$ ($\mathrm{Pa/m}$ or $\mathrm{kg{\cdot}m/m^3{\cdot}s^2}$). All terms in equations (3.3) and (3.4) represent change in volumetric momentum with respect to time and have units of $\mathrm{N/m^3}$, $\mathrm{Pa/m}$ or $\mathrm{kg{\cdot}m/m^3{\cdot}s^2}$. In both of the momentum equations, the first terms on the right-hand side contain the fluid stress tensor, which for a Newtonian fluid has the form

$$\sigma_{ik} = -p\delta_{ik} + \lambda \frac{\partial u_m}{\partial x_m} \delta_{ik} + \mu \left[\frac{\partial u_i}{\partial x_k} + \frac{\partial u_k}{\partial x_i} - \frac{2}{3} \delta_{ik} \frac{\partial u_m}{\partial x_m} \right] \tag{3.5}$$

where p is the static pressure of the fluid in Pa, λ is bulk viscosity and μ is the dynamic viscosity of the fluid both with units of Pa·s. For the solids phase, the stress tensor for the locally average properties is assumed to have the same form as a Newtonian fluid (Anderson and Jackson, 1967) and therefore is given as

$$\sigma^s_{ik} = -p^s\delta_{ik} + \lambda^s \frac{\partial \upsilon_m}{\partial x_m} \delta_{ik} + \mu^s \left[\frac{\partial \upsilon_i}{\partial x_k} + \frac{\partial \upsilon_k}{\partial x_i} - \frac{2}{3} \delta_{ik} \frac{\partial \upsilon_m}{\partial x_m} \right] \tag{3.6}$$

where velocity, pressure and viscosities have been substituted for those of the solids phase, for which constitutive relations will be required. Note, that the isothermal assumption removes the need for the third balance equation for conservation of energy. The two-fluid equations (3.1) to (3.6) provide a foundation, to which the third and final assumption was applied.

The final assumption (A3) was that a one-dimensional representation of the flow will provide suitable accuracy. A one-dimensional representation for the pipe bounded flow implies, as presented in section §3.1.1, that: flow properties are averaged over the pipe cross-section, velocities other than in the axial direction are zero, and that there will need to be some approximation of viscous stresses (since the Newtonian correlation with velocity gradients is not possible). These observations allow for the modeling equations to be simplified substantially. With the ascribed assumptions and simplifications, the governing equations for the fluid phase continuity and momentum balance respectively were

$$\rho_f \frac{\partial \varepsilon_f}{\partial t} + \rho_f \frac{\partial}{\partial x}\left(\varepsilon_f u\right) = 0 \tag{3.7}$$

$$\rho_f \varepsilon_f \left[\frac{\partial u}{\partial t} + u\frac{\partial u}{\partial x}\right] = -\varepsilon_f \frac{\partial p}{\partial x} + \varepsilon_f \frac{\partial}{\partial x}\left(\frac{4}{3}\mu \frac{\partial u}{\partial x}\right) + S^f \tag{3.8}$$

where Cartesian subscripts have been dropped for convenience because there is only a single dimension. The stress tensor, equation (3.5), was reduced and substituted directly into the momentum balance producing the first and second terms on the right hand side of equation (3.8); representing contributions from pressure and viscous diffusion in the axial direction, parallel to the flow. The remaining viscous stress terms have either been eliminated or are accounted for in the fluid momentum source term, equation (3.9), as wall friction. The bulk viscosity component of the fluid stress tensor has been removed because it is negligible for incompressible flow (Gidaspow, 1994, p.202). Additionally, all external forces such as gravity, fluid-wall friction, and fluid-particle interaction have been combined into the source term such that

$$S^f = S^f_{gravity} + S^f_{friction} - M \tag{3.9}$$

which produces a form better suited to discretization (seen in the following sections). The equations for the solids phase were treated in the same manner, and after simplification to

one-dimension become

$$\rho_s \frac{\partial \varepsilon_s}{\partial t} + \rho_s \frac{\partial}{\partial x}\left(\varepsilon_s \upsilon\right) = 0 \tag{3.10}$$

$$\rho_s \varepsilon_s \left[\frac{\partial \upsilon}{\partial t} + \upsilon \frac{\partial \upsilon}{\partial x}\right] = \varepsilon_s \left[-\frac{\partial p}{\partial x} + \frac{4}{3}\mu \frac{\partial^2 u}{\partial x^2}\right] - \frac{\partial p_s}{\partial x} + \frac{\partial}{\partial x}\left[\left(2\mu_s + \lambda_s\right)\frac{\partial \upsilon}{\partial x}\right] + S^s \tag{3.11}$$

$$S^s = S^s_{gravity} + S^s_{friction} + M \tag{3.12}$$

where again the external forces in the momentum equation have been grouped into a source term for convenience. Note that the interphase momentum exchange (M) was given the opposite sign in the solids source term, reinforcing that momentum is transferred between the phases and not lost or gained. Taken together, equations (3.7), (3.8), (3.10) and (3.11) represent the one-dimensional governing equations for pipe bounded gas-particle flow that were the basis for simulation.

3.1.3 Auxiliary Equations

Along with the four governing equations, multiple auxiliary equations were required for closure of the mathematical model of the flow. They provided several proportionality constants and critically the source terms which were present in the momentum equations for both phases. As a consequence of simplification to a one-dimensional model, momentum loss due to viscous friction with the pipe wall must be approximated and introduced as a source term. Fluid wall friction was therefore calculated using the Darcy-Weisbach equation (found in any fluid mechanics textbook, for example White 2011)

$$S^f_{friction} = \frac{dp}{dx} = f\frac{\rho_f u^2}{2d} \tag{3.13}$$

where d is the pipe inner diameter and f is the Darcy friction factor. For computational efficiency, the Haaland equation (as reviewed by Genić et al., 2011) was used as an explicit approximation of the friction factor in place of the more common and implicit Colebrook equation. The approximation of Haaland is given as

$$f = \left\{ -1.8 \log \left[\left(\frac{\epsilon}{3.7} \right)^{1.11} + \frac{6.9}{Re} \right] \right\}^{-2} \tag{3.14}$$

where ϵ is the relative pipe roughness and Re is the pipe Reynolds number.

Gravitational effect on the momentum of the fluid appear in the source term (3.9) and is calculated as

$$S^f_{gravity} = \varepsilon_f \rho_f \mathrm{g} \cos\theta \tag{3.15}$$

where θ is the angle between the pipe axis and the direction of gravitational acceleration. The equivalent expression for the solids is obtained simply by substituting volume fraction and density for their respective values for the solids phase.

Momentum exchange between fluid and particles appears in the momentum equations for both phases and is the primary source of coupling between fluid and solids. Momentum exchange occurs through both form drag and viscous drag imparted by the fluid on the suspended particles (van Wachem and Almstedt, 2003). The fluid-particle interaction is very complex in reality and includes phenomenon such as turbulent dispersion, particle rotation, Saffman lift force, virtual mass, etc. In very sophisticated models, the fluid-particle interaction may be calculated by resolving the flow field around individual particles. However, for the present simplified model, it must be accounted for using empirical correlations for a bulk or volume averaged drag force between fluid and particles. The drag force model presented by Gidaspow (1994) was used herein, and is based off the work of several earlier authors. It is given as

$$M = \beta\,(u - v) \tag{3.16}$$

$$\beta = \frac{3}{4} C_D \frac{\varepsilon_f \varepsilon_s \rho_f |u - v|}{d_p} \varepsilon_f^{-2.65}; \qquad \varepsilon > 0.8 \tag{3.17}$$

$$C_D = \frac{24}{Re_s}\left(1 + 0.15\,(Re_s)^{0.687}\right); \qquad Re_s < 1000 \tag{3.18}$$

$$C_D = 0.44; \qquad Re_s \geq 1000 \tag{3.19}$$

$$Re_s = \frac{\varepsilon_f \rho_f\,(u - v)\,d_p}{\mu} \tag{3.20}$$

where β is the friction coefficient, C_D is the drag coefficient, d_p is the diameter of a single particle, and Re_s is a modified Reynolds number. Note, that the above drag model is not able to account for the more advanced aspects of fluid-particle interaction listed above. Volume fraction provides a second source of coupling between the two phases. For a continuous mixture of two constituents, any space which is not occupied by the first must be occupied by the second since no part of the volume may be vacant. Therefore, the volume fractions for the solids and fluid phases are related simply as

$$\varepsilon_s = (1 - \varepsilon_f) \tag{3.21}$$

The solids momentum equation (3.11 and 3.12) contains contributions from several source terms. Two of these - momentum contribution from gravity ($S^s_{gravity}$) and inter-phase momentum transfer (M) - have already been addressed. The final external source component is friction losses due to particle collisions with the pipe wall. In fluid-particle flow, entrained particles experience random motion which causes them to collide periodically with the pipe wall. For elastic materials, each collision results in a reduction in particle momentum which

must be replaced from the mean flow. The approach of Eskin et al. (2007) was used for approximating the frictional losses for the solids phase. Therein, the frequency of particle-wall collisions is estimated from kinetic theory for granular flows and per-collision momentum loss is related to a restitution coefficient. Conjointly, they are used to estimate the shear stress for the solids phase caused by particle collisions with the wall (τ^s_{wall}), given as

$$\tau^s_{wall} = (e_{wall} - 1)\,\varepsilon_s \rho_s \upsilon \frac{\Theta^{1/2}}{\sqrt{2\pi}} \tag{3.22}$$

where e_{wall} is the coefficient of restitution for particle-wall collisions, and Θ is the granular temperature of the solids phase from kinetic theory. For pipe bounded flow, axial momentum loss due to wall collisions is a function of the wall shear stress, such that

$$S^s_{friction} = \frac{4\tau^s_{wall}}{d} \tag{3.23}$$

In the solids phase governing equations, there are several unfamiliar solid's properties (viscosity and pressure) which appear in the momentum equation. While they are analogous to their familiar fluid counterparts, their values are neither clear nor constant. They must be calculated using constitutive relations which relate them to know flow properties. These properties are: solids dynamic viscosity μ_s, solids bulk viscosity λ_s, and solids pressure p_s; and are calculated using the following expressions (Ansys, Inc., 2017; Sarrami Foroushani and Nasr Esfahany, 2015)

$$\mu_{s,col} = \frac{4}{5}\varepsilon_s^2 \rho_s d_p g_0 \,(1 + e_{ss}) \left(\frac{\Theta}{\pi}\right)^{1/2} \tag{3.24}$$

$$\lambda_s = \frac{4}{3}\varepsilon_s^2 \rho_s d_p g_0 \,(1 + e_{ss}) \left(\frac{\Theta}{\pi}\right)^{1/2} = \frac{5}{3}\mu_{s,col} \tag{3.25}$$

$$p_s = \varepsilon_s \rho_s \Theta \left(1 + 2\varepsilon_s g_0 \left(1 + e_{ss}\right)\right) \tag{3.26}$$

where g_0 is a radial distribution function and e_{ss} is the coefficient of restitution for particle-particle collisions.

The radial distribution function is a correction factor which accounts for changes in the frequency of particle collisions as the number of particles in a given volume increases and decreases. For monodisperse flows, g_0 is a function of volume fraction and can be calculated using the relation proposed by Ding and Gidaspow (reported by Gidaspow, 1994) as

$$g_0 = \left[1 - \left(\frac{\varepsilon_s}{\varepsilon_{s,max}}\right)^{1/3}\right]^{-1} \tag{3.27}$$

where $\varepsilon_{s,max}$ is the maximum packing density of the particles. The granular temperature which appears in equations (3.22), and (3.24) to (3.26) can be calculated by different methods. In more sophisticated simulations, it is often treated as a unique flow property and modeled with its own transport equation complete with production and dissipation terms. In the current work a simpler approximation was used (that of Jenkins and Savage, as presented by Gidaspow, 1994). Simplified for one-dimension, the granular temperature is simply a function of the mean particle velocity, such that

$$\Theta = \frac{1}{3}\left\langle v^2 \right\rangle . \tag{3.28}$$

3.1.4 Comments on the Modeling Equations

In the interest of transparency and completeness, there are several points concerning the governing equations that should be noted.

The first is in regards to the primary assumption made by Anderson and Jackson (1967) in the derivation of the two-fluid equations. The averaging procedure which they employed was based on the premise that the area over which properties are averaged is "large compared with the particle spacing and small compared with the scale of macroscopic variations from point to point in the system". Alternatively, "when particle spacing becomes comparable with the dimensions of the containing system" the validity of the averaging procedure becomes suspect. In the present case, which concerns dilute pneumatic conveying of large particles, this assumption is very likely a poor one. As such, there is some question as to the validity of the two-fluid model for the present case. However, the Eulerian-Eulerian model was previously identified as the most promising based on demands of the intended application (see section §2.5). Thus, despite questions of validity for the present case it was employed, with accepted limitations, as the best available alternative.

The second point relates to the viscous diffusion terms in the momentum equations. In highly convective flows the viscous component of momentum transfer (i.e. diffusion) is usually much smaller than the more dominant convection component. It is common in many applications to ignore viscous diffusion; reducing the momentum equations to their *inviscid from* (known as the *Euler Equations*). The current case is an example of a convection dominant flow, and thus the inviscid assumption is applicable. However, viscous diffusion (in the axial direction) was retained for two reasons. These being that: a) the one-dimensional equations are not greatly simplified by elimination of the viscous term, and b) diffusion is a naturally *dissipative* force, being proportional to an even derivative, and thus can provide added stability in numerical solutions (Wendt, 2009, p.204). The impact of diffusion on stability in the present case was admittedly unquantified, however, there was little advantage (and possibly disadvantage) in its removal.

3.2 Numerical Methodology

To achieve tangible results (i.e. simulated data), the modeling equations must be solved to obtain solutions to the problems of interest. However, obtaining an exact solution to equations of this form is difficult if it is possible at all. Solving the equations must, therefore, rely upon numerical methods implemented on computers. With the modeling equations defined, an appropriate method for obtaining an approximate numerical solution must be implemented. In the case of computational fluids, the numerical method typically consists of four elements: dividing the physical domain into discrete computational points, discretization of the governing equations into their algebraic analogs, the solution of systems of algebraic equations, and a specialized routine for ensuring convergence of the coupled sets of equations. These aspects are presented in the following subsections.

3.2.1 Discretization of the Governing Equations

For numerical solution, the continuous physical domain must be divided up to create the *discrete* computational domain on which the approximate solution to the differential equations is calculated. This process is referred to as *meshing* and produces a mesh or grid of discrete points. The discrete computational domain serves as the base from which the equations are *discretized*. There are numerous meshing strategies available with varying degrees of complexity. Some advanced meshes can provide advantages in accuracy and computational efficiency for certain problems, geometries, and coordinate systems at the cost of additional complexity. The simple geometry and one-dimensional model used herein allowed for an equally simple mesh to be employed. Figure 3.1 shows the uniform rectangular mesh and resulting grid used in the current solution. Although the control volumes appear rectangular, in reality, each represents a cylindrical section of the pipe. All control volumes are of a uniform size and so the distance between grid points (Δx) is equal across the domain. The common notation used by several authors (Patankar, 1980; Versteeg and Malalasekera, 1995) is retained herein, where the current control volume is denoted by the subscript P, and adjacent control volumes to the left (west) and right (east) are denoted by subscripts W and E respectively.

To avoid unrealistic solutions such as checker-boarding a *staggered grid* is used, as de-

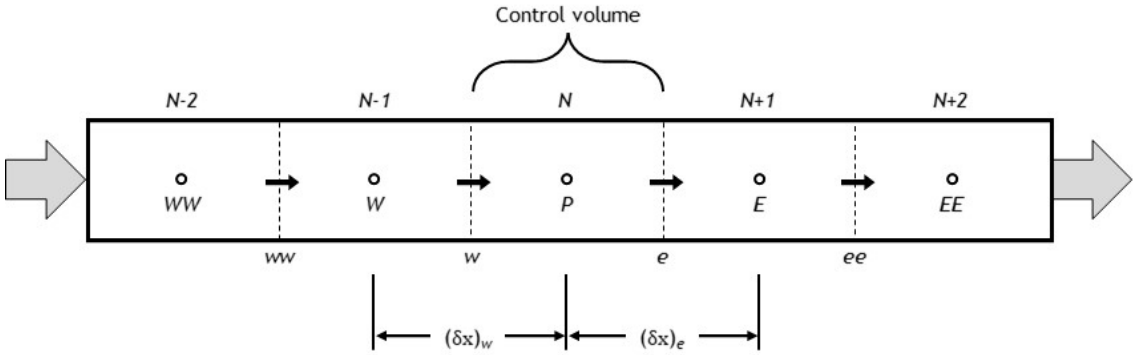

Figure 3.1: The one-dimensional staggered grid used for discretization of the model equations. Scalar and vector quantities are calculated at different locations. Uppercase lettering denotes scalar grid points at control volume centres while lowercase lettering denotes vector grid points at control volume faces.

scribed by Patankar (1980). In the staggered grid arrangement, scalar and vector quantities are stored and calculated at different locations within the computational domain. Scalar quantities such as pressure and volume fraction are stored at control volume centres (denoted by uppercase lettering W, P, E, etc.) while vector quantities such as velocity are stored at control volume faces (denoted by lowercase lettering w, e, ee, etc). In figure 3.1, nodes on the scalar grid are represented as circles while nodes on the vector grid are represented with small black arrows. The distinction is important for proper interpretation of the discrete equations.

Discretization of the modeling equations requires that a choice is made of which discretization methods and schemes are utilized. There are several methods for transforming the continuous partial differential equations into their discrete analogs. The *finite volume method* (FVM) was used in the present case (Wendt, 2009). In the FVM, the differential equations are integrated over a control volume to produce the integral forms of the conservation equations; and it is the integral form of the equations which are discretized. Use of the integral forms guarantees conservation of properties for every control volume (or grid cell) regardless of size. When properly formulated, this ensures that the discrete equations are inherently conservative and that solutions will be realistically bounded regardless of accuracy (Patankar, 1980); an advantage over other methods, particularly for multiphase flow. In addition, an appropriate interpolation scheme for relating properties at control volume faces to

adjacent cell centres is necessary for treatment of the convective terms. The *upwind scheme* was used herein for its simplicity; the value of relevant variables at control volume faces are inherited from the upwind cell, and thus are dependent upon the direction of flow. The upwind scheme assumes the flow to be convection dominant and should be applicable to the current application. Finally, integrals with respect to time appearing in the derivation must be approximated using either an explicit, implicit, or intermediate scheme. Following the procedure of Patankar (1980) in compliance with the SIMPLER algorithm (see section §3.2.2) an implicit scheme was used.

The described method and schemes were used to discretize the governing equations into forms suitable for numerical solution. The resulting discrete algebraic equations - which were solved numerically in simulation - are presented below.

3.2.1.1 Fluid Phase Discrete Equations

The discrete fluid momentum equation, which is *solved* for the dependent variable fluid velocity (u), is:

$$a_e u_e - a_w u_w - a_{ee} u_{ee} - A_e \left(p_P - p_E\right) = b \tag{3.29}$$

where,

$$a_e = a_w + a_{ee} + a_e^0 - \bar{S}_p A_e \Delta x,$$

$$a_w = D_P + \max\left[F_P, 0\right],$$

$$a_{ee} = D_E + \max\left[0, -F_E\right],$$

$$a_e^0 = \left(\varepsilon_f \rho_f\right)_e^0 \frac{A_e \Delta x}{\Delta t},$$

$$b = \bar{S}_c A_e \Delta x + a_e^0 u_e^0,$$

$$F_P = \left(\varepsilon_f \rho_f\right)_P \frac{\left(u_e + u_{ee}\right)}{2},$$

$$D_P = \frac{4}{3} \frac{\mu_P A_P}{\Delta x}.$$

The pseudo-velocity equation, which is used to *calculate* an approximate velocity field is

$$\hat{u}_e = \frac{a_w u_w + a_{ee} u_{ee} + b}{a_e} \tag{3.30}$$

where the coefficients and constant (a_w, a_{ee}, a_e, and b) have the same value as those used in equation equation (3.29).

The discrete pressure equation, which is *solved* for the dependent variable fluid pressure (p), is:

$$a_P p_P - a_W p_W - a_E p_E = b \tag{3.31}$$

where,

$$a_W = \frac{(\varepsilon_f \rho_f)_w A_w^2}{a_{w,central}},$$

$$a_E = \frac{(\varepsilon_f \rho_f)_e A_e^2}{a_{e,central}},$$

$$a_P = a_W + a_E,$$

$$b = \left[(\varepsilon_f \rho_f)_P^0 - (\varepsilon_f \rho_f)_P\right] \frac{A_P \Delta x}{\Delta t} + \left[(\varepsilon_f \rho_f \hat{u})_w - (\varepsilon_f \rho_f \hat{u})_e\right] A_P.$$

The pressure correction equation, which is *solved* for a correction to the initial pressure field is:

$$a_P p_P^{'} - a_W p_W^{'} - a_E p_E^{'} = b \tag{3.32}$$

where a_W, a_E, and a_P are the same as in equation (3.31) and the new mass source is calculated using the intermediate velocity u^* as

$$b = \left[(\varepsilon_f \rho_f)_P^0 - (\varepsilon_f \rho_f)_P\right] \frac{A_P \Delta x}{\Delta t} + \left[(\varepsilon_f \rho_f u^*)_w - (\varepsilon_f \rho_f u^*)_e\right] A_P.$$

The velocity correction equation, used to *calculate* a corrected fluid velocity field after pressure is determined is

$$u_e = u_e^* + \frac{A_e \left(p_P^{'} - p_E^{'}\right)}{a_e} \tag{3.33}$$

where coefficient values are the same as in the momentum equation (3.29).

3.2.1.2 Solids Phase Discrete Equations

The discrete solids momentum equation, which is *solved* for the dependent variable solids velocity (v), is:

$$av_e - a_w v_w - a_{ee} v_{ee} - \varepsilon_e^s A_e \left(p_P - p_E\right) - A_e \left(p_P^s - p_E^s\right) - \varepsilon_P^s D_P (u_w - u_e) + \varepsilon_E^s D_E (u_e - u_{ee}) = b, \tag{3.34}$$

where,

$$a_w = D_P^s + \max\left[F_P^s, 0\right],$$
$$a_{ee} = D_E^s + \max\left[0, -F_E^s\right],$$
$$a_e = a_w + a_{ee} + a_e^0 - \bar{S}_p^s A_e \Delta x,$$
$$b = \bar{S}_c^s A_e \Delta x + a_e^0 v_e^0,$$
$$D_P^s = \frac{\left(2\mu_s + \lambda_s\right)_P A_P}{\Delta x},$$
$$F_P^s = \left(\varepsilon_s \rho_s\right)_P \frac{\left(v_w + v_e\right)}{2}.$$

The discrete solids continuity equation, which is *solved* for the dependent variable solids volume fraction (ε^s), is:

$$a_P \varepsilon_P^s - a_E \varepsilon_E^s - a_W \varepsilon_W^s = b \tag{3.35}$$

where,

$$a_W = \max\left[\upsilon_w A_w, 0\right],$$

$$a_E = \max\left[0, -\upsilon_e A_e\right],$$

$$a_P = a_P^0 + \max\left[\upsilon_e A_e, 0\right] + \max\left[0, -\upsilon_w A_w\right],$$

$$b = \bar{S}_c^s A_P \Delta x + a_P^0 \varepsilon_P^0,$$

$$a_P^0 = \frac{A_P \Delta x}{\Delta t}.$$

3.2.2 Solution of the Discrete Equations using the SIMPLER Algorithm

The discrete algebraic equations developed in the previous section were the basis for numerical solution of the governing equations. Applying the discrete equations to each control volume within the domain produces a set of algebraic equations, which when solved gives an approximate solution for the dependent variables ε, p, u, and υ; a process commonly referred to as *simulation*. The algebraic equations can be written in matrix form and solved using linear algebra techniques (standard or specialized). However, in fluid flow problems, tight coupling between the PDE's (especially pressure and velocity) can make obtaining a solution to the equations difficult. Special techniques are often required to ensure that the numerical solution converges. The solution procedure used in the present case was the Semi-Implicit Method for Pressure-Linked Equations Revised (SIMPLER) developed by Patankar (1980). The SIMPLER algorithm makes use of several intermediate equations to assist in convergence of the fluid velocity and pressure solutions; resulting in the unique discrete fluid equations (3.30 to 3.33). Without special procedures, direct application of the FVM to the momentum and continuity equations produces discrete equations like those of the solids phase (3.34 and 3.35).

The SIMPLER method uses an implicit discretization scheme and so relies on an *iterative* solution. The discrete equations are solved sequentially, and successive iteration improves the accuracy of the solution. Implicit methods are iterative and require more computation

per time step, however, their improved stability over explicit schemes often allows them to be less computational demanding and faster overall (Wendt, 2009). Nonlinearity is handled through the iterative procedure since coefficients for the discrete equations are recalculated on every iteration. Thus, the iterative loop that is the SIMPLER algorithm involves the successive recalculation of coefficients and solution of the discrete linear equations until suitable convergence of the solution is obtained. For transient problems, this procedure is conducted anew for each time step, with the solution of the previous time step acting as a starting point for the next. The sequence of operations for solution of the discrete equations (adapted from Patankar, 1980) is given below:

1. Start with an initial velocity field (from initial conditions or previous time step).
2. Calculate the coefficients for the discrete fluid momentum equations, including linearized source terms using auxiliary equations.
3. Calculate fluid pseudo-velocities ($\hat{u}$) using equation (3.30).
4. Calculate the coefficients for the pressure equation (3.31) using pseudo-velocities and then solve for the pressure field (p^*).
5. Using the above pressure field, solve the fluid momentum equations to obtain u^*.
6. Calculate the new mass source b and solve the pressure correction equation (3.32) to obtain $p^{'}$.
7. Correct the velocity field using equation (3.33).
8. Calculate the coefficients for the discrete solids momentum equations, including linearized source terms using auxiliary equations.
9. Solve the solids momentum equation (3.34)to obtain solids velocity field (υ).
10. Solve the solids continuity equation (3.35) to obtain volume fraction (ε).
11. Return to step 2 and repeat until convergence. Once converged, advance to next time step.

3.3 Implementation

The process of solving the discrete modeling equations using specified numerical methods is referred to as simulation. In the present work, the solution of the equations using the SIMPLER algorithm was implemented in MATLAB® (The Mathworks, Inc., 2015). MATLAB® offers a convenient development environment and a high-level scientific computing language. It is commonly used in both academic research and industry. Following the initial development and validation, the simulation program can be migrated to any suitable programming language or environment. In particular, MATLAB® offers tools for conversion to C and C++ languages; allowing easy implementation on embedded hardware and potential performance acceleration (The Mathworks, Inc., 2015).

3.4 Summary

In this chapter, the mathematical model which is the basis of simulation was determined. Several important assumptions were posed and their implications for simplifying the model discussed. Using an established form of the *Eulerian-Eulerian* (or *two-fluid*) equations for fluid-particle flows, a simplified one-dimensional mathematical representation of the flow was developed. The mathematical description consists of four partial differential governing equations accompanied by multiple auxiliary equations. Discretization of the modeling equations, via the finite volume method and a staggered grid, was conducted and the discrete equations presented. Finally, the solution procedure, using the SIMPLER algorithm and implemented using a computer code developed in MATLAB®, was briefly outlined.

Chapter 4

Evaluation of Accuracy and Performance

To be useful for control application, the model and simulation must predict flow conditions quickly and with suitable accuracy. The purpose of this chapter is to investigate model accuracy and simulation performance, in fulfillment of objectives #3 and #4. It includes a summary of the experimental apparatus and equipment, validation of the model through a comparison of simulated and experimental data, and evaluation of the simulation's performance in the context of the control application.

4.1 Collection of Experimental Data

Validation was conducted through comparison to measured experimental data. The required measured data were collected using existing experimental pneumatic conveying equipment located in the University of Saskatchewan Air Handling Laboratory. The experimental equipment was instrumented with multiple sensors for measurement of both fluid pressure and bulk particle velocity.

4.1.1 Overview of the Experimental Apparatus

The laboratory apparatus used for collection of experimental data consisted of a custom-built pneumatic conveying system. The apparatus was designed to approximate a single conveying line from a modern air seeder. It was equipped with an array of sensors and computer equipment which were used to control, monitor, and record air-particle flow within the conveying line. A simplified schematic of the experimental apparatus is provided in figure 4.1.

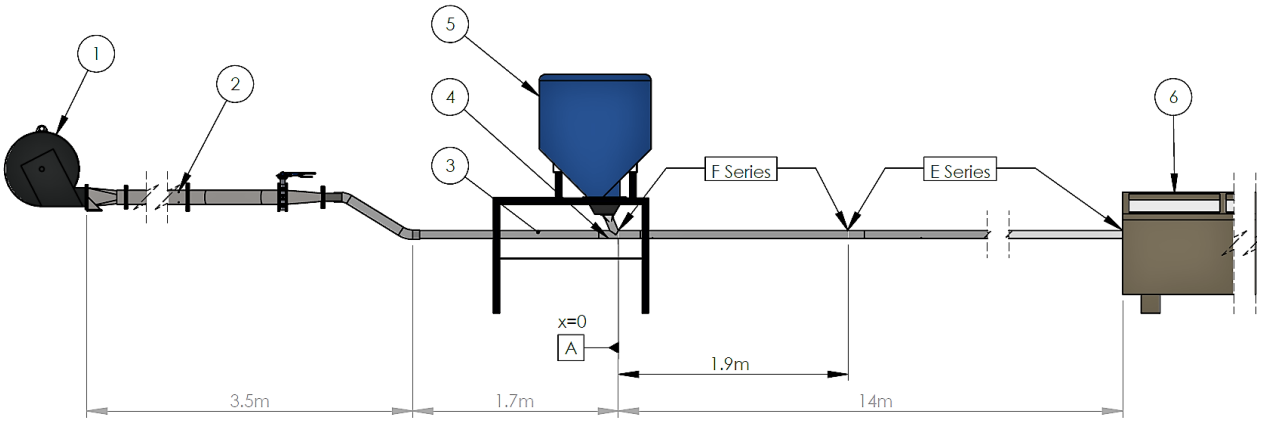

Figure 4.1: Schematic of the pneumatic conveying line laboratory apparatus used for collection of experimental data. Components: 1. Fan (supplies air flow), 2. Venturi air flow meter (used for fan control), 3. Internal flow straightening device, 4. Inclined T-section for particle injection, 5. Pressurized product tank, air lock and metering device, 6. Product collection box. (CAD files courtesy of Keep, T.)

Additional components not shown in the schematic include electric motors which drive both the meter roller and air supply fan, and the computer terminal which controlled operation and data acquisition. The span of both sets of pressure transducers are indicated with the 'F Series' and 'E Series' labels. All sensor location measurements are in reference to the downstream edge of the particle injection T-section marked in the diagram as datum [A], taken to be the location x = 0 m. The total length of the conveying line downstream of the injection point was 14 m. Additional dimensions are provided in the schematic. The conveying line was constructed from multiple sections of clear acrylic pipe with an internal diameter of 0.0574 m. The sections were joined with air tight collars. Care was taken to ensure the line was straight and the impact of joints and other defects on flow minimized.

4.1.2 Instrumentation

The conveying line apparatus was instrumented with multiple sensors for measurement of experimental data. Two sensor types, differential pressure transducers and electrostatic sensors, were used to measure fluid pressure and solids velocity respectively. Both types were installed along the full length of the line, but with greater frequency immediately downstream of the particle injection point. This provided better spatial resolution of measured data in

the acceleration region where higher rates of change were anticipated. Location information for pressure and velocity sensors is provided in the Appendix. Additional instrumentation used for system control is not discussed here. Further information on the data collection instrumentation follows.

To properly resolve transient components of measured data, a sufficiently high sampling rate was required. Experience and prior testing suggested that compared to other dynamic systems, the experimental conveying apparatus was relatively slow; exhibiting reduced excitation to inputs of 1 Hz and faster. Note that this excludes fluid phase dynamics such as shock waves, which would be on the order of 20 Hz for a line of this length, but are not expected in the present case. After modification of the existing data acquisition software (programmed in NI LabVIEW^{TM}) an average sampling rate of 20 Hz was achieved for control and fluid related measurements. This was reasoned sufficient to resolve expected system transients, and was well above the estimated system Nyquist frequency. The sampling rate is not constant and fluctuates around the mean value of 20 Hz, a consequence of the non-deterministic nature of the data acquisition computer software. However, observed fluctuations did not appear to significantly impact the quality of the collected data.

4.1.2.1 Static Pressure Transducers

Differential pressure transducers were installed at regular intervals along the length of the experimental conveying line, providing measurements of static fluid pressure. The sensors were connected via flexible plastic hose to static pressure taps drilled through the top centre of the acrylic conveying line. Pressure transducers were divided into two sets, the F series and the E series. The former was installed over the front 1.9 m of the line in the particle acceleration zone while the later covered the remainder of the conveying line. For the two series, two models of pressure transducer were used:

Series	Make	Model	Range	Accuracy
F Series	Dwyer	648B-4	0-1 inH20 (0-249 Pa)	0.8% FS
E Series	Dwyer	648B-5	0-2.5 inH20 (0-622 Pa)	0.8% FS

The pressure transducers measure the difference in pressure between two adjacent pressure

taps; interpreted as the pressure gradient ($\Delta p/\Delta x$) with units Pa/m. Overall (gauge) pressure was also of interest and had to be calculated in post-processing. To calculate overall pressure, differential pressures were summed sequentially beginning at the furthest downstream pressure tap (considered open to atmosphere). Because of the reliance on downstream pressure measurements, measured gauge pressure had higher uncertainty which increased with the number of pressure measurements which were summed. This is the reason for increasing error bars toward the front of the conveying line in later graphs.

4.1.2.2 Electrostatic Velocity Sensors

Measurement of solids velocity (i.e. bulk or average particle velocity) was made possible through the use of specialized electrostatic sensors developed previously by the air handling research group. A total of 8 velocity sensors were installed along the length of the experimental conveying line. A diagram showing the basic design of the sensor is given in the figure below, followed by a brief summary the operating principles. For further details, see Ouyang (2017); Pastl and Noble (2014).

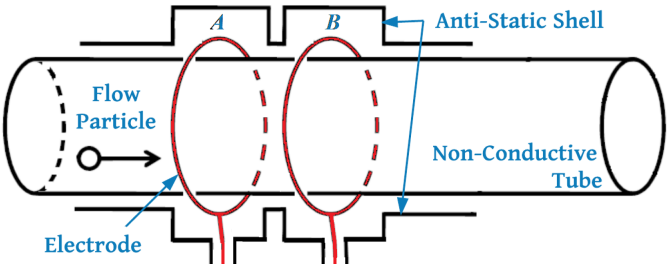

Figure 4.2: Conceptual design of the electrostatic velocity sensor showing the two electrodes, A and B, which detect passing particles. Image credit: Ouyang (2017).

The velocity sensors use electrostatic charge carried by conveyed particles to detect their passing and determine velocity. When a particle possessing electrostatic charge moves through the electrode ring (see figure 4.2), a small current is induced in the electrode wire. The small amount of current generated by the particle's electric field is amplified and converted by embedded electrical circuitry connected to the electrode. After amplification and conversion, this signal is measured as a raw voltage by the data acquisition system. Induced electrostatic current manifests as spikes in the raw signal which correspond to charged par-

ticles passing by the electrode. If two electrodes are placed sufficiently close together that a particle's velocity and trajectory do not change significantly while passing between them, then the signals produced by the two electrodes will have similar profiles. This can be verified by examining actual raw signal data, as shown in figure 4.3.

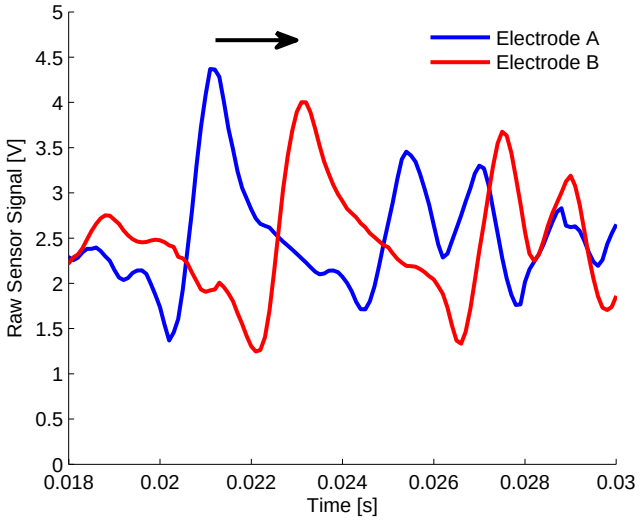

Figure 4.3: Raw signals for the two electrodes of an electrostatic velocity sensor, showing the self-similar profile and lag which is exploited to determine velocity.

Cross-correlation of the two signals gives the relative lag (i.e. time difference) between the signals. Because the distance between the two electrodes is known, the average velocity of particles moving between the electrodes can be calculated (distance between electrodes divided by the time lag between them, thus $v = \frac{\Delta x}{\Delta t}$).

Only raw electrode signals were measured during the experiment, and determination of velocity required additional processing. The raw electrostatic signals were sampled at a relatively high rate of 10 kHz, required to capture high frequency signal component, as particles traverse the small gap between electrodes quickly. In post-processing, the cross-correlation was performed using a windowed approach. This allowed the effective sampling rate of calculated solids velocity to be specified. For data presented in this report solids velocity was sampled at a rate of 20 Hz, consistent with measurements for the fluid phase.

4.1.3 Particles

The experimental apparatus can be configured for different particle types. Typically, this includes agricultural products, such as different fertilizers and seed varieties, which are unique in pneumatic conveying applications for their wide variations in size, shape, density and other material properties. Although wheat seed was tested, all experiments reported herein exclusively used spherical polyethylene pellets as the conveyed particles. The polyethylene pellets had a mean diameter of 3.56 mm and a density of 1420 kg/m^3. Plastic pellets offered a dust free, uniform particle with a simplified geometry that was convenient for experimentation while also being a good approximation of granular fertilizers products commonly used with air seeders. The use of spherical particles removes potential effects (and errors) due to particle shape, which is significant because most of the equations for fluid-particle flow are developed assuming spherical particles. Therefore, validating the model for spherical particles first, before examining other shapes, was a logical beginning. However, because many agricultural products are non-spherical the effects of particle shape on the accuracy of the model should be investigated in the future.

4.1.4 Fan Control & Limitations

The fan which produces the air flow has a substantial impact on operation of the conveying system. Fans have operating characteristics which change based on their design, but generally interrelate three variables: rotational speed, back-pressure and volumetric air flow rate. For many designs, increasing the back-pressure (i.e. pressure difference between the fan's inlet and outlet) will cause a reduction in volume flow rate. This posses a problem when trying to measure the conveying line's dynamic response which requires rapid increase in particle feed rates. The presence of particles creates additional back-pressure in the system, causing a drop in air velocity referred to as a *disturbance*. The simulation currently does not account for fan related dynamics and so cannot replicate this event. Therefore, disturbances to air velocity result in simulation boundary conditions no longer being accurate approximations of the experiment. To ensure comparable conditions between simulation and experiment, air speed should ideally remain near constant when particle are introduced. Deviations in air

speed during tests may obscure the results, making it difficult to distinguish other dynamics such as those associated with the particles. Thus, special consideration was required.

The air supply fan on the experimental apparatus was controlled via a software implemented PID controller. To minimize disturbances in air velocity generated by the introduction of particles, the fan controller was optimized for disturbance rejection. System identification techniques were employed to develop a more aggressive PID controller tuning with better disturbance rejection capabilities.

The aggressive controller was found to have greatly improved disturbance rejection performance. Figure 4.4 shows measured air velocity during two dynamic tests involving a near step increase in particle metering rate. The previous controller exhibited poor disturbance rejection capability, requiring a minimum of 16 sec to re-stabilize on the target air velocity of 25 m/s. The aggressive controller produced superior dynamic performance, regaining the target air velocity within approximately 3 sec of particles being introduced. The maximum deviation in air velocity was reduced from 3 m/s (12%) to 1.5 m/s (6%) with the use of the aggressive fan controller. However, the optimized controller is not able to completely remove disturbances in the air velocity. Figure 4.4 clearly shows that there is still a noticeable drop in air velocity upon particle introduction. Evidently, some disturbance to air velocity will be present in the experimental data, and must be remembered during analysis.

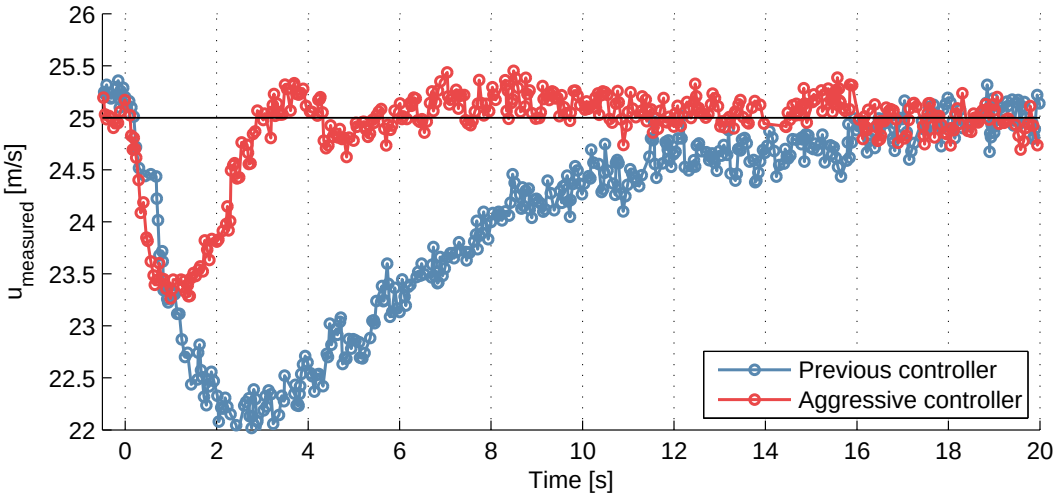

Figure 4.4: Comparison of measured air velocity (u) for the previous (non-aggressive) and updated (aggressive) fan controller designs regarding disturbance rejection.

While the more aggressive controller design provides superior disturbance rejection, it comes at the expense of stability. If the system is operated too far away form the operating point for which the controller was designed, the controller becomes unstable and will cause the fan to runaway. This was especially evident during startup. Proper treatment of the nonlinear nature of the fan would require a more intensive design process and possibly a more advanced controller design to achieve both high performance and stability. In the scope of this project, this was deemed unfeasible. Instead, two controller tunings were used with manual switching between them. The previous controller was used for regular system control and particularly startup. The aggressive controller was enabled only during dynamic testing and after the system had been brought to the desired air velocity. This allowed for the fan's impact on the dynamics of the conveying line to be reduced (but not eliminated), improving the quality of the experimental data.

4.2 Validation of the Model

Utility of the model and simulation is ultimately dependent upon its ability to accurately predict experimental observations. In this section, simulated results are validated through comparison to measured data for fluid pressure and solids velocity. To begin with, the model is calibrated to determine several unknown parameters. After calibration, validation of the model is conducted in two parts. The first examines prediction of steady-state flow conditions. The second compares the time dependent dynamic response of simulated vs. experimental data. The numerical solution procedure was examined for error extensively during development and determined free of error because it generally produced stable, bounded solutions. Furthermore, any significant faults would be expected to manifest noticeably in the simulation results.

4.2.1 Model Calibration

The model equations presented in the previous chapter contain several quantities for which definite values are not readily available, and which must be either estimated or assumed. These include: particle-wall and particle-particle restitution coefficients (e_{wall} and e_{ss} respec-

tively), particle velocity at the inlet and to a lesser extent the drag coefficient, C_d (known for spheres, requires assumption or additional equation(s) for non-spherical particles). Values for these parameters must be either estimated or assumed. To provide direction for estimation and calibration efforts, an elementary sensitivity analysis was performed to determine the impact of these four parameters on simulation results. Greater effort should be taken to determine accurate estimates for parameters with higher sensitivity as simulation accuracy will be impacted more significantly.

The sensitivity analysis revealed the responsiveness of the simulated output data to changes in the four named parameters. It was found that the steady-state solution had very low sensitivity to e_{ss}, high sensitivity to e_{wall}, and marginal sensitivity to both the inlet velocity (for the same grid configuration) and drag coefficient. For the case of spherical plastic particles, the value of C_d should be consistent with that presented in equations (3.18) and (3.19) and the relatively low sensitivity provides little reason for its adjustment. This may not be the case for non-spherical particles, as is the case for many agricultural crop seeds. The solids inlet velocity was estimated from the geometry of the experimental apparatus at a value of 1.2 m/s; assuming that particles exit the meter roller with zero velocity and are accelerated by gravity in free fall before entering the conveying line proper. For higher resolution simulations the value had small significance and, therefore, should not be adjusted without cause or a better estimate. Greater sensitivity was observed as the mesh was made coarser. The remaining two parameters are both restitution coefficients and functions of particle and conveying line material properties. While restitution coefficients can be measured they are commonly estimated due to difficulty in obtaining accurate results reflecting real conditions. In the present work they are used as calibration parameters, their values assumed to be those which provided the best fit to the experimental calibration data set. Values of $e_{wall} = 0.9986$ and $e_{ss} = 0.7$ were found, through trial and error, to provide a good fit to the calibration data. It should be noted that the reported value of e_{wall} is higher than what is typical seen in similar cases, based on manufacturer practices (CNH Industrial, 2018). Furthermore, the coefficient of restitution was measured in the laboratory to be 0.88 for current materials, suggesting erroneous over-prediction of solids friction with the present model.

Sensitivity of the simulated dynamic response to the above parameters was also examined.

For the dynamic response a high sensitivity to e_{wall}, moderate sensitivity to C_d and low sensitivity to solids inlet velocity was observed. Therefore, no additional consideration was given to these parameters aside from that described above. The simulated dynamic response was found to have higher sensitivity to e_{ss} than seen for steady-state, particularly for solids velocity. However, adjustment of e_{ss} alone was not able to adequately approximate the calibration data and so it was not altered.

To provide a better fit to the calibration data with respect to the dynamic response, scaling was introduced to the solids pressure term (eq. 3.26) of the form $p_s^* = \psi p_s$ where ψ is the scaling factor. This provided two benefits: first, it improved the stability of the simulation, and second, it improved the approximation of solids velocity behavior seen in the elevated solids velocity along the particle front. Elevated solids velocity along the front is entirely due to the solids pressure term and disappears completely in its absence. The solids pressure term was found to have a negligible effect on steady-state results. Therefore, the solids pressure term was scaled to 10% of its calculated value, thus $\psi = 0.1$. The need for this correction is likely due to overestimation of granular temperature resulting from the simplified calculation used herein; solids pressure being highly dependent on this quantity. More accurate calculation of granular temperature - possibly using a transport equation - would likely improve the results but was beyond the scope of the present work.

The calibration values described above were used for all simulations in the following sections.

4.2.2 Constants and Physical Properties for Simulation and Experiment

In addition to the calibrated values discussed in the previous section, several constants are required to describe the geometry and physical properties of fluid and particles. The values used for the simulation data in this work are summarized in table 4.1 and were selected to match experimental conditions.

Table 4.1: Constants and Physical Properties for Simulation and Experiment

Parameter	Value	Unit
fluid density, ρ_f	$1.12 \cdot 10^{0}$	kg/m^3
fluid dyanmic viscosity, μ	$1.83 \cdot 10^{-5}$	Pa·s
particle density, ρ_s	$1.42 \cdot 10^{3}$	kg/m^3
particle diameter, d_p	$3.56 \cdot 10^{-3}$	m
particle-particle resitiution coeff.	*	-
particle-wall resitution coeff.	*	-
pipe inner diameter, d	$5.74 \cdot 10^{-2}$	m
pipe length	$1.4 \cdot 10^{1}$	m
pipe relative roughness, ϵ	0	-

* See section 4.2.1

4.2.3 Steady-State Model Validation

The first component of model validation is evaluation of the simulation's ability to predict steady-state conditions in the testing apparatus. Simulations and experiments were conducted for flow conditions with different particle metering rates and nominal air speeds. Three validation test cases are presented in addition to the calibration data set used to fit unknown parameters. The testing conditions used for validation are summarized in table 4.2. Test conditions were selected to approximate air seeding conditions and to have overlap between the two independent variables (solids mass flow rate and nominal air speed), allowing for the sensitivity of simulation accuracy to be assessed for each.

For each test condition, steady-state simulation and experimental results were compared for solids velocity, gauge pressure and pressure gradient along the length of the conveying line. Prediction accuracy for solids velocity and gauge pressure give a general indication of the model's accuracy and ability to predict those macroscopic flow quantities of interest for control application. Pressure gradient provides a better indication of how applicable the subcomponents of the model (e.g inter-phase momentum transfer from drag) are to the given case, particularity through the acceleration zone where the flow is not fully developed.

Table 4.2: Summary of the testing conditions used for model validation along with important parameters

Data Set	Nominal Air Velocity [m/s]	Nominal Air Mass Flow [kg/s]	Metering Step Time [s]	Solids Mass Flow Rate [kg/min]	Solids Mass Loading Ratio	Solids Vol. Fraction* [m^3/m^3]	Superficial Reynolds Number
Calibration	25	0.0756	0.50	4.55	1.00	0.00317	93500
Test 1	30	0.0907	0.50	4.55	0.84	0.00264	112100
Test 2	20	0.0604	0.50	4.55	1.25	0.00396	74900
Test 3	20	0.0604	1.25	16.99	4.68	0.01479	75700

*Solids volume fraction is an estimate provided as a reference to flow density, calculated according to $\varepsilon_{s,avg} = \dot{m}_s / A\rho_s v_{avg}$ where average solids velocity over the length of the conveying line is approximated as $v_{avg} = 0.3 \cdot u_{nominal}$ based on experimental observations.

4.2.3.1 Steady-State Simulation and Experimental Data

Conditions for test 1 consisted of a moderate solids mass flow rate (4.55 kg/min) and a high nominal air velocity (30 m/s). Figure 4.5 compares simulated and experimental data for test 1. The top graph (figure 4.5(a)) shows excellent agreement between simulated and experimental solids velocity, with an average percent error (relative to experiment) of 4.66%. The largest relative error was found on the first data point at 13.22%. Across the remaining length of the conveying line, excluding the first data point, relative error remains below 5.5%. Predicted fluid pressure, reported in figure 4.5(b), was also found to have excellent agreement with experimental data. Average error was calculated as 4.60%. A maximum error of 12.16% was observed for the second to last data point (#20). It should be noted that the measured pressure at point 20 was consistently high across all data sets, possibly the result of a defect in the apparatus, sensor or sensor calibration. The final graph, figure 4.5(c), presents the fluid pressure gradient. Good overall agreement between simulation and experiment was found. The average error in pressure gradient prediction was 9.25% with a maximum of 27.41%. The trend in pressure gradient was replicated well by the simulation; an observation of note given that the drag model is intended only for fully developed flow and was anticipated to have limited accuracy in the acceleration zone near where particles are introduced. Taken as a whole, the capability of the model in predicting the measured variables for conditions of test 1 appears very good.

Conditions for test 2 consisted of the same moderate solids mass flow rate (4.55 kg/min)

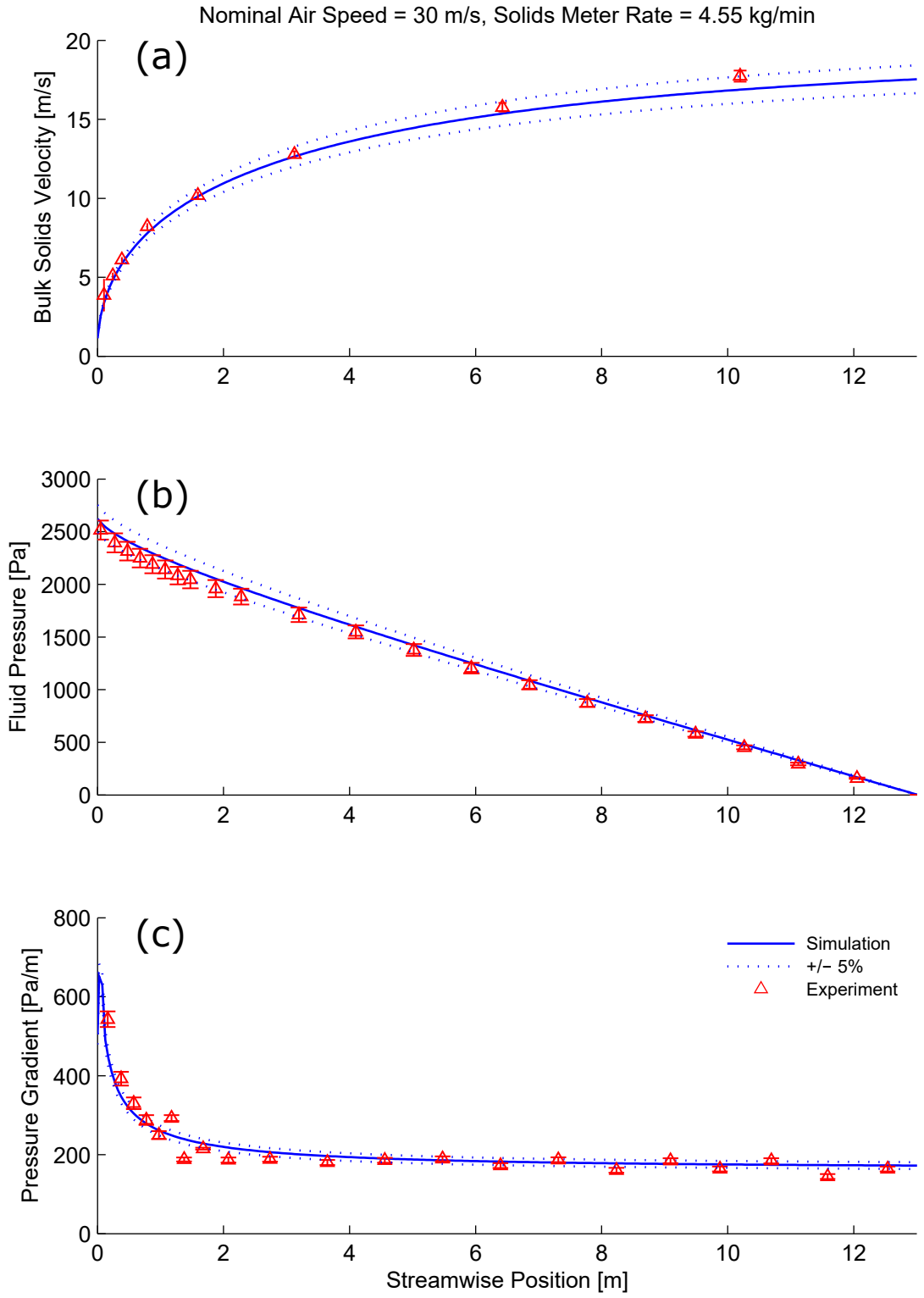

Figure 4.5: Steady-state results from simulation and experiment for test 1, consisting of a high air velocity ($u = 30$ m/s) and a moderate solids flow rate ($\dot{m}_s = 4.55$ kg/min). Solids velocity (a), fluid pressure (b), and pressure gradient (c) are recorded at multiple locations along the conveying line.

and a low nominal air velocity (20 m/s). Figure 4.6 presents simulated and experimental data for test 2. Good agreement was demonstrated between simulated and experimental solids velocity at the lower conveying speed[1]. The average error was found to be 8.10% and the general trend was well observed over the entire line. The results for gauge pressure were also positive, showing excellent agreement with experiment. An average error of only 3.93% was observed. Error for gauge pressure was quite consistent over all measured points, with the exception of tap #20 as was seen in test 1. Pressure gradient showed good agreement although slightly poorer than the previous test condition, particularly in the developing (i.e. particle acceleration) region of the flow. The average error in pressure gradient for test 2 was found to be 8.35% with a maximum value of 30.29%. The trend was again well represented in the simulated results. The model's ability to predict the experimental data for conditions found in the second test case seems quite good.

Conditions for test 3 consisted of a high solids mass flow rate (16.99 kg/min) and a low nominal air velocity (20 m/s), results for which are found in figure 4.7. In figure 4.7(a), observe that relatively poor agreement between simulated and experimental solids velocity was found. The average error was 25.28% with a maximum of 44.31%. Simulated particle velocity does not observe the overall trend seen in the experimental data; plausibly due to the experimental flow departing from the fully suspended and homogeneous flow expected by the model. However, excellent agreement was again seen for fluid pressure. Average error in fluid pressure for test 3 was 3.72% and the maximum error was 18.88%. Error was biased toward the end of the line where measured pressure was lower, inflating the relative error percentages. Simulated gradient pressure, reported in the third graph, showed good agreement with experiment. The average percent error in gradient pressure was 7.62% with a maximum of 22.81%. The trend was predicted quite well even through the acceleration region, despite the assumptions of the drag force model. For more dense flow (i.e. higher solids loading and lower air velocity) the model seems very capable at predicting fluid pressure, while relatively poor at predicting solids velocity.

Error bars, in figures 4.5 to 4.7, represent the estimated measurement uncertainty. For

[1]Note that the 8th measured velocity point (V8) has been removed from tests 2 and 3 due to instrument malfunction causing erroneous measurements.

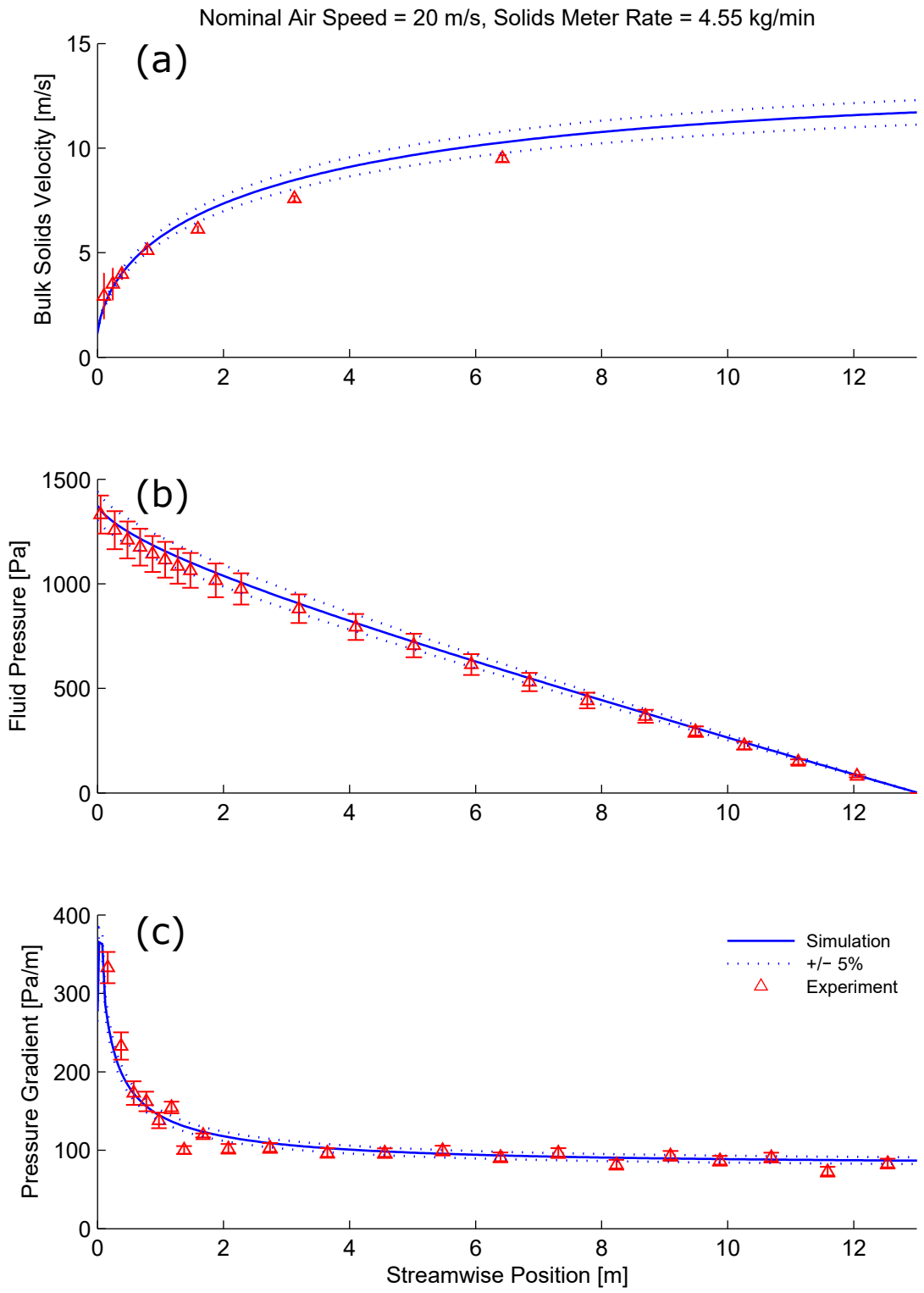

Figure 4.6: Steady-state results from simulation and experiment for test 2, consisting of a low air velocity (u = 20 m/s) and a moderate solids flow rate ($\dot{m}_s$= 4.55 kg/min). Solids velocity (a), fluid pressure (b), and pressure gradient (c) are recorded at multiple locations along the conveying line.

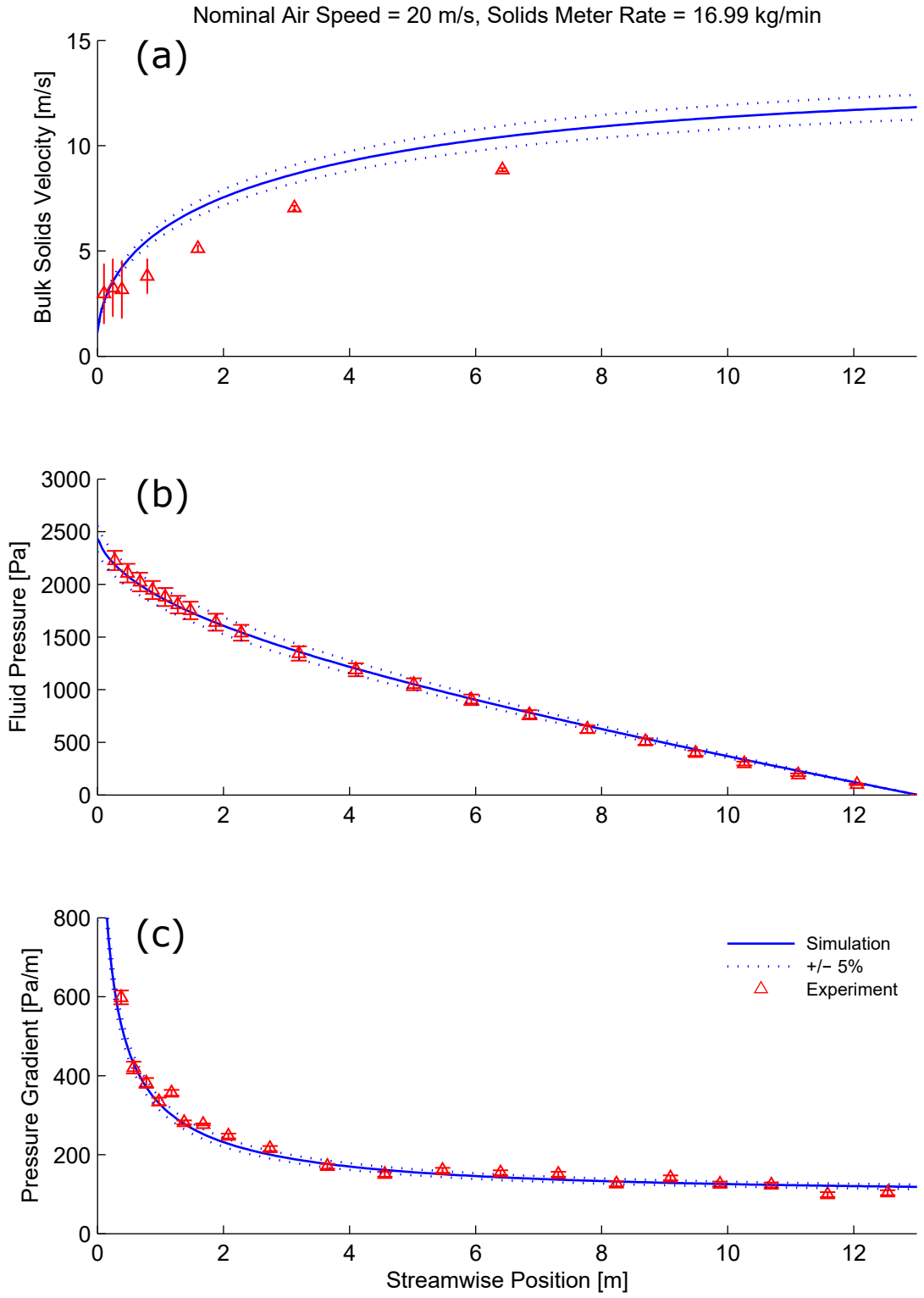

Figure 4.7: Steady-state results from simulation and experiment for test 3, consisting of a low air velocity (u = 20 m/s) and a high solids flow rate ($\dot{m}_s$= 16.99 kg/min). Solids velocity (a), fluid pressure (b), and pressure gradient (c) are recorded at multiple locations along the conveying line.

solids velocity, they represent one standard deviation in the measured velocity data for the period over which the steady-state value (i.e. average) was calculated. For pressure, error bars report the uncertainty due to accuracy of the pressure sensors (typically 0.8% FS). In cases where adjacent sensors are summed, such as for gauge fluid pressure, the uncertainty is cumulative and increases approaching the start of the conveying line ($x = 0$ m).

4.2.3.2 Interpretation of Steady-State Validation Results

The present model validation was by no means exhaustive, utilizing a limited set of three test conditions and one calibration point, and was intended only to provide a general assessment of capability. From the validation results presented in figures 4.5 to 4.7, several general conclusions can be made regarding steady-state accuracy.

First, simulation results indicate the current model to be very capable of predicting macroscopic fluid pressure over a relatively wide range of flow conditions. Between all test conditions, total pressure loss ranged from approximately 1350-2400 Pa, nominal air speed ranged from 20-30 m/s and solids mass flow rate ranged from 4.5-17 kg/min. For all tests, average error between simulated and experimental pressure was below 6%, and with only a few exceptions so was each measured point. This level of accuracy is very good and demonstrates that the one-dimensional Eulerian-Eulerian model is well suited to the pneumatic conveying of large particles. Pressure gradient (per unit length) was also seen to agree consistently across all three tests in both magnitude and overall behaviour. Notably, this included the acceleration zone following the particle entrainment point in which flow is not fully developed. This was in violation of the fully developed assumption of the drag force model. Closer examination of the acceleration region did show increasing differences between simulation and experiment approaching x = 0 m. This is indicative that the drag model is not perfectly suited to the developing region resulting in lower accuracy. However, it does not appear significant enough to seriously degrade the overall results.

Second, the ability to predict solids velocity was unfortunately not as robust, proving to be inconsistent across the range of conditions tested. Both test 1 and 2 consisted of a moderate solids mass loading. For test 1 with higher air velocity excellent agreement was observed, and relatively good agreement was seen for test 2 with lower air velocity as well. However, for

the more dense flow present in test 3 there was significant deviation between simulated and measured solids velocity. The most likely explanation is degeneration of the flow structure away from fully suspended homogeneous flow. As the two-phase flow becomes more dense and air velocity decreases, the flow structure can degenerate (section §2.3) into more complex and unstable patterns. This creates more complex particle movement - including sliding, pickup, settling, saltation, and dune formation - which could significantly impact intrinsic flow mechanisms such as inter-phase momentum exchange and particle friction. The current model assumes that the flow is homogeneous and fully suspended and cannot account for the more complex flow patterns. Therefore, as the flow structure degenerates, prediction of solids velocity grows increasingly inaccurate. The current model was able to provide accurate prediction results for flow conditions where the solids loading rate was sufficiently low to ensure comparatively well developed homogeneous flow.

Third, examination of the pressure graph for all three data sets shows that the simulation generally over predicted pressure slightly compared to experimental measurements. Interestingly, this was also observed for air-only flow in the absence of particles. Figure 4.8 compares simulated and experimental pressure for air-only flow at a flow rate of 25 m/s, for which the average error was found to be 5.37%. This is curious since for air-only flow pressure drop is sourced solely from the industry standard Darcy-Weisbach pressure loss equation. Even this amount of error was unexpected for air-only flow, and is likely a significant contribution to error in the two-phase simulations. Furthermore, similar observations were made in simulation data obtained with commercial CFD software. Potential explanations for this observation include: i) error in measured experimental air velocity and therefore an inaccurate setpoint for experiments, or ii) the geometry of the experimental apparatus (including the flow straightener located upstream from the particle introduction point) attenuates turbulence and/or alters the flow structure sufficiently to noticeably alter pressure loss from fluid pipe friction. However, neither has been verified.

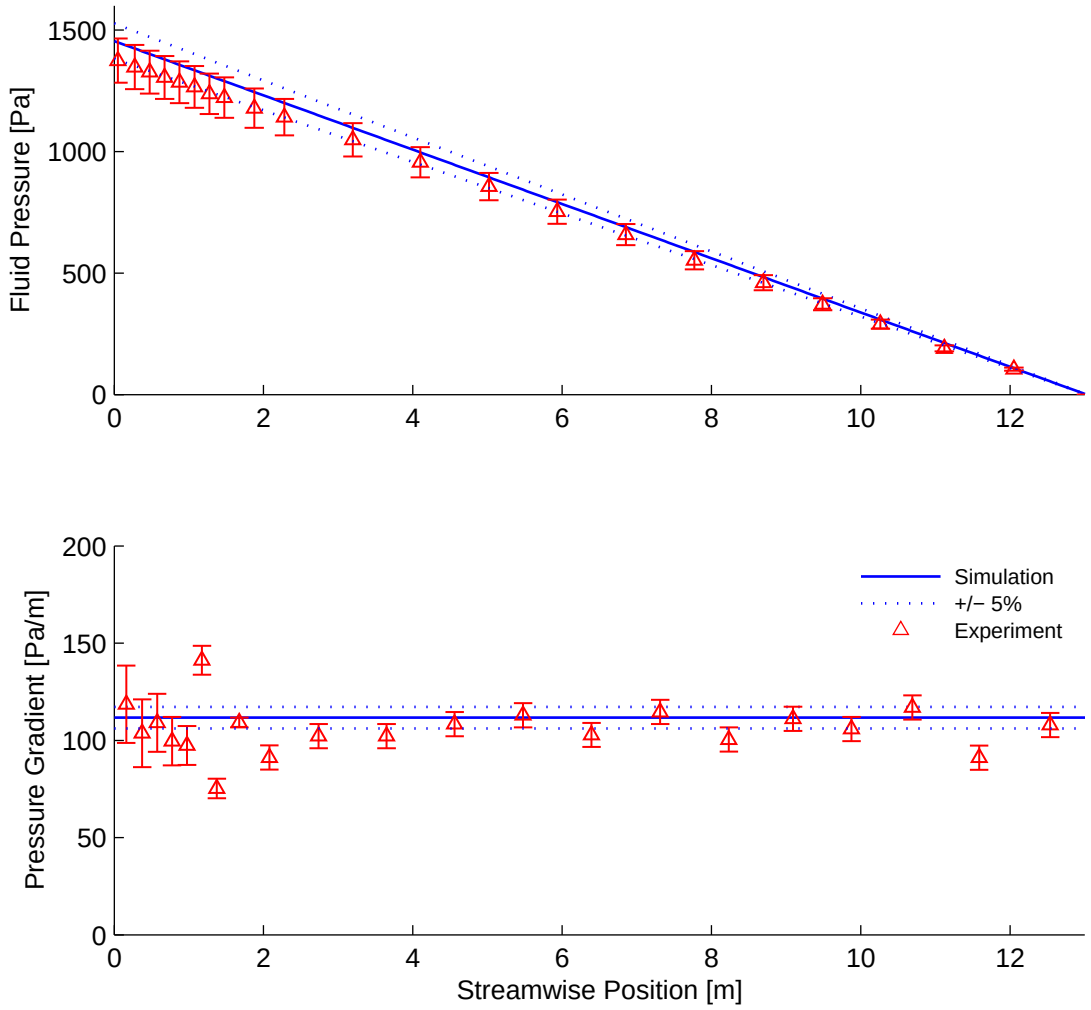

Figure 4.8: Simulated and experimental pressure for air-only flow without particles for a nominal air velocity of $u = 25$ m/s demonstrating error in single phase pressure predictions.

4.2.4 Dynamic Model Validation

The previous section examined the steady-state performance of the model. The discussion on control in section §2.2 established that the dynamic or transient response of the system is also important. Subsequently, the model's ability to accurately predict the dynamic response of the experimental pneumatic conveying flow must be evaluated.

As before, solids velocity and fluid pressure are the two dependent variables which were experimentally measured and were used for dynamic validation. The same test conditions used in the steady-state analysis were retained for consistency. The dynamic tests involve a near step increase in the solids metering rate, transitioning from zero to the specified rate for each test condition. For an ideal step input this transition would be instantaneous, but acceleration limitations of the metering motor means that, in reality, solids flow rate increases over a brief ramping interval. The ramp time to transition from zero to the specified solids flow rate at the inlet is indicated in table 4.2 for each test. Note, dynamic validation does not include variation of the second control variable, air velocity. Because the model assumes incompressible flow, it cannot account for dynamics associated with the fluid phase. Neither has accommodation been made in the model for fan dynamics. Therefore, the model is only capable of predicting dynamic behavior directly associated with the particles and its capabilities should be well examined by the testing method described above.

4.2.4.1 Dynamic Simulation and Experimental Data

Each of the following figures present three graphs comparing simulated and experimental dynamic results for one of the three test conditions. Measured air velocity, solids velocity and normalized fluid pressure are displayed vs. time in each of the three plots respectively, from top to bottom. Solids velocity and pressure are each reported at four separate locations along the length of the conveying line. Normalized solids metering rate (step input) is also shown in the third graph for reference. In all cases, the step introduction of particles begins at $t = 0$ s. Pressure values were normalized according to the following formula,

$$\tilde{p_i} = \frac{(p_i - p_0)}{(p_{\infty,\,sim} - p_{0,\,sim})}, \tag{4.1}$$

where $\tilde{p_i}$ is normalized pressure for point i in the current data set, p_i is the original pressure for point i, p_0 is the initial pressure[2] for the current data set, $p_{\infty,sim}$ is the final pressure for the reference simulation, and $p_{0,sim}$ is the initial pressure for the reference simulation.

Dynamic results for test 1 consisting of a moderate solids flow rate and a high air speed are given in figure 4.9. Therein, measured air velocity was seen to deviate from the set point (30 m/s) by approximately 2 m/s or 6.7% upon introduction of particles. This was the expected response of the air supply fan, volumetric flow rate decreasing in the presence of elevated back-pressure caused by particles. Air velocity was seen to recover relatively quickly, regaining setpoint +/- 2.0% within $\approx$ 2.7 s. In the second graph, simulated solids velocity was seen to have predicted the correct behaviour as observed in the experimental data; including the overshoot in velocity along the solids front. The front refers to the leading edge of persistent solids mass which advances along the length of the conveying line as it fills with particles. However, despite demonstrating the correct behavior, simulated solids velocity was seen to lead experimental results consistently by $\approx$ 0.15 s. This suggests that the solids front moves faster in the simulation than in reality. Solids velocity also appears relatively insensitive to the drop in air velocity, at least for the current operating conditions. Moving to examine the graph of normalized air pressures, substantial disagreement between simulation and experiment was observed. The simulated data predicted that air pressure within the conveying line should stabilize at steady-state values within $\approx$ 1.5 s, while experimental data showed stabilization required approximately 4.0 s. Additionally, experimental data revealed a momentary drop in air pressure immediately following particle introduction. A feature which was not replicated in the simulated data. This discrepancy suggests, as might be surmised, that air pressure is highly sensitive to the response of the fan. Initially, it appears that the models ability to predict transient fluid pressure response was quite poor, yet further discussion of this will follow. Finally, the spatial distribution of pressure during the transient response seems consistent between experimental and simulated data; with pressures at different locations having similarly shaped curves and proportional spacing.

Dynamic results for test 2 consisting of a moderate solids flow rate and a low air speed

[2]For simulation data, p_0 is the initial air-only pressure and is constant for all time $t \leq 0$ s. For experimental data, p_0 is the measured air-only pressure drop, taken as the average pressure for the period before particle introduction as $p_0 = avg(p(t \leq 0))$.

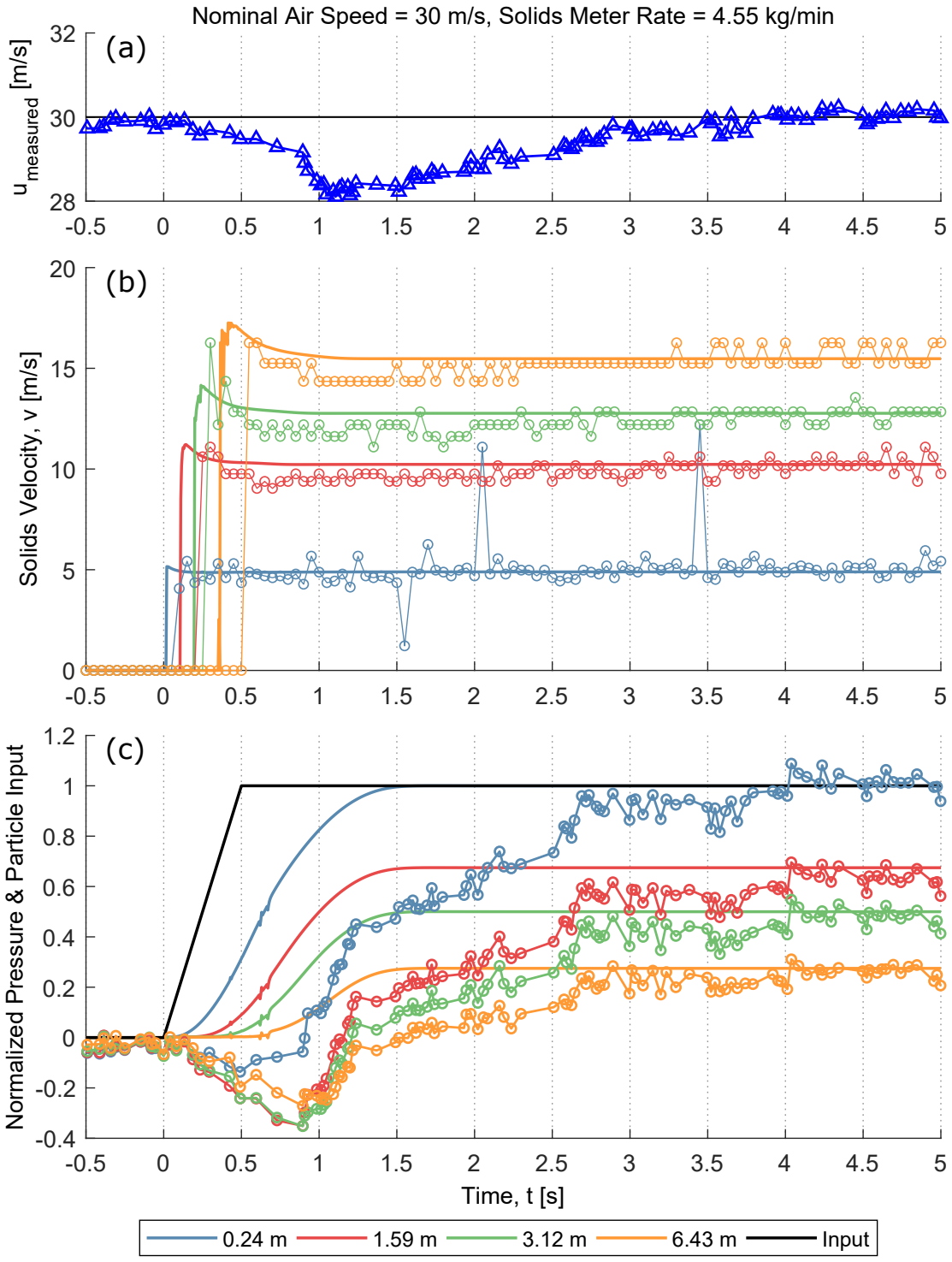

Figure 4.9: Dynamic results from simulation and experiment for test condition 1 (u = 30 m/s, $\dot{m}_s$= 4.55 kg/min). Solid lines represent simulated data while lines with markers represent experimental data. Measured air velocity is presented (a). Solids velocity (b) and normalized fluid pressure (c) are recorded at 4 distances downstream from the particle introduction point. Normalized particle input is given for reference (c).

are given in figure 4.10. Similar observations can be made for test 2 as were stated in the previous paragraph. The same disturbance in air velocity ($\approx$ 2 m/s or 10%) caused by particle introduction was seen to occur. Recovery of the setpoint is slower in the second test, requiring 5.05 seconds to stabilize within +/- 2% of the setpoint. Controller performance appears to decrease and there was noticeable overshoot at the lower air velocity. Solids velocity was seen to respond similar to the previous test. The correct response was predicted in the simulation but again leads the experimental results, in this case by approximately 0.2 s. This again suggests that the front moves too fast in the simulation. With respect to fluid pressure, similarity with the first test remains, with substantial disagreement in transient pressure between simulated and experimental data. The simulation predicted that the transient portion of the pressure response should be complete by $\approx$ 2 s after particle introduction. Experimental measurements, however, indicated a transient interval of between 4.5 and 5 s. The same qualitative differences in the trend were also present, i.e. initial drop in pressure following particle introduction and a sizable overshoot. This provides further evidence of the high sensitivity of fluid pressure to air velocity and the ability of the fan to influence dynamic flow behaviour.

Dynamic results for test 3 consisting of a high solids flow rate and a low air speed are given in figure 4.11. A more severe drop in air velocity was observed following particle introduction, the disturbance measured $>$ 3.5 m/s or 17.5% of the nominal value. Recovery from the disturbance to air velocity was slower, taking $\approx$ 4.25 s to recover within 1 m/s and $\approx$ 9.4 s to stabilize within 2% of the setpoint. A minor overshoot in air velocity was recorded. A similar response to the two previous tests was seen for solids velocity, with the exception of more pronounced impact from the drop in air velocity. Both simulation and experiment exhibited elevated velocity along the solids front; which again moved faster in simulation, by approximately 0.25 s, compared to experimental data. However after the initial rise, solids velocity dips before recovering to its final value. The path of solids velocity recovery tracks closely with air velocity seen in the top graph. Additionally, experimental solids velocity data exhibits more noise than the previous two tests. This is possibly due to less uniform entrainment of particles at the higher mass loading rate. Regarding fluid pressure, significant disagreement between the simulated and measured response persists for test 3. Simulated

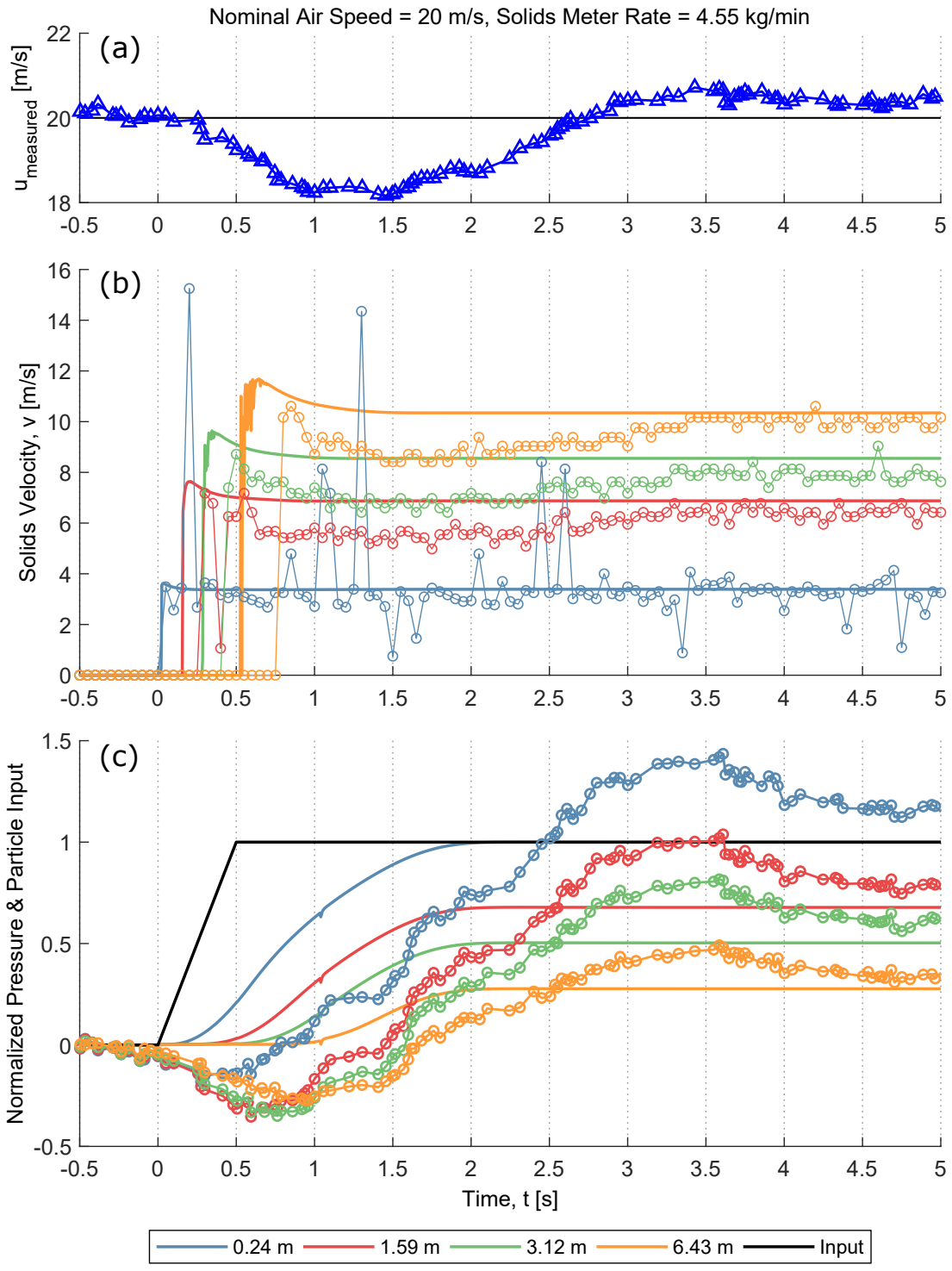

Figure 4.10: Dynamic results from simulation and experiment for test condition 2 (u = 20 m/s, $\dot{m}_s$= 4.55 kg/min). Solid lines represent simulated data while lines with markers represent experimental data. Measured air velocity is presented (a). Solids velocity (b) and normalized fluid pressure (c) are recorded at 4 distances downstream from the particle introduction point. Normalized particle input is given for reference (c).

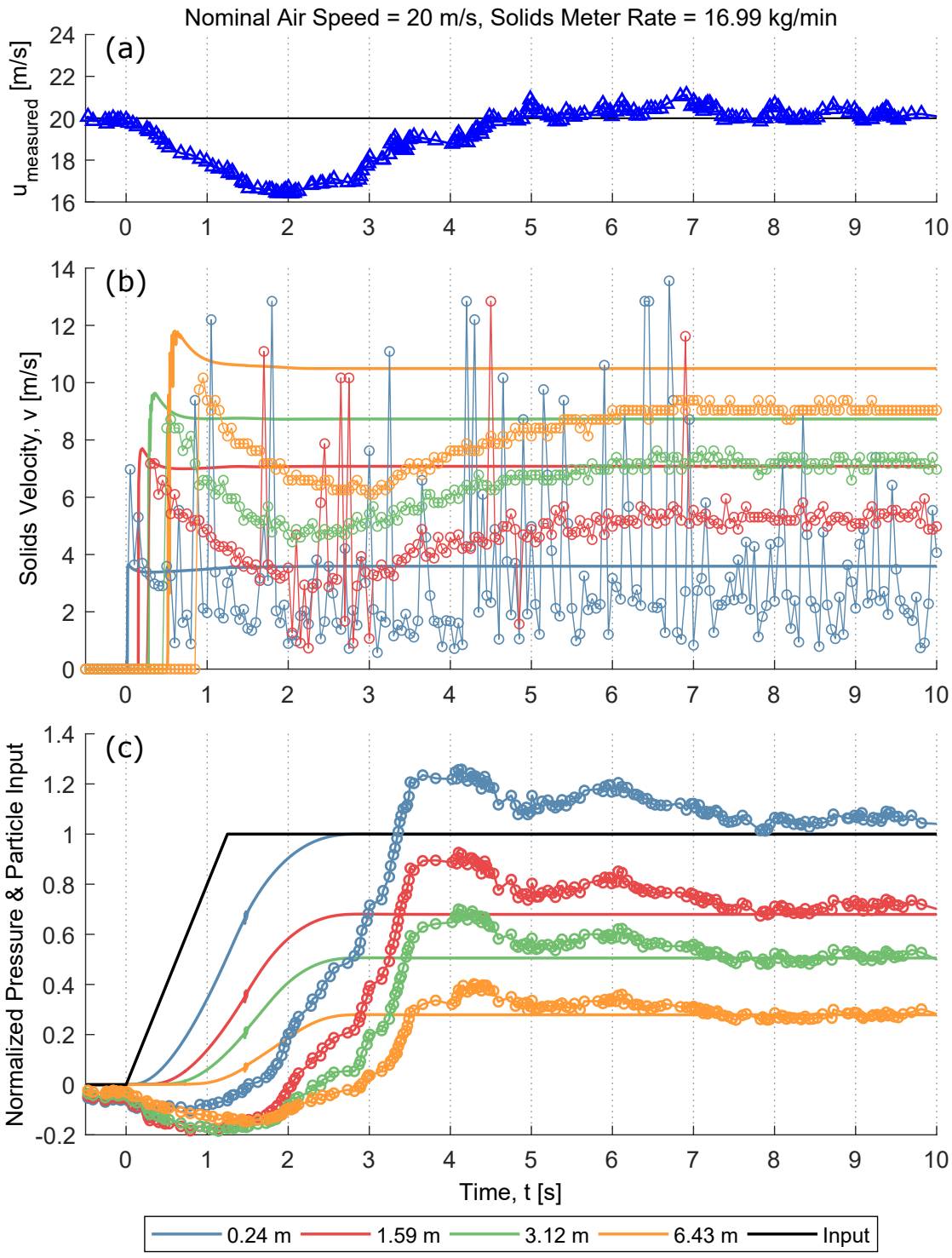

Figure 4.11: Dynamic results from simulation and experiment for test condition 3 (u = 20 m/s, $\dot{m}_s$= 16.99 kg/min). Solid lines represent simulated data while lines with markers represent experimental data. Measured air velocity is presented (a). Solids velocity (b) and normalized fluid pressure (c) are recorded at 4 distances downstream from the particle introduction point. Normalized particle input is given for reference (c).

pressure transients end after ≈ 2.7 s while for the experiment steady-state was not reached until 7-8 s after particle introduction. Moderate overshoot in pressure was observed in the experimental data as was the momentary drop in pressure following particle introduction see in previous tests. Neither of these phenomena were replicated in the simulated data.

4.2.4.2 Interpretation of Dynamic Validation Results

Dynamic validation testing examined the simulation's ability to predict three variations of a near step increase in solids mass flow rate entering the conveying line. It was determined that qualitative prediction of solids velocity transient response was relatively good across all three test conditions. Simulation results correctly predicted a moving solids mass front which travels streamwise down the length of the pipe as it fills with particles. Elevated solids velocity along this front, as predicted by the simulation, was also observed in the experimental data. In the simulation, the elevated velocity is generated entirely by the solids pressure term (eq: 3.26). However, some quantitative error between simulation and experiment did exist. The solids front advanced faster in the simulation than in the experiment for all three tests. The amount by which the simulation leads was found to increase with solids mass loading (combination of lower air velocity and/or higher particle flow rate). In this case, disagreement between the two sources is not entirely surprising. The faster propagation of solids velocity seen in the simulated results is due to an inherent characteristic of the continuous equations. In reality, particles are discrete units representing the minimum amount of mass (above zero) that can exist in a location or be accelerated through drag force. This fact is not enforced by the continuous equations used to model the solids phase, for which any amount of mass can be present, even quantities far less than a single particle. In figures 4.9 to 4.11, solids velocity becoming non-zero at location x in the simulated data indicates that particle mass traveling at velocity v has entered that location of the conveying line. It gives no indication of how much particle mass is present at location x. Therefore, it is appropriate to investigate not only solids velocity but also solids mass flow rate in the simulated results.

Simulated solids velocity, experimental solids velocity and simulated solids mass flow rate are presented in figure 4.12 for a single location on the conveying line. Examination of the figure shows that although simulated velocity becomes non-zero at $t = 0.355$ s, the amount

of solids mass possessing that velocity at that time was negligibly small. In fact, the solids mass flow rate of 5.318×10^{-6} observed at $t = 0.355$ s is equivalent to less than a 1/4 particle/s (or 0.007% of final value). To negate this, experimental velocity and simulated solids mass flow rate were compared; the latter acting as a mass corrected version of solids velocity (being the product of particle density, velocity and volume fraction). In the figure, the lag between simulated velocity and solids mass flow rate is evident and marked with arrows. The rise in solids mass flow rate, indicating that a meaningful amount of mass is present and traveling at the corresponding velocity, aligns very closely with the experimental solids velocity. At the time when particles first appeared in the experimental data, the simulated solids mass flow rate translates to ≈ 12 particles/s (or 0.34% of final value). Simulated solids mass flow rate seems a better predictor of experimental results. In a second graph (figure 4.13) simulated solids velocity has been removed and three additional locations added for the same test conditions. The strong temporal alignment between simulated solids mass flow rate and measured solids velocity was seen to persist across the length of the conveying line. This suggests that predicted solids dynamics are better than might be assumed from from figures 4.9 - 4.11. However, due to the inherent effects of modeling the discrete particles using continuous equations, simulated solids velocity leads experimental results in time. This is an acknowledged limitation of the chosen model.

Increased solids loading also produced larger deviations between simulation and experiment following the passing of the initial solids front. After the initial rise from zero, experimental solids velocity was observed to temporarily drop before slowly regaining its final value. This was significantly more pronounced at higher solids loading rates (tests 2 and 3). The gradual drop and subsequent rise are believed to be primarily due to the disturbance to air velocity; which was in turn caused by the fan's response to increased back-pressure, with a larger step causing a larger disturbance.

With respect to fluid pressure, simulation data were observed to have a poor agreement (thus far at least) with dynamic measurements across all three test conditions. Simulation results predicted that the fluid pressure transient response would be complete between 1.5 and 2.7 seconds following particle introduction; the transient interval increasing with solids loading ratio. Experimental results meanwhile revealed that far more time was required,

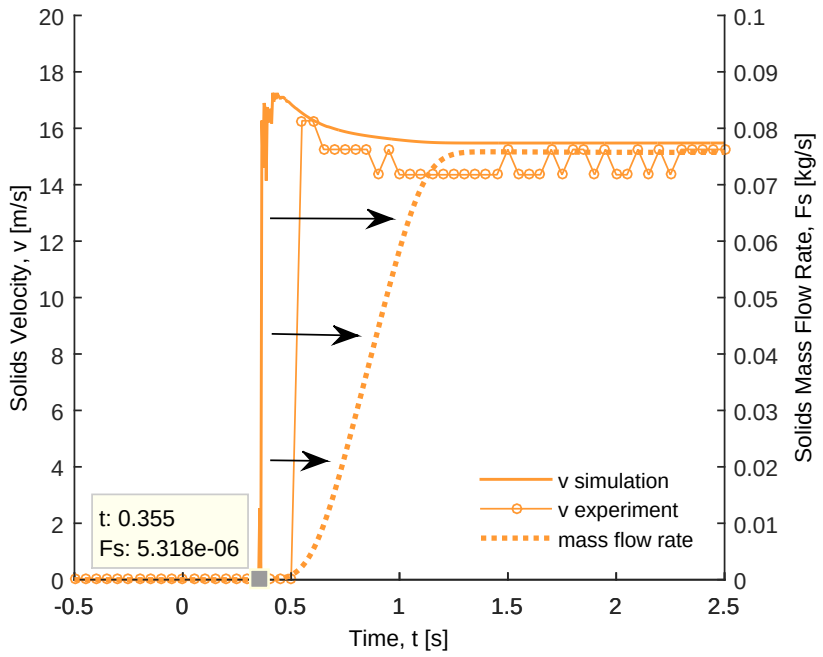

Figure 4.12: Simulated solids velocity, experimental solids velocity, and simulated solids mass flow rate for a single location (x = 6.43 m) demonstrating the temporal lag between solids velocity and solids mass flow rate in simulation. Data is for test condition 1 (u = 30 m/s, $\dot{m}_s$= 4.55 kg/min).

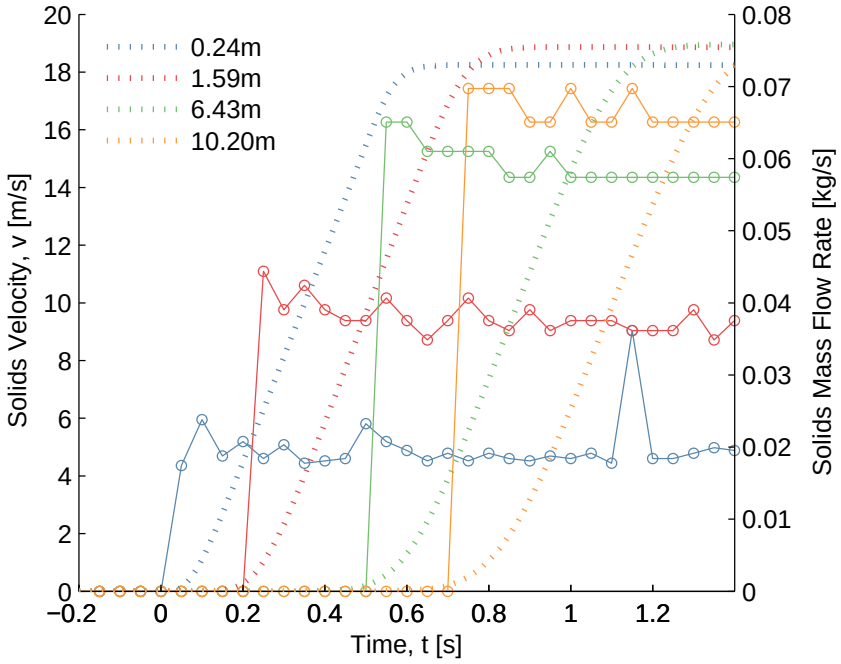

Figure 4.13: Experimental solids velocity and simulated solids mass flow rate reported at four locations, showing the strong temporal alignment between the two variables across the length of the conveying line. Data are for test condition 1 (u = 30 m/s, $\dot{m}_s$= 4.55 kg/min).

approximately 2.5 times that of simulation, for pressure to stabilize at steady-state values. There are two probable explanations for the observed discrepancies in pressure response: a) the model is inherently inaccurate for dynamic flow conditions, or b) simulated conditions were not an accurate representation of the experimental conditions. Further analysis is therefore required to determine, to the extent it is possible with the available data, which of these is the case.

In figure 4.14(a), measured air velocity is reported for two experimental tests with the same input conditions. The two experimental tests were conducted using the aggressive and non-aggressive fan controllers, respectively. For both tests, measured air velocity was clearly observed to drop immediately following the introduction of particles, reaffirming earlier dynamic results. In the case using the non-aggressive controller, the drop in air velocity was larger and persisted for a longer period of time. The unintended drops in air velocity are designated as disturbances and their occurrence was not unexpected given what is known about the operating characteristics of the air supply fan (refer to section §4.1.4). However, the simulation expects the setpoint air velocity of 25 m/s to be constant for the duration of the test. Consequently, simulated and experimental boundary conditions (w.r.t. fluid inlet velocity) are no longer in agreement when the fan's output drops. Aware of the non-ideal change in air velocity and its implications regarding simulation boundary conditions, it must be determine if this change is the primary cause of the observed discrepancies in the dynamic pressure response.

To analyze and compare the observed deviations in pressure and velocity, calculated values are presented in the remaining graphs of figure 4.14. The middle graph (figure 4.14(b)) reports normalized pressure response for the aggressive controller experiment, the non-aggressive controller experiment, and for the simulation. Particle input is also given for reference. All pressure data was normalized to the simulation data set (for $u = 25$ m/s) according to the formula in equation (4.1)[3]. The graph of normalized pressure clearly shows the disagreement between experiment and simulation remarked upon earlier. To determine if the observed differences between simulation and experiment can be attributed to the noted differences in

[3]In the case of p_{sim22} since the air velocity is lower, air-only pressure drop (i.e. p for $t < 0$) is also lower. To preserve the offset this pressure data set was normalized taking $p_0 = p_{0,sim25}$.

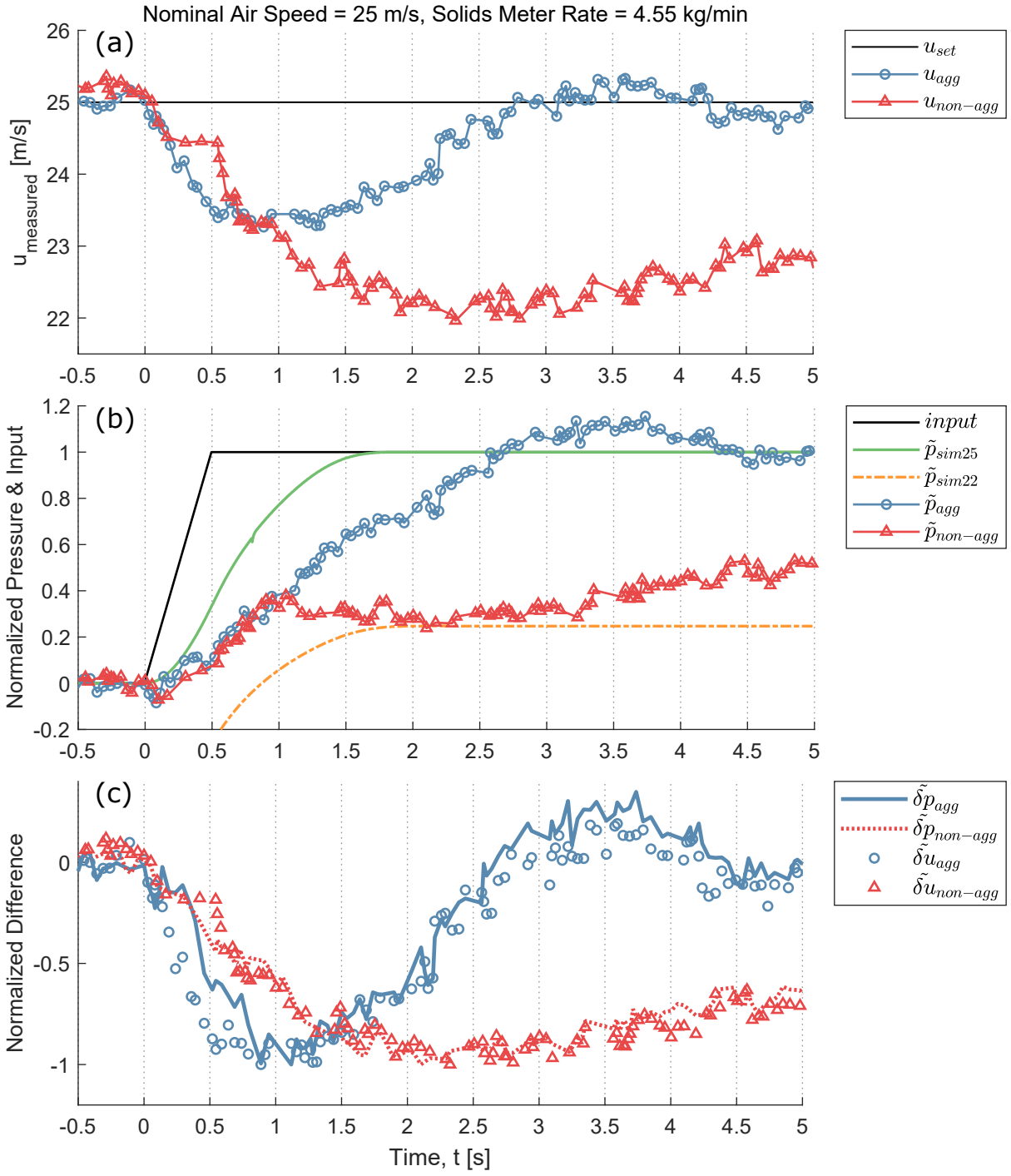

Figure 4.14: Analysis of experimental pressure response demonstrating the strong correlation between errors in predicted pressure and the air velocity disturbances. Measured air velocity (a), normalized pressure response (b) and normalized differences for pressure and air velocity (c).

air velocity, it is useful to compare them directly. Normalized differences between experiments and simulation for both pressure and air velocity are presented in figure 4.14(c). The normalized differences are calculated as follows:

$$\tilde{\delta p_i} = \frac{(\tilde{p}_{i,\,exp} - \tilde{p}_{i,\,sim})}{\max(\mid \tilde{p}_{exp} - \tilde{p}_{sim} \mid)}, \tag{4.2}$$

where $\tilde{\delta p}$ is the normalized difference in pressures, $\tilde{p}_{exp}$ is the normalized pressure for the experimental data set, $\tilde{p}_{sim}$ is the normalized pressure for the simulation data set, and a subscript indicates the value is the ith element of the time series; and

$$\tilde{\delta u_i} = \frac{(u_i - u_{set})}{\max(\mid u - u_{set} \mid)}, \tag{4.3}$$

where $\tilde{\delta u}$ is the normalized difference in air velocities, u is the measured experimental air velocity, u_{set} is simultaneously the simulated air velocity and the experiment setpoint and is constant, and the subscript has the same meaning as before. Normalization removes differences in scale which allows for trends in the calculated values to be compared more equitably. Inspection of figure 4.14(c) shows a very strong correlation between the observed pressure difference ($\tilde{\delta p}$) and velocity difference ($\tilde{\delta u}$) for both experimental sets. This provides evidence that the observed discrepancies between simulated and measured pressure response were the result of disturbances in air velocity during experimental testing, rather than inherent faults of the model. The simulation may, therefore, be more accurate than was suggested by the data presented in figures 4.9 - 4.11.

To justify the observed dynamic pressure results, the hypothesis is put forward that the measured pressure response contains two superimposed dynamic components. The *primary response* was induced directly by particles interacting with the fluid and results in an increase in pressure. The *secondary response* encompasses fluctuations in pressure caused by disturbances to air velocity; a result of the fan's inability to maintain constant flow rate when subjected to increasing back-pressure. Simulated pressure ($\tilde{p}_{sim25}$) is an approximation

of only the primary response (i.e. particle induced) because the simulation does not include a model for fan dynamics. Experimental pressures $\tilde{p}_{agg}$ and $\tilde{p}_{non-agg}$ meanwhile are the sum of both the primary and secondary (i.e. disturbance induced) responses. By subtracting simulated pressure from experimental pressure to yield $\tilde{\delta p}$, the disturbance component of the response is isolated. This assumes the simulation produces a time-accurate representation of the particle-induced pressure increase; the magnitude having been verified in the steady-state analysis. If the proposed analysis is valid then the secondary response represented by $\tilde{\delta p}$ should track closely with its source, namely, the disturbance in air velocity ($\tilde{\delta u}$). This is confirmed in figure 4.14(c) and suggests that the primary pressure response due to particles alone is accurately represented by the simulated data; at least in form.

The case for the model being accurate, in the absence of air velocity disturbances, is furthered by simulation data for a setpoint air velocity of 22 m/s. Simulated pressure ($\tilde{p}_{sim22}$) for the reduced air speed is given in figure 4.14(b). The reduced air velocity of 22 m/s was selected because it is the minimum value which $u_{non-agg}$ reduces to after particle introduction. Reasonable agreement is witnessed between $\tilde{p}_{sim22}$ and $\tilde{p}_{non-agg}$ for the period before $t \approx 2.5$ sec. This is understandable since conditions of the lower velocity simulation would more accurately approximate the experiment prior to air velocity beginning to increase (which occurred slowly and after some delay under the non-aggressive control scheme).

Operating under the premise of a dual pressure response, a final point of inquiry presents itself. Can the interval over which the primary response occurs be estimated from the experimental data? Obtaining an estimate for the primary response provides additional evidence for or against the dynamic accuracy of the model. To begin, the presence of both a primary (particle induced) and secondary (fan induced) pressure response are assumed. The effect of particles is to increase pressure and thus can only decrease air velocity. The effect of the fan controller is to compensate for changes and thus should only increase air speed (when operating below the setpoint). Therefore, the following supposition was made. The decreasing trend in air velocity (beginning at $t = 0$) is caused by particles and can stop only when one of two events occur; either particle related dynamics have concluded, or the controller has built up sufficient compensation so as to negate further decrease. Thus, the point in time when air velocity stops decreasing, defined as $t_{min(u)} = t\left(\min(u_{measured})\right)$, is an important marker.

It serves as a definite left side limit (earliest possible conclusion) of the particle response; if particles are the only source of decreasing velocity then their effects cannot be complete while velocity is decreasing. Unfortunately, the unknown contribution from controller compensation prevents the right side limit (maximum time) from being determined definitively; the particle response could at any time be negated by the fan controller increasing air speed. In the case of the non-aggressive controller, however, it is not unreasonable to assume that $t_{min(u),non-agg}$ does approximate the right side limit because in this case controller action was gradual and delayed. Thus, the interval over which the primary response occurs was estimated from figure 4.14 to be between $t_{min(u),agg} \approx 0.8$ and $t_{min(u),non-agg} \approx 2.2$ seconds; a result which is more consistent with simulated data (simulated response concluded $t \approx 1.6$ seconds) than was observed in the previous section.

The data presented in figure 4.14 and accompanying arguments imply that the simulation's ability to predict pressure transients is better than previously stated. The evaluation was hindered by dynamics associated with the fan, however, and an improved experimental design is required for definitive assessment. The secondary response caused by disturbances in air velocity (related to the fan's dynamic response to increased back-pressure) was slower than the response predicted by simulation, extending the time required for the conveying line to reach steady-state. Clearly, despite optimization of the controller, fan dynamics continue to exert considerable influence. Because the current model's scope is limited to the conveying line and does not include the air supply fan, it was unable to account for the fan's response to back-pressure and resulting changes in air flow rate. Therefore, despite the implication of better accuracy regarding the primary response (particle induced), the simulation cannot replicate the dynamic experimental data for fluid pressure. Incorporating fan dynamics into the model in the future is advised, and would be expected to yield improved results.

4.3 Simulation Performance

In addition to accurate prediction of experimental observations, computational speed is a critical factor in determining suitability of the model and simulation. Timely delivery of information is essential for successful control applications, and was a primary criteria for the simulation and this project. Evaluating the simulation's performance with respect to computing speed and its relation to accuracy is the focus of this section. This addresses the fourth and final project objective.

Investigating simulation performance in the present context requires answering several questions. How fast can simulation data be calculated? What is the relationship between computing speed and accuracy? Can a suitable level of both be achieved concurrently? The answer to these questions are not trivial. Computing speed is undeniably influenced by the hardware used to run the simulation. Furthermore, possibly computing speed and certainly accuracy, are dependent upon the conditions being simulated (demonstrated in the previous section). Obtaining a complete description of simulation performance would require an extensive investigation and generate a large amount of data. Therefore, only a preliminary analysis is included here, which is both concise and sufficient for the purposes of the project.

The method employed to evaluate simulation performance was relatively simple: simulate a standardized test condition under different simulation configurations and compare the results. The use of a standard simulation target - designed to contain ramps, holds and sinusoidal variations of varying rate - allowed for direct comparison between data sets. It also ensured that a large portion of the simulation is transient, negating the possibility of fast computing speed being due to the simulation reaching steady-state. In the absence of experimental data approximating the standardized test condition, accuracy was interpreted as consistency between simulated data sets (the steady-state and dynamic accuracy of the simulation having already been investigated). Thus, the three evaluation metrics included steady-state consistency, consistency during transients and elapsed computing time.

A standardized performance test case was used for all simulations in this section. The physical domain was a 14 m straight pipe section consistent with the experimental apparatus. Air velocity at the pipe inlet ($x = 0$ m) was held constant at 25 m/s. Spherical plastic particles

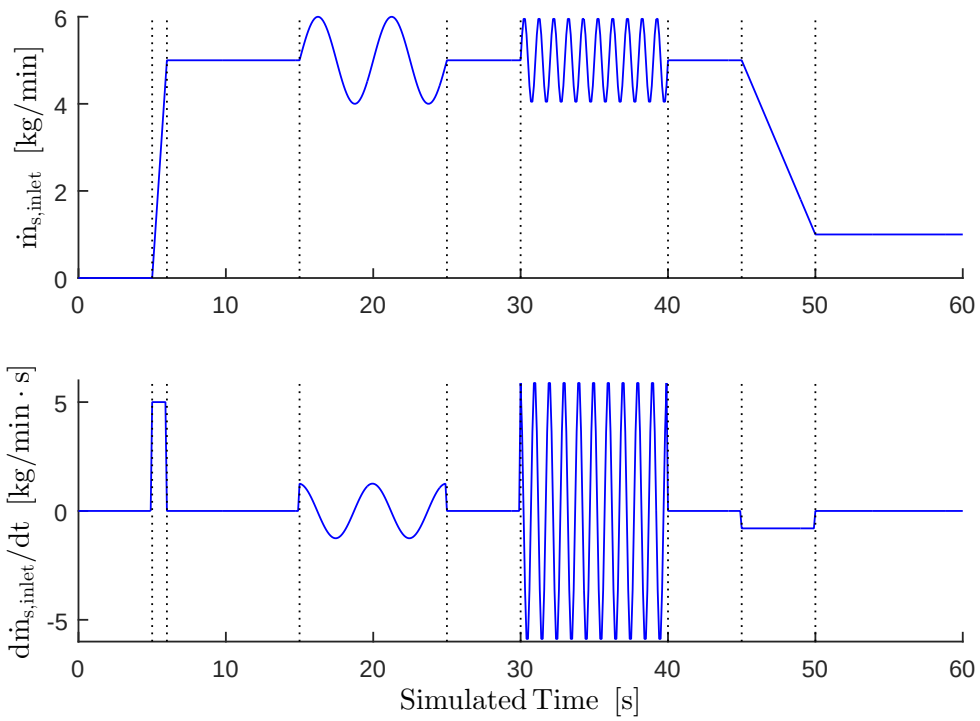

Figure 4.15: Solids mass flow rate boundary condition ($\dot{m}_{s,inlet}$) and its derivative ($\dot{m}_{s,inlet}/dt$) for the standardized simulation target used to evaluate simulation performance, containing both ramps and sinusoidal variations with differing rates of change.

were introduced to the line at the location $x = 1.0$ m, at a rate which was varied over a 60 second interval according to the prescribed schedule seen in figure 4.15. The particle mass flow rate into the conveying line included: a ramp from 0 to 5 kg/min between 5 and 6 s, two periods of sinusoidal variation (5 ± 1 kg/min) between 15-25 s and 30-40 s with frequencies of 0.2 Hz and 1.0 Hz respectively, and finally a ramp reduction to 1 kg/min occurring between 45 and 50 seconds. The time-rate-of-change of the boundary condition by design possess different magnitudes in each of these dynamic components. The standardized test contained different rates of change and a relatively large transient proportion, providing a consistent and demanding means of comparing the simulation's performance.

4.3.1 Host Hardware Specifications

Computational speed is highly dependent upon the hardware specifications of the host computer used to run the simulation. In the interest of repeatability and unbiased assessment,

Table 4.3: Specifications of host machine used to simulate performance test data

Software:	Windows 7 enterprise SP1 (64 bit) / MATLAB 2014a
Processor:	Intel® Xeon® CPU E3-1245 v3 @3.40GHz (4 core, 8 thread)
Memory:	8.00 GB RAM
Storage:	Micron HP 128GB 6GB/s SSD
GPU:	None

specifications of the host computer are provided in table 4.3. All simulations reporting computational speed or run time were executed consistently on the same computer with the listed hardware specifications. Additionally, no specific allowance for parallelization has been made at present.

4.3.2 Computing Time for Different Grid Configurations

Multiple simulations of the standardized test condition were performed with four different configurations of the calculation grid (i.e. Δt and Δx). In general, increasing step size would be expected to decrease computational effort because the number of required calculations is reduced. Increasing step size would also be expected to have a negative impact on stability and accuracy. To make the comparison as unbiased as possible, step sizes were chosen to maintain a constant Courant number (Cr). This reduced the influence of step size on simulation stability between tests. The four simulation tests, important parameters and simulation run times are summarized in table 4.4.

Table 4.4: Simulation configurations for comparison of accuracy vs. computational effort with constant Courant number. All tests were 60 seconds of simulated time.

#	Test	u_{inlet} [m/s]	Δt [s]	Δx [m]	Cr	# Nodes	Max Itr.	Max Res.	Run Time [s]
1	constCFL_veryHighRes	25	0.005	0.05	2.5	3,360,000	100	$1{\cdot}10^{-4}$	850.1
2	constCFL_highRes	25	0.01	0.1	2.5	840,000	100	$1{\cdot}10^{-4}$	96.3
3	constCFL_lowRes	25	0.02	0.2	2.5	210,000	100	$1{\cdot}10^{-4}$	20.3
4	constCFL_veryLowRes	25	0.05	0.5	2.5	33,600	100	$1{\cdot}10^{-4}$	5.0

The Courant number is a dimensionless number and an important stability criterion

for the numerical solution of hyperbolic partial differential equations (Wendt, 2009). It is calculated as:

$$Cr = u\frac{\Delta t}{\Delta x} \tag{4.4}$$

where Cr is known as the Courant number, Δt and Δx are the time and spatial step sizes respectively, and u is the flow velocity. For numerical methods using explicit time integration (e.g. time marching methods) the Courant number is a strict limit on stability, and must have a value of $Cr_{max} \leq 1$. This is alternatively known as the Courant–Friedrichs-Lewy (CFL) condition, developed by Courant et al. (1967) and discussed in Wendt (2009); Wikipedia (2017). For numerical methods utilizing implicit time integration - such as SIMPLER - stability can be retained with higher Courant numbers. However, as the Courant number becomes larger there is increased chance of the simulation becoming unstable, as has been observed by the author in the present case.

Step size for both time (Δt) and space (Δx) were varied by one order of magnitude through the four test simulations. This results in a 100x difference in the number of nodes - the product between the number of spatial grid points and the number of temporal grid points when the full domain is discretized - between the highest and lowest resolution simulations. Table 4.4 shows that the running time for the four test simulations ranges from 850 sec for the highest resolution down to 5 sec for the lowest resolution simulation; a significant difference in computing speed. Furthermore, both simulations #3 and #4 were seen to execute faster than real-time, simulating 60 seconds worth of single-line data in 20.3 and 5.0 seconds respectively. It is apparent that the answer to the first question is that...the simulation is, in fact, able to achieve faster than real-time execution; at least for the conditions tested presently.

4.3.3 Relative Accuracy for Different Grid Configurations

Overall consistency between simulations is presented through a side by side comparison of the entire simulated data set comprised of the four dependent variables, air velocity, pressure, solids velocity and volume fraction. Figure 4.16 presents the simulated results for the highest

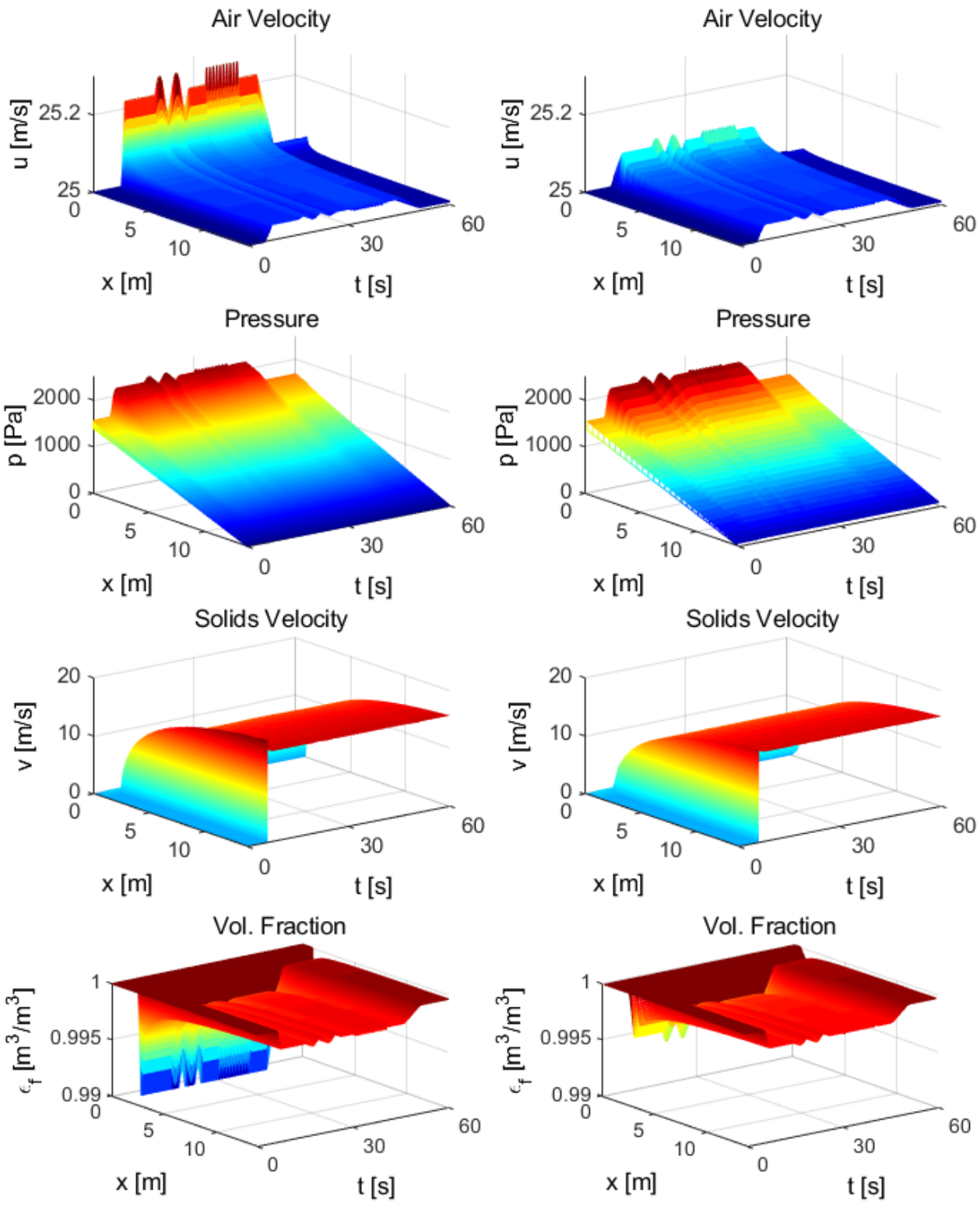

Figure 4.16: Comparison of the four dependent variables: fluid velocity, fluid pressure, solids velocity and void ratio, between the high resolution and the low resolution simulations. (left: veryHighRes-sim#1; right: veryLowRes-sim#4)

resolution and the lowest resolution simulations, sim #1 and sim #4 respectively. Simulated results between the two data sets were seen to agree very well. Fluid pressure and solids velocity were nearly identical between the two sets. Initially, there appears to be disagreement in both air velocity and void ratio, but this is largely due to smoothing resulting from the coarse mesh. In the lower resolution simulations, spatial grid points are not numerous enough to properly resolve the sharp changes that occur near the entrainment point. In the case of both air velocity and void ratio, the values that appear in the low resolution data (right) are consistent with the high resolution data (left). However, values between grid points at the lower resolution are lost, smoothed out by averaging over larger control volumes. Fortunately, localized loss of higher magnitude data in the large gradient regions of the flow is not of high importance for system level control.

Steady-state solids velocity and fluid pressure were used previously for experimental validation. They were again used here and shown in figure 4.17 for the simulations listed in table 4.4. The steady-state results were for the entire pipe length and reported at time $t = 14.5$ s, after the system had stabilized following the first ramp in solids mass flow rate. Both plots show relatively good agreement between all four simulated data sets. The fourth simulation (very coarse) begins to show some deviation, but much of this can again be attributed to smoothing. The loosely spaced grid cannot properly reconstruct curvature in the nonlinear regions. The same observations can be made for solids velocity which exhibits very good agreement. Overall, steady-state predictions remain very consistent between the four simulations despite the large variation in computational effort observed.

Simulated step-response to particle injection is presented in figure 4.18. Recall that the input of solids mass occurs between 5-6 s (referred to as a step but actually a fast ramp, compliant with experimental limitations). Simulated fluid pressure was reported near the upstream end of the pipe at location $x = 2.0$ m while solids velocity was reported further downstream where the flow was more developed, at location $x = 10.0$ m. Attending first to fluid pressure, very consistent agreement is observed with respect to time (position on the horizontal axis) between all four simulations. In all simulations, the transient response begins at 5.0 s and concludes by ≈ 7.0 s. Some disagreement in the initial and finally values (i.e. steady-state) was observed for sim #4 - more apparent here than in the previous figures - but

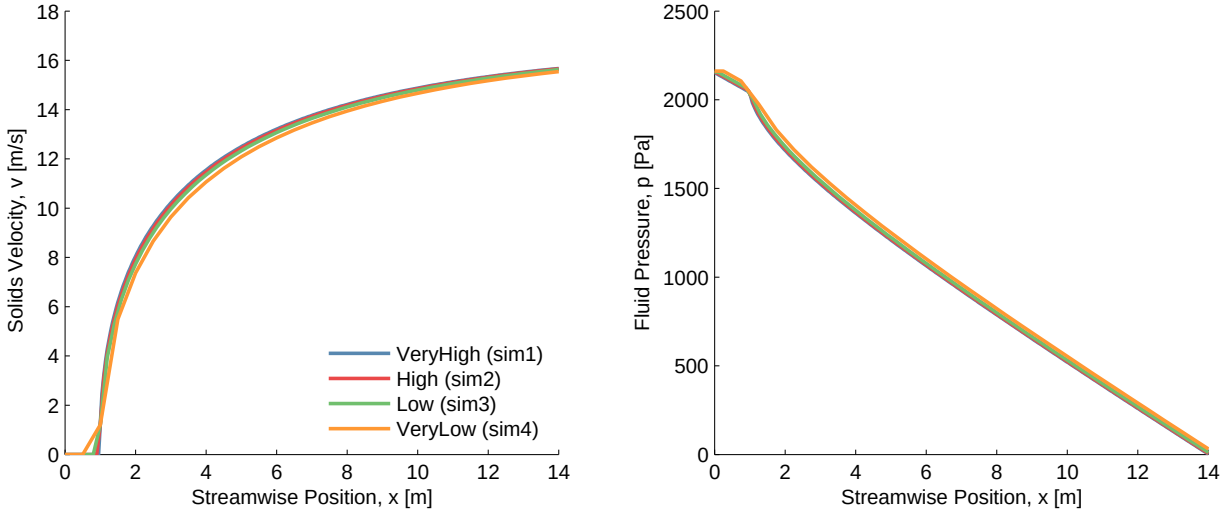

Figure 4.17: Steady-state results of four simulations with different grid configurations and computing times, as given in table 4.4, for solids velocity (left) and fluid pressure (right).

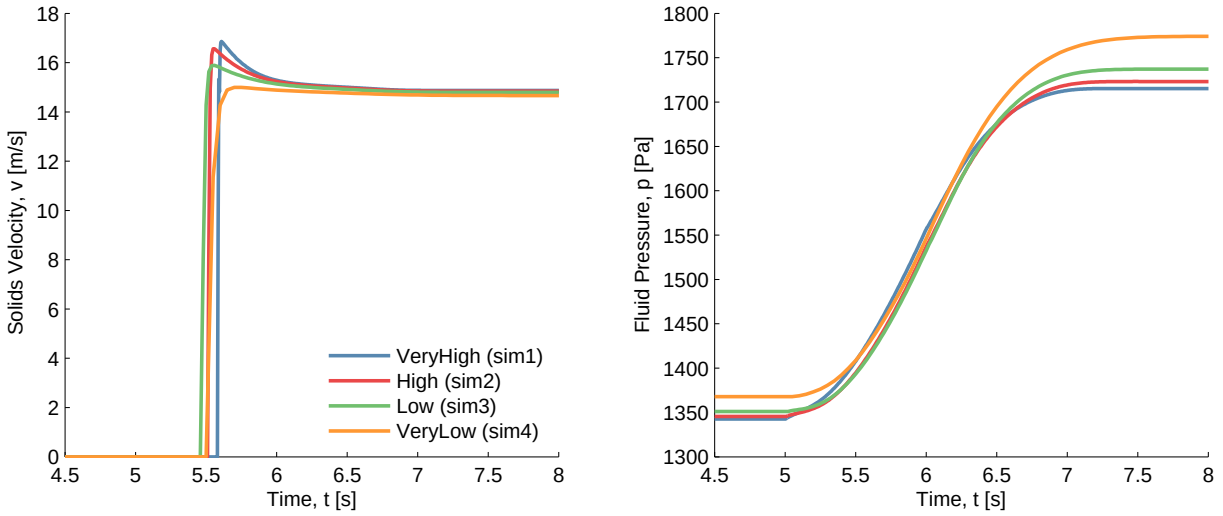

Figure 4.18: Dynamic step-response results of four simulations with different grid configurations and computing times, as given in table 4.4, for solids velocity (left) and fluid pressure (right).

was still reasonable given the large reduction in execution time. Furthermore, sim #3, was noticeably better at replicating the higher resolution simulations. The third simulation also executed faster than real-time, with a recorded run time of 20.3 s for 60 s of simulated data; demonstrating opportunity for optimization between accuracy and computational speed in the future. Good transient results were also obtained for solids velocity, which exhibits strong agreement between all simulations. The fourth data set does suffer from some smoothing as a result of the coarse spatial grid as has been remarked previously. Despite some smoothing the approximation of the higher resolution simulations was still quite good; and the significant increase in computational speed easily justifies the observed loss of accuracy. Future optimization may improve the results further.

4.3.4 Assessment of Simulation Capability

To be practical for application to control of a pneumatic conveying system, the model and simulation must successfully meet two criteria. First, the model must predict two-phase flow conditions within the conveying lines with suitable accuracy. Second, the simulation must be capable of fast execution and timely delivery of calculated results. The development of the model and simulation presented herein was focused on these criteria.

In the previous sections, simulation results were compared to experimental measurements. The model was found to be very capable of predicting steady-state experiments, provided that flow conditions were sufficient to ensure well developed flow. Prediction of dynamic measurements was decidedly less accurate. However, analysis was presented which argued strongly that dynamic accuracy was negatively impacted by the fan response and could be improved in the future. Subsequently, the performance of the simulation regarding computing time was examined. Simulation results were observed to be relatively insensitive to the size of time step and spatial step used; allowing computing times to be drastically reduced without significantly impacting accuracy of the results. The simulation was found to be capable of running significantly faster than real-time while maintaining acceptable accuracy.

The developed model and simulation has demonstrated potential for successful application to control of the air seeder conveying system. The simulation was capable of accurately predicting experimental observations (for most conditions examined) and can do so consid-

erably faster than real-time. This will allow for timely prediction of the conveying system's response to commands and disturbances, which can be used to enhance performance of the conveying system through more advanced control architecture. The two criteria of accuracy and computational speed have been achieved, although currently only for a single conveying line. Extensive development is still needed before anything practical is realized, but the outlook for control application appears favorable.

4.4 Summary

In this chapter, model accuracy and simulation performance were examined. The laboratory apparatus and instrumentation used to collect experimental data were introduced, including control of the air supply fan to minimize its influence. The procedure for calibration of the model was described. Simulation results for both steady-state and dynamic flow conditions were presented and compared to experimental measurements. The model's accuracy was examined and discussed. The performance of the simulation with respect to computing time and its relation to accuracy were investigated. Finally, the potential of the developed simulation for application to control was addressed.

Chapter 5

Conclusions and Recommendations

5.1 Conclusions

There is a demand within the agricultural industry for better performing and more capable equipment. Leading air seeder manufacturers continually pursue innovations that will increase productivity, efficiency, and agronomic performance. Limitations of the pneumatic conveying system represent a significant obstacle to further increases in functionality and precision of air seeding technology. It is theorized that real-time prediction of multiphase flow within the conveying lines could be used to improve controllability and performance characteristics of existing pneumatic conveying systems. The purpose of this study was to develop a model and simulation to predict multiphase flow conditions found on air seeders and to evaluate its accuracy and potential for control applications.

To achieve this goal and provide a foundation for further development, the present research pursued four objectives:

1. To research existing modeling methodologies and select a suitable candidate for the given conditions and application,

2. To develop a model and simulation for prediction of multiphase flow conditions within an air seeder conveying system,

3. To validate the model and simulation using experimentally collected data, and

4. To assess the suitability of the developed model and simulation for future expansion and for control system application.

A review of the literature was conducted in Chapter 2 to determine the available methods for modeling of multiphase flow and pneumatic conveying. Examples found in the literature were grouped into three types: empirical models, correlations and computational models. Computational models, involving the solution of differential equations, were found to be the most suitable and several variations in methodology were investigated. Ultimately, a modeling approach using the Eulerian-Eulerian or "two-fluid" framework was identified as most appropriate for application to control; successfully completing objective #1.

A mathematical representation of the multiphase flow within the conveying lines was developed in Chapter 3. Based upon established "two-fluid" equations for fluid-particle flows, the simplified, one-dimensional model comprised a set of four partial differential governing equations and multiple auxiliary equations. The equations were converted into discrete analogs using the finite volume method and presented in a form consistent with the SIMPLER algorithm. Obtaining a numerical solution to the discrete equations using the prescribed algorithm was the function of the computer simulation program developed in MATLAB® (The Mathworks, Inc., 2015). The model presented in Chapter 3 and the resulting simulation program fulfilled the requirements of objective #2.

In Chapter 4, the model's accuracy and performance of the simulation program were investigated. Experimental measurements of fluid pressure and bulk solids velocity were obtained using a laboratory apparatus which replicated a straight horizontal pneumatic conveying line. Measurements included both steady-state flow conditions and transient conditions following the introduction of particles to the conveying line. Objective #3 was addressed via comparison of simulated and experimental data for three test conditions; evaluating the steady-state and dynamic accuracy of the model. In addition to accuracy, fast delivery of information is an important criterion for control application. To assess performance of the simulation program in fulfillment of objective #4, computing speed and its relation to accuracy were examined. The following results were obtained:

- Steady-state accuracy of the model is acceptable when the flow is sufficiently well developed. Prediction of steady-state fluid pressure was excellent across all test conditions examined. Prediction of steady-state solids velocity was accurate for flow conditions adequately dilute and well developed. At higher mass loading ratios, prediction accuracy

for solids velocity began to deteriorate.

- Dynamic accuracy of the model is believed to be suitable, but the analysis was not conclusive. Evidence suggests that dynamics associated with suspended particles were accurately represented in simulation data; including transport of solids mass within the conveying line and the corresponding increase in fluid pressure. However, the simulation was unable to exactly replicate dynamic experimental observations for either fluid pressure or solids velocity. Limitations of using continuous equations to represent discrete particles and non-ideal fan behaviour are suspected of causing the discrepancies and complicating the analysis.

- Simulation performance with respect to computing speed is excellent. Simulated results were found to be relatively insensitive to the resolution of the computational grid, with the minor exception of rounding in areas of high spatial variation. As a result, the simulation was capable of running significantly faster than real-time with minimal reduction in accuracy.

In conclusion, the developed model and simulation demonstrate sufficient potential for control application. The two principal criteria for application to control are accuracy and quick delivery of information. Accuracy of the model at predicting experimental observations is promising, despite some deficiencies, and results can be computed faster than real-time. The hypothesis, that a simplified one-dimensional model can predict bulk flow properties in the conveying lines with suitable accuracy and speed to be useful for real-time control, has been substantiated. The established model and simulation provide a foundation for future improvement and expansion. Based on the finding presented herein, continued research and development is warranted.

5.2 Limitations

The design philosophy which guided model selection and development prioritized fast execution of the simulation. Concessions were made to reduce the computational intensity of the model at the expense of detail and capability. The consequences of the various simplifications and assumptions need to be understood.

- The two-fluid model was simplified to a one-dimensional representation applicable for pipe bounded flow, greatly reducing the number of equations which need to be solved. While a one-dimensional model is more efficient, it does forfeit certain capabilities. For instance, the simplified model cannot resolve the internal structure of the flow and is only suitable for calculation of bulk, streamwise flow properties. It cannot be applied to bodies with complex geometry. Furthermore, many complex phenomena (e.g. fluid turbulence and its effects) cannot be resolved in one-dimension as they involve higher dimensional properties (e.g. velocity gradients).

- The two-fluid model approximates the dispersed phase as a continuous medium. While this greatly reduces computational requirements, it is an unrealistic representation of discrete particles. The continuous equations are not restricted to the minimum quantum of mass representing a single particle. Therefore, correct solutions to the continuous equations can produce erroneous behavior in some quantities. Overestimated convection of solids momentum, for example, was observed in section §4.2.4.

- The incompressible fluid assumption simplified the modeling equations and numerical procedure. In the present case, compressible effects are estimated to be of minor importance. However, pressure variation in longer conveying lines can cause a significant change in air density (Klinzing et al., 2010), challenging the validity of this assumption. With the simulation program established, this assumption could be revisited in the future with potential benefit to accuracy.

- The scope of the model is currently limited to the conveying line only and does not include the air supply fan. Despite compensation efforts, the dynamic characteristics

of the fan had a substantial influence on flow behaviour during experimental testing. Lacking the capability to account for fan-related dynamic effects, the simulation was not able to replicate the experimental response. Moreover, it significantly hindered dynamic validation of the model. Given the impact of fan dynamics on the overall behaviour of the conveying system, it is unlikely that suitable prediction of system dynamics will be possible without extending the simulation to include the fan.

During model and simulation testing, several deficiencies were discerned which have hitherto not been noted. While these shortcomings did not impede validation efforts, they may prove important to future application and development.

- Simulation instability was observed for the case of emptying the conveying line (i.e. solids mass flow rate into the line becoming zero). Solids mass flow rate at the inlet can be reduced, for example by half, without issue. However, as solids mass flow rate into the conveying line approaches zero, the simulation becomes unstable, causing the numerical solution to diverge. The source of the instability has not been thoroughly investigated.

- Large spikes in fluid pressure were observed upon changing the fluid velocity boundary condition ($u_{x=0}$). This is at least in part a consequence of the incompressible assumption. For incompressible pipe flow, fluid velocity must be equal everywhere to satisfy continuity, assuming constant cross-sectional area. A change in inlet velocity thus necessitates instantaneous change over the whole domain. In the absence of an external force, a large change in the pressure gradient is required to balance the momentum equation and achieve the corresponding change in velocity. This creates large deviations in simulated pressure which persist for the span of a single time-step. This becomes problematic when adapting the single-line model to the simulation of multiple lines run in parallel, for which the velocity boundary conditions will need to be continually adjusted to balance air flow. Some means of compensating for the momentum change - possibly ad hoc modification of values from the previous time-step or incorporation of a pseudo momentum source - might be required.

5.3 Recommendations for Future Work

The investigation of model accuracy and simulation performance conducted as part of this work was by no means exhaustive and was intended only to evaluate suitability for continued development. Further analysis should be conducted to thoroughly test the model and determine limits for its application. Specifically, further validation should consist of the following.

- An expended set of flow conditions covering the operating range of a typical air seeder pneumatic conveying system. Limits should be established for the range of flow conditions over which the model provides suitable accuracy.

- Additional particle varieties as encountered in agriculture. This should include a range of sizes and shapes, particularly non-spherical, to establish limits of applicability.

The developed simulation code provides a testing platform; organized for easy substitution of individual components and source terms. Components of the model can be individually examined, improved or replaced as appropriate to enhance accuracy and efficiency. Several elements of the model have already been identified as candidates for future development.

- Solids friction estimation. The high sensitivity of simulation results to solids friction makes it a priority. Despite adequate results, the calibrated value for the particle-wall restitution coefficient is higher than expected suggesting the current model overestimates solids friction. Substitution with an alternative model may improve results.

- Calculation of granular temperature. An important model parameter, granular temperature was estimated using a simplified formula. Alternative methods in the literature calculate granular temperature via a differential transport equation (Eskin et al., 2007). Although more complex, the latter method has the potential for greater accuracy.

- Drag force model. Alternative drag force models are available in the literature, including examples which account for non-spherical particle shapes. This may provide better accuracy, particularly for the acceleration zone.

- Compressible flow assumption. As noted, compressible effects can be important in pneumatic conveying over large distances. With a stable simulation program to use as a base, the modeling equations could be reformulated to account for compressible flow.

- Alternative models and correlations, available in the literature or developed internally, can be incorporated into the simulation and tested for improved accuracy and performance.

Although promising results have been obtained, significant development is required before any practical means of improving conveying system performance is realized. The model and simulation, having been investigated for a single horizontal conveying line, must be expanded to the larger conveying system. Future development should address the following issues.

- Code optimization. The model and simulation were designed for fast execution. However, the scope of this work was a preliminary investigation and did not include extensive optimization of the simulation program. Optimization of the code for speed and efficiency is advised.

- Incorporation of fan dynamics. The importance of the fan's dynamic response was observed during dynamic validation and is believed to be the primary source of error in simulated results. Extending the model to include the air supply fan would improve predicted dynamic behaviour of the conveying system.

- Incorporation of additional pipe elements. The current model was developed for straight horizontal pipe flow. To predict flow conditions throughout the entire conveying system, the model must include additional pipe elements, e.g. curves, bends, dividers and valves.

- Expansion to parallel lines. Air seeder conveying systems are comprised of multiple conveying lines run in parallel and coupled through the common air supply. The current model can be replicated for additional conveying lines; however, a means of coupling must be introduced. An iterative procedure - where pressure drop for each line is calculated and used to adjust air flow boundary conditions, continuing until the simulation converges on a common pressure - may be possible.

- Control system integration. To achieve tangible improvement in conveying system performance the simulation must be integrated into a suitable control system architecture. Simulation data will guide control decisions, provide operating knowledge and improve performance for air seeder conveying systems.

References

Anderson, T. B. and R. Jackson (1967). Fluid mechanical description of fluidized beds: Equations of Motion. *Industrial and Engineering Chemistry Fundamentals 6*(4), 527–539.

Andrews, M. and P. O'Rourke (1996). The Multiphase Particle-in-Cell (MP-PIC) Method for Dense Particulate Flows. *Int. J. Multiphase Flow 22*(2), 379–402.

Ansys, Inc. (2017). *Ansys Fluent Theory Guide*. Canonsburg, PA. http://www.ansys.com.

Baker, K. D., R. L. Stroshine, K. J. Magee, G. H. Foster, and R. B. Jacko (1986). Pressure Pneumatic Conveying System. *Transactions of the ASABE 29*(3), 840–847.

Barbosa, P. and P. Seleghim (2003). Improving the Power Consuption in Pneumatic Conveying Systems By Adaptive Control of the Flow Regime. *Journal of the Brazilian Society of Mechanical Sciences & Engineering 25*(4), 373–377.

Binsirawanich, P. (2011). *Mass flow sensor development for an air seeding cart*. M.Sc. Thesis, University of Saskatchewn.

Brennen, C. E. (2005). *Fundamentals of multiphase flow*. Cambridge: Cambridge University Press.

Cabrejos, F. and G. Klinzing (1992). Solids mass flow rate measurement in pneumatic conveying. In *Winter Annual Meeting of the American Society of Mechanical Engineers*, Anaheim, CA, 8-13 November 1992, pp. 1–7.

CNH Industrial (2018, July). Personal communication.

Conservation Technology Information Center (2017). Top 10 Conservation Tillage Benefits. Accessed December 2017. http://www.ctic.purdue.edu/resourcedisplay/293/.

Courant, R., K. Friedrichs, and H. Lewy (1967). On the Partial Difference Equations of Mathematical Physics. *IBM Journal of Research and Development 11*(2), 215–234.

Crowe, C. T. (2006). *Multiphase Flow Handbook*. Boca Raton, FL: CRC Press.

Ellis, G. (2004). *Control System Design Guide: Using Your Computer to Understand and Diagnose Feedback Controllers* (Third ed.). San Diego, CA: Academic Press.

Eskin, D., Y. Leonenko, and O. Vinogradov (2007). An engineering model of dilute polydisperse pneumatic conveying. *Chemical Engineering & Processing 46*(3), 247–256.

Gasterstadt, J. (1924). Die experimentelle Untersuchung des pneumatischen Fordervorganges. *V.D.I. Zeitschrift 68*(24), 617–624.

Genić, S., I. Arandjelović, P. Kolendić, M. Jarić, N. Budimir, and V. Genić (2011). A Review of Explicit Approximations of Colebrook ' s Equation. *FME Transactions 39*(2), 67–71.

Gidaspow, D. (1994). *Multiphase flow and fluidization : continuum and kinetic theory descriptions with applications*. Boston: Academic Press.

Gore, R. A. and C. T. Crowe (1989). Effect of particle size on modulating turbulent intensity. *Int. J. Multiphase Flow 15*(2), 279–285.

Henthorn, K. H., J. S. Curtis, and K. Park (2005). Measurement and prediction of pressure drop in pneumatic conveying: Effect of particle characteristics, mass loading, and reynolds number. *Industrial and Engineering Chemistry Research 44*(14), 5090–5098.

Hossain, M. S. (2015). *Development of Semi-Empirical Models to Measure Mass Flow Rate of Solids in an Air Seeder*. M.Sc. Thesis, University of Saskatchewan.

Industry Canada (2017). Trade Data Online. Accessed December 2017. https://www.ic.gc.ca/eic/site/tdo-dcd.nsf/eng/Home.

Janzen, H. H. (2004). Carbon cycling in earth systems - A soil science perspective. *Agriculture, Ecosystems and Environment 104*(3), 399–417.

Keep, T. R. (2016). *Effect of a Localized Velocity Increase on Overall Power Consumption and Flow Characteristics in Pneumatic Conveying Systems*. M.Sc. Thesis, University of Saskatchewan.

Klinzing, G., F. Rizk, R. Marcus, and L. Leung (2010). *Pneumatic Conveying of Solids: A theorical and practical approach* (Third ed.). New York: Springer.

Konno, H. and S. Saito (1967). Pneumatic conveying of solids. *Journal of Chemical Engineering of Japan 2*(2), 211–217.

Laín, S. and M. Sommerfeld (2012). Characterisation of pneumatic conveying systems using the Euler/Lagrange approach. *Powder Technology 235*, 764–782.

Mando, M., M. F. Lightstone, L. Rosendahl, C. Yin, and H. Sorensen (2009). Turbulence modulation in dilute particle-laden flow. *Int. J. Heat Fluid Flow 30*(2), 331–338.

Mason, D. J., P. Marjanovic, and A. Levy (1998). A simulation system for pneumatic conveying systems. *Powder Technology 95*(1), 7–14.

Minnesota Department of Agriculture (2017). Conservation Tillage. Accessed December 2017. https://www.mda.state.mn.us/protecting/conservation/practices/constillage.aspx.

Mittal, L. (2017). *Identifying the Flow Conditions in Pneumatic Conveying of Wheat Grains through Horizontal Straight and Bent Pipe using Pressure Drop*. M.Sc. Thesis, University of Saskatchewan.

Ouyang, Y. (2017). *Measuring Seed Velocity and Seed Counting in a Pneumatic Conveying System using Electrostatic Sensors.* M.Sc. Thesis, University of Saskatchewan.

Pastl, D. and S. D. Noble (2014). Design and Testing of an Electrostatic Particle Sensor for Lean-Phase Pneumatic Conveying. In *2014 ASABE and CSBE/SCGAB Annual International Meeting*, Montreal, Quebec Canada, 13-16 July 2014.

Patankar, S. (1980). *Numerical heat transfer and fluid flow.* Washington: Hemisphere Publishing Corporation.

Pirker, S., D. Kahrimanovic, C. Kloss, B. Popoff, and M. Braun (2010). Simulating coarse particle conveying by a set of Eulerian, Lagrangian and hybrid particle models. *Powder Technology 204*(2-3), 203–213.

Roser, M. and H. Ritchie (2017). Yields and Land Use in Agriculture. Accessed December 2017. https://ourworldindata.org/yields-and-land-use-in-agriculture#global-agricultural-land-use-today.

Sæther, A., C. Arakaki, C. Ratnayake, and D. Di Ruscio (2009). Prediction of Mass Flow Rate in Pneumatic Conveying Using a System Identification Modeling Approach. *Particulate Science and Technology 27*(4), 314–326.

Salahshoor, K., S. Zakeri, and M. Haghighat Sefat (2013). Stabilization of Gas-lift Oil Wells by a Nonlinear Model Predictive Control Scheme based on Adaptive Neural Network Models. *Engineering Applications of Artificial Intelligence 26*(8), 1902–1910.

Sarrami Foroushani, A. and M. Nasr Esfahany (2015). CFD Simulation of Gas-Solid Two-Phase Flow in Pneumatic Conveying of Wheat. *Iranian Journal Of Chemistry & Chemical Engineering-International English E 34*(4), 123–140.

Saskatchewan Trade & Export Partnership (2016). 2016 Saskatchewan State of Trade. Technical report. Accessed December 2017. https://www.sasktrade.com/public/ uploads/userfiles/files/Saskatchewan State of Trade 2016 - February 2017.pdf.

Satpati, B., C. Koley, P. S. Bhowmik, and S. Datta (2014). Nonlinear Model Predictive Control of Pneumatic Conveying and Drying Process. In *IEEE Conference on Control Applications*, Antibes, France, 8-10 October 2014, pp. 492–497.

Schellander, D., S. Schneiderbauer, and S. Pirker (2013). Numerical study of dilute and dense poly-dispersed gas-solid two-phase flows using an Eulerian and Lagrangian hybrid model. *Chemical Engineering Science 95*, 107–118.

Statistics Canada (2017). Seeding decisions harvest opportunities for Canadian farm operators. Technical report. Accessed December 2017. https://www150.statcan.gc.ca /n1/en/pub/95-640-x/2016001/article/14813-eng.pdf?st=y986BP1S.

The Mathworks, Inc. (2015). MATLAB. https://www.mathworks.com/products/matlab.html.

United Nations (2017). Global Issues: Food. Accessed December 2017. http://www.un.org/ en/sections/issues-depth/food/index.html.

van Wachem, B. G. and A. E. Almstedt (2003). Methods for multiphase computational fluid dynamics. *Chemical Engineering Journal 96*(1-3), 81–98.

Versteeg, H. K. and W. Malalasekera (1995). *An introduction to computational fluid dynamics : the finite volume method*. Harlow, Essex, England: Longman Scientific & Technical.

Wen, C. (1959). Flow Characteristics in Solids-Gas Transportation Systems. Technical report, US Dept of the Interior, Bureau of Mines, Pennsylvania.

Wendt, J. F. (2009). *Computational Fluid Dynamics An Introduction*. Berlin, Heidelberg: Springer.

White, F. M. (2011). *Fluid mechanics* (7th ed.. ed.). McGraw-Hill series in mechanical engineering. New York, N.Y.: McGraw Hill.

Wikipedia (2017). Courant-Friedrichs-Lewy condition. Accessed 4 July 2018. https://en.wikipedia.org/wiki/Courant—Friedrichs—Lewy_condition.

World Bank Group (2015). Future of Food: Shaping a Climate-Smart Global Food System. Technical report, Washignton, DC. Accessed December 2017. http://documents.worldbank.org/curated/en/645981468189237140/pdf/100046-WP-PUBLIC-dislcose-7am-10-8-15-Box393216B.pdf.

Wu, Z., A. Aguirre, A. Tran, H. Durand, and D. Ni (2017). Model Predictive Control of a Steam Methane Reforming Reactor Described by a Computational Fluid Dynamics Model. *Industrial & Engineering Chemisty Research 56*, 6002–6011.

Appendix A

Details of the Experimental Apparatus

The experimental apparatus used to collect measured data was instrumented with a multitude of differential pressure and velocity sensors. Sensor placement was biased toward the front section of the conveying line to provide greater spatial resolution in the particle acceleration zone where rates of change are highest. A total of 21 differential pressure transducers and 8 electrostatic velocity sensors were used, the locations of which are given in table A.1 and table A.2 below. Measurements are referenced to the particle entrainment point (refer to section 4.1.1).

Table A.1: Pressure sensor locations for the experimental apparatus

Tap #	Position (m)	Upstream tap for	Downstream tap for
1	0.050	F1	-
2	0.274	F2	-
3	0.475	F3	F1
4	0.675	F4	F2
5	0.875	F5	F3
6	1.075	F6	F4
7	1.275	F7	F5
8	1.475	F8	F6
9	1.876	E0	F7, F8
10	2.280	E1	E0
11	3.196	E2	E1
12	4.100	E3	E2
13	5.020	E4	E3
14	5.934	E5	E4
15	6.854	E6	E5
16	7.772	E7	E6
17	8.696	E8	E7
18	9.490	E9	E8
19	10.264	E10	E9
20	11.120	E11	E10
21	12.052	E12	E11
22	13.024	-	E12

Sensor	dx (m)
F1	0.425
F2	0.401
F3	0.400
F4	0.400
F5	0.400
F6	0.400
F7	0.601
F8	0.401
E0	0.404
E1	0.916
E2	0.904
E3	0.920
E4	0.914
E5	0.920
E6	0.918
E7	0.924
E8	0.794
E9	0.774
E10	0.856
E11	0.932
E12	0.972

The output from the differential pressure transducers is differential pressure between adjacent pressure taps. The gauge pressure curves presented in the report were constructed by summing consecutive differential pressures. The consequence of this is that measurement uncertainty also sums, which is the cause of increasing error bars is some graphs showing gauge pressure.

Table A.2: Velocity sensor locations for the experimental apparatus

Sensor	Position (m)
V1	0.102
V2	0.244
V3	0.388
V4	0.790
V5	1.592
V6	3.124
V7	6.426
V8	10.198

Appendix B

Alternative Form for Momentum Equations

The momentum equations (alternatively the Navier-Stokes equations when referring to the fluid phase) presented in section §3.1 were based on the work of Anderson and Jackson (1967). The form of the momentum equations is consistent with that of the originating work, however, certain elements of the equations can appear to contradict other notations of the Navier-Stokes equations. This is due to the fact that there are two forms in which the momentum equations can be represented, arising from differences in their derivation. The left hand side of both equation (3.3) and equation (3.4) are examples of the *non-conservation* form of the momentum equations; derived by considering a fluid element which moves through space. Alternatively, by considering a fluid element which is fixed in space, it is possible to derive the *conservation* form of the momentum equations (Wendt, 2009). This terminology should not be confused with the fact that both forms are expressions of the physical concept of conservation of momentum.

In general, the two forms of the momentum equation are equal and it is possible to derive one from the other. Beginning with the product rule and the identity for divergence of the product of a scalar and vector term, respectively given as

$$\frac{\partial\left(\varepsilon u_i\right)}{\partial t} = \varepsilon\frac{\partial u_i}{\partial t} + u_i\frac{\partial \varepsilon}{\partial t} \tag{B.1}$$

and,

$$\frac{\partial\left(\varepsilon u_i u_k\right)}{\partial x_k} = u_i\frac{\partial\left(\varepsilon u_k\right)}{\partial x_k} + \varepsilon u_k\frac{\partial u_i}{\partial x_k} \tag{B.2}$$

the left side of equation (3.3) can be rewritten, through substitution of the above equations and with subscripts f and s dropped for convenience, as

$$\rho\varepsilon\left[\frac{\partial u_i}{\partial t} + u_k\frac{\partial u_i}{\partial x_k}\right] = \frac{\partial\left(\rho\varepsilon u_i\right)}{\partial t} - u_i\left[\rho\frac{\partial \varepsilon}{\partial t} + \rho\frac{\partial\left(\varepsilon u_k\right)}{\partial x_k}\right] + \rho\frac{\partial\left(\rho\varepsilon u_i u_k\right)}{\partial x_k} \tag{B.3}$$

where the term in brackets on the right side is simply the continuity equation and thus, is equal to zero. Simplifying the right side equation (B.3) of results in the expression

$$\rho\varepsilon\left[\frac{\partial u_i}{\partial t} + u_k\frac{\partial u_i}{\partial x_k}\right] = \frac{\partial\left(\rho\varepsilon u_i\right)}{\partial t} + \frac{\partial\left(\rho\varepsilon u_i u_k\right)}{\partial x_k}. \tag{B.4}$$

The left side of equation (B.4) represents the local and convective derivatives (i.e. the first terms in the momentum balance equation) denoted in their *non-conservation* form while the right side of equation (B.4) represents the *conservation* form. While the two forms are seen to be equivalent, the conservation form is often better suited for numerical solution (Wendt, 2009). The discrete equations used for simulation herein were derived from the conservation form of the momentum equations. The conservation form of equation (3.3) is given below for reference.

$$\frac{\partial\left(\rho_f \varepsilon_f u_i\right)}{\partial t} + \frac{\partial\left(\rho_f \varepsilon_f u_i u_k\right)}{\partial x_k} = \varepsilon_f \frac{\partial \sigma_{ik}}{\partial x_k} + \varepsilon_f \rho_f \mathrm{g}_i - M_i \tag{B.5}$$